Aus der V. Medizinischen Klinik (Nephrologie/Endokrinologie/Rheumatologie) der
Medizinischen Fakultät Mannheim der Universität Heidelberg
(Direktor: Prof. Dr. med. Bernhard Krämer)

The use of stem cells as a therapeutic modality for amelioration of chronic renal damage after warm or cold ischaemic insults

Inauguraldissertation
zur Erlangung des akademischen Grades
Doctor scientiarum humanarum (Dr. sc. hum.)
der
Medizinischen Fakultät Mannheim
der Ruprecht-Karls-Universität
zu
Heidelberg

vorgelegt von
Sara Medina Balbuena

aus
Las Palmas de Gran Canaria, Spanien
2020

Dekan: Prof. Dr. Sergij Goerdt
Referent: Prof. Dr. Benito Yard

Table of Contents

Abbreviations……1-4
1. Introduction and aims ……5-16
1.1. Acute kidney injury: an overview……....5
1.1.2. Pathophysiology of kidney ischaemia-reperfusion injury …..... 5
1.1.3. Progression to chronic kidney disease…….....6
1.1.4. Animal models of warm ischaemia ……8
1.2. Kidney transplantation: an overview…….....8
1.2.1. Alloantigen–dependent factors affecting transplantation outcome……...9
1.2.2. Alloantigen-independent factors affecting transplantation outcome……. 10
1.2.3. Fischer to Lewis model of chronic renal allograft rejection …… 11
1.3. Rationale of the use of mesenchymal stromal cell in kidney injuries…….. 11
1.3.1. Immunomodulation……... 12
1.3.2. Role in fibrosis, angiogenesis and apoptosis…….. 14
1.3.3. MSC secretome: conditioned media ……..14
1.4. Aims of the thesis ……..16
2. Material and Methods…….....17-40
2.1. Experimental designs.....17
2.1.1. Assessment of long-term renal outcomes in a model of ischaemia-induced acute kidney injury without contralateral nephrectomy……17
2.1.2. Assessment of long-term renal outcomes using two different models of ischaemia induced acute kidney injury……18
2.1.3. Assessment of the therapeutic efficacy of human adipose-derived mesenchymal stromal cells in an ischaemia-induced AKI model……...18
2.1.4. Assessment of therapeutic efficacy of human ABCB5+ cells and its derived CM in a chronic kidney allograft rejection model …….....19
2.2. Surgical methods…….....20
2.2.1. Warm ischaemia model ……..……20
2.2.2. Kidney transplantation ……...23
2.3. Blood and urine collection and analysis…….....29
2.4. Transcutaneous assessment of renal function……...30
2.5. Cells and conditioned media…….....32
2.5.1. Human adipose-derived mesenchymal stromal cells (hASC)……32
2.5.2. Human ABCB5 positive mesenchymal stromal cells (hABCB5+) ……...33
2.5.3. ABCB5-derived conditioned media ……...33
2.6. Organ collection…….. 33
2.7. Histology methods……... 34
2.7.1. Haematoxylin-eosin staining …… 34
2.7.2. Masson-Goldner staining…… 34
2.7.3. Periodic Acid-Schiff staining ……34
2.8. Immune histology…… 35
2.8.1. ED1 staining……35
2.8.2. CD3 staining ……...35
2.9. Quantification of ED1 and CD3 positive cells……....36
2.10. Quantification of kidney fibrosis…….. 37
2.11. Banff classification…… 38
2.12. Exclusion criteria……39
2.13. Statistical analysis …… 40

3. Results.....41-73
3.1. Assessment of long-term renal outcomes in a model of unilateral kidney ischaemia without contralateral nephrectomy……...41
3.1.1. Clinical parameters……41
3.1.2. Macroscopic and histological changes ……..45
3.2. Assessment of long-term renal outcomes using two different models of ischaemia-induced acute kidney injury……...50
3.2.1. Clinical parameters ……50
3.2.2. Histopathology findings ……51
3.3. Assessment of the therapeutic efficacy of human adipose-derived mesenchymal stromal cells (hASC) in an ischaemia-induced AKI model ……57
3.3.1. Clinical parameters …… 57
3.3.2. Renal histology ……...57
3.4. Therapeutic efficacy of human ABCB5+ and its derived CM in a chronic kidney allograft rejection model ……61
3.4.1. Animal general condition ……...61
3.4.2. Clinical parameters ……62
3.4.3. Renal histology……...65
4. Discussion……74-83
4.1. Long-term renal outcomes of unilateral ischaemia without contralateral nephrectomy.....74
4.2. Role of the kidney mass at the time of ischaemic injury in the long-term renal outcomes …….....75
4.3. Role of human adipose-derived MSC (hASC) in the amelioration of chronic renal damage caused by warm ischaemia……..77
4.4. Role of human ABCB5+ cells and its CM in the amelioration of chronic renal damage after cold ischaemia and minor MHC disparity……79
4.5.Conclusions……83
5. Summary 84
6.References……..85--97
7.Curriculum Vitae and Publications……..98-99
8. Acknowledgements..... 100

Abbreviations

A	
ABCB5	ATP-binding cassette subfamily B, member 5 P-glycoprotein
AKI	Acute kidney injury
AMR	Antibody-mediated rejection
Ang-1	Angiopoietin-1
ASC	Adipose-derived mesenchymal stromal cells
α-SMA	Alpha smooth muscle actin
ATP	Adenosine triphosphate
B	
Bcl-2	B-cell lymphoma 2
Bcl-XL	B-cell lymphoma extra large
BD	Brain death
BDD	Brain dead donor
BDNF	Brain-derived neurotrophic factor
bFGF	Basic fibroblast growth factor
BM-MSC	Bone marrow-derived mesenchymal stromal cells
BMP-7	Bone morphogenetic protein 7
Bregs	Regulatory B cells
BSA	Bovine serum albumin
BW	Body weight
C	
CCL	Chemokine CC-Motif Ligand
CCR	Chemokine CC-Motif receptor
CD	Circulatory death
CD80/CD86	Cluster of differentiation 80/86
CDD	Circulatory death donor
Cdh11	Cadherin 11
CKD	Chronic kidney disease
CM	Conditioned media
Col1a1	Collagen 1a1
CX3CR1	CX3C chemokine receptor 1
CXCR	CX chemokine receptor
Cyr61	Cysteine-rich protein 61
D	
DAMPs	Danger-associated molecular patterns
DC	Dendritic cell
DCE-MRI	Dynamic contrast enhanced magnetic resonance imaging
DEPC	Diethyl pyrocarbonate-treated water
DMEM	Dulbecco’s modified eagle medium
E	
ECM	Extracellular matrix

EGF	Epidermal growth factor
eGFR	Estimated glomerular filtration rate
EP2/EP4	Prostaglandin E2 receptor subtype 2/ subtype 4
EPO	Erythropoietin
EPOR	Erythropoietin receptor
ESRD	End-stage renal disease
ET-1	Endothelin-1
EVs	Extracellular vesicles
F	
Fbln-1	Fibulin-1
FBS	Foetal Bovine Serum
FITC –S	FITC-sinistrin/ Fluorescein isothiocynate
Fn-1	Fibronectin-1
FOXP3	Forkhead box P3
G	
GDNF	Glial cell line-derived neurotrophic factor
GFR	Glomerular Filtration Rate
H	
hABCB5+	Human ABCB5 positive mesenchymal stromal cells
hASC	Human adipose-derived mesenchymal stromal cells
HC	Hyaline casts
H-E	Haematoxylin-eosin
HGF	Hepatocyte growth factor
HIF-1α	Hypoxia-inducible factor 1 alpha
HLA	Human Leukocyte Antigen
HO-1	Heme-oxygenase 1
HTK	Histidine-tryptophan-ketoglutarate solution
HUVECS	Human umbilical vein endothelial cells
I	
ICAM-1	Intracellular adhesion molecule 1
IDO	Indoleamine 2,3-dioxygenase
IF	Interstitial fibrosis
IFN-γ	Interferon gamma
IF-TA	Interstitial fibrosis and tubular atrophy
IGF	Insulin-like growth factor
IgM/ IgG	Immunoglobulin M/ Immunoglobulin G
IL	Interleukin
IL1-R	Interleukin 1 receptor
IL1-RA	Interleukin 1 receptor antagonist
iNOS	Inducible nitric oxide synthase
IP	Intraperitoneally
IRI	Ischaemia-reperfusion injury

IV	Intravenously
J	
K	
KTx	Kidney transplantation
L	
LD	Living donor
LEDs	Light-emitting diodes
M	
MCP-1	Monocyte chemoattractant protein 1
M-CSF	Macrophage colony stimulating factor
M-G	Masson-Goldner staining
MHC	Major histocompatibility complex
MIP-1α/β	Macrophage inflammatory protein -1alpha/beta
miRNA	Micro RNA
mRNA	Messenger RNA
MSC	Mesenchymal stromal cells
MSC-CM	Mesenchymal stromal cell-derived conditioned media
MSC-EV	Mesenchymal stromal cell-derived extracellular vesicles
N	
NF-κB	Nuclear factor kappa-light-chain-enhancer of activated B cells
NGF	Nerve growth factor
NK	Natura killer cell
NO	Nitric oxide
Nx	Nephrectomy
O	
P	
PAS	Periodic acid–Schiff
PBMC	Peripheral blood mononuclear cells
PCNA	Proliferating cell nuclear antigen
p-Crea	Plasma creatinine
PDL1	Programmed death-ligand 1
PGE2	Prostaglandin E2
PIGF	Placental growth factor
p-Urea	Plasma urea
Q	
R	
ROS	Reactive oxygen species
S	
SDF-1	Stromal cell-derived factor 1
SC	Subcutaneously
SOCS3	Suppressor of cytokine signalling 3
SVF	Stromal vascular fraction

T	
t½	Half-life
TA	Tubular atrophy
TBS	Tris-buffered saline
TD	Tubular dilation
TGF-β1	Transforming growth factor beta 1
TLR	Toll-like receptor
TMR	T-cell-mediated rejection
TNF-α	Tumour necrosis factor alpha
Tregs	Regulatory T cells
TSG-6	Tumour necrosis factor-inducible gene 6 protein
TxA_2	Thromboxane A_2
U	
uNx	Uninephrectomy/Uninephrectomised
UW	University of Wisconsin solution
V	
VCAM-1	Vascular cellular adhesion molecule 1
VEGF	Vascular endothelial growth factor

1. Introduction

1.1. Acute kidney injury: an overview

Acute kidney injury (AKI), previously known as acute renal failure is characterised by a rapid decline in glomerular filtration rate (GFR) with retention of blood urea nitrogen and serum creatinine (SCr). Even though AKI is heterogeneous in its aetiology, as it may be caused by interstitial nephritis, glomerulonephritis, obstructive nephropathy or renovascular complications, it is more commonly the consequence of ischaemic and toxic insults. It is associated with high morbidity and mortality, particularly in critically ill and elderly patients, with mortality numbers reaching up to 60%[1-3]. Because no specific pharmacologic therapy is effective in AKI patients, their care is limited to supportive management such as renal replacement therapy. The high mortality rate and its associated cost make AKI a serious public health concern and an important economic burden for healthcare systems world-wide.[4-6]. To be more specific, it has been reported to cost 434-620 million pounds in the United Kingdom and 10 billion dollars in the United States, due to prolonged hospitalization and co-morbidities.[7-9]

Renal ischaemia-reperfusion injury (IRI) is a common cause of AKI. It occurs when the blood supply to the kidney is reduced or completely abolished and then restored. Both the deprivation and restoration of oxygen and nutrients contribute to tissue damage. While tissue damage is initiated by the former, restoration of blood flow causes exacerbation of tissue injury culminating in a profound inflammatory response (reperfusion injury). IRI takes place in the clinical setting during kidney transplantation, kidney tumour resections, and cardiac or aortic surgery among others.[10,11]

1.1.2. Pathophysiology of kidney ischaemia-reperfusion injury

Kidney ischaemia-reperfusion injury triggers a cascade of complex mechanisms that lead to epithelial and endothelial cell injury, as well as hemodynamic instability. As a result, the innate and adaptive immune responses are activated, leading to sterile inflammation and oxidative stress that further aggravate injury (**Fig.1**). The lack of oxygen will lead to ATP depletion and will cause damage in all segments of the nephron. Due to their higher metabolic rate proximal tubular epithelial cells in the S3 segment will suffer the most, losing their apical brush border, detaching from the basement membrane and causing tubular dilation[10].

Likewise, endothelial cells are profoundly damaged when subjected to ischaemia. Increased levels of endothelin-1, angiotensin II as well as reduced production of NO cause vasoconstriction in the small arterioles of the post-ischaemic kidney. This, together with activation of the coagulation system and oedema formation, causes vascular occlusion, thereby further reducing blood flow to the outer medulla[12]. Endothelial injury also leads to impairment of the vascular barrier, supporting oedema formation and leucocyte egress. Subsequently, these leucocytes become activated, starting to produce inflammatory cytokines that upregulate the expression of ICAM-1 and VCAM-1 on endothelial cells[13].

Both innate and adaptive immune responses play an important role in IRI. The innate response acts as early as 30 min after IRI, in a non-antigen-specific fashion, involving neutrophils, monocytes, macrophages, DC, NK cells and NKT cells (natural killer T cells). The role of adaptive immune response in kidney IRI is not yet fully understood, but it is

believed that T-cell activation occur both through antigen-specific and antigen-independent mechanisms, and it takes place hours or days after the initial injury [14,15]. The first wave of immune cells are neutrophils, which attach to the endothelium and produce proteases, ROS and cytokines, leading to increased vascular permeability and cell injury. Facilitated by the action of CCR2 and CX3CR1 signalling pathways, the second wave of cells that infiltrate the kidney consists of monocytes. Their main action is phagocytosis and digestion of cellular debris. They also can differentiate into M1 or M2 tissue macrophages, special subsets of macrophages that maintain the inflammatory process or initiate inflammation resolution respectively.[16,17]

In the course of IRI the complement system is activated, mostly but not exclusively, through the alternative pathway. This further propagates the inflammatory cascade. In particular, formation of C5a supports neutrophil recruitment, macrophage activation and chemokine production by the tubular epithelium[18,19]. In response to epithelial cell damage, these cells express toll-like receptors (TLRs), mostly TLR2 and TLR4, which associated molecular patterns (DAMPs) in the extracellular milieu of damaged cells and upon receptor engagement execute a pro-inflammatory response reflected by cytokine production and more recruitment of inflammatory cells. TLR expression/activation is increased under hypoxic conditions (TLR2) or conditions of oxidative stress (TLR4).[20,21]

The role of T-cells in kidney IRI has not been fully elucidated yet. Rodent models of IRI using T-cell deficient animals have suggest a pivotal role for CD4 T cells [22,23]. Likewise it seems that NKT cells, a subset of T-cell receptor expressing NK cells, infiltrate the post-ischaemic kidney as soon as 3 hours after IRI producing large amounts IFNγ [24]. The later mediator, also upregulates MHC class I and II molecules on non-hematopoietic cells, like tubular epithelial cells, making the tissue more prone to T-cell mediated immune attack.[25]

Generation of ROS in IRI comes from four pathways: the mitochondrial respiratory chain; NADPH oxidases; reaction of arachidonic acid catalysed by cyclooxygenase 2; and xanthine and hypoxanthine via xanthine oxidase. The latter is activated under ischaemic conditions, enabling the oxidation of hypoxanthine to xanthine upon reperfusion concomitantly with formation of free oxygen radicals[26]. ROS may cause direct damage to cells through lipid peroxidation of the cell membrane, or indirectly via the formation of the highly toxic peroxynitrite. The huge amount of ROS overwhelms the capacity of oxidant-scavenging systems, leading to mitochondrial dysfunction, compromised ATP production, cytoskeleton alterations and cell death by apoptosis.[27-29]

1.1.3. Progression to chronic kidney disease

For several years it was believed that AKI was a reversible process that would eventually lead to full recovery in absence of co-morbidities. However, evidence from several epidemiological studies suggests that AKI is a risk factor for the progression to chronic kidney disease (CKD)[30-35]. Kidney fibrosis is a key feature of progressive chronic kidney disease and it is characterised by an excessive deposition of a collagenous extracellular matrix (ECM). This is mainly attributed to the secretion of profibrotic cytokines by inflammatory cells, resulting in fibroblast and myofibroblast activation[36].

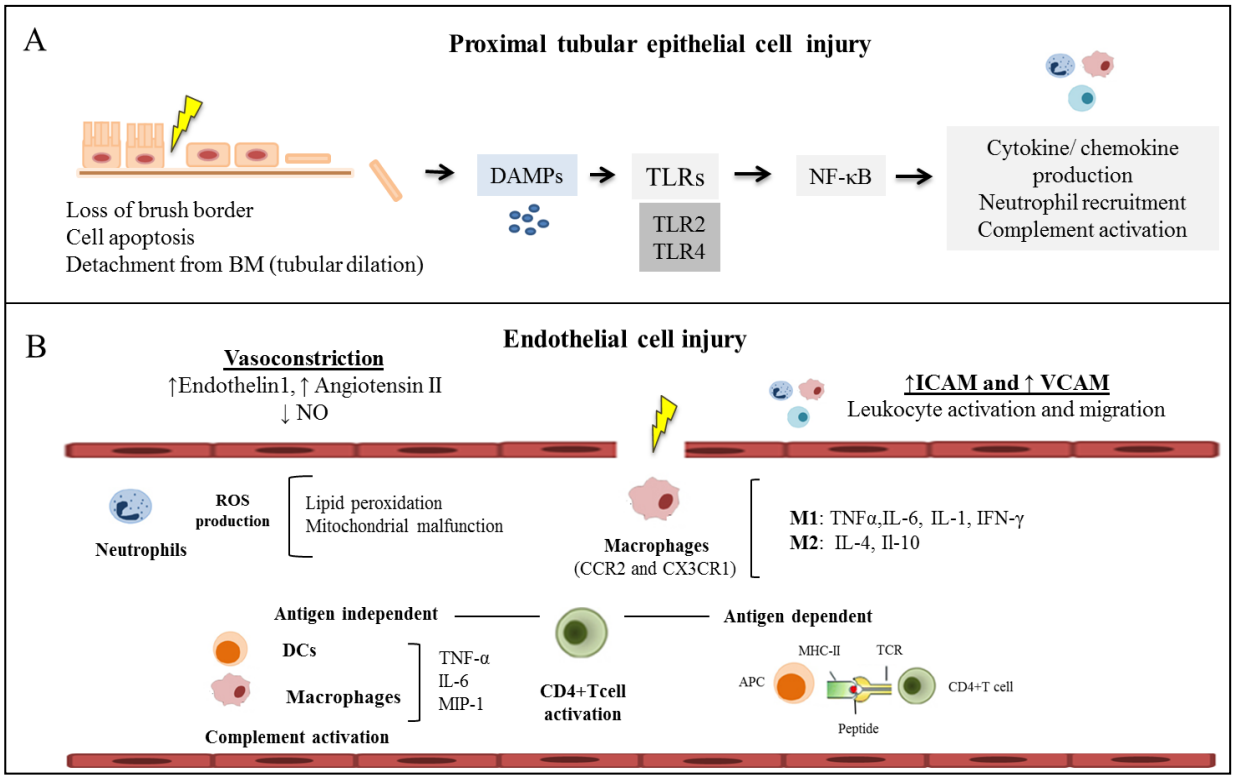

Figure 1: Main pathophysiological events occurring during kidney ischaemia-reperfusion injury.

A. Proximal tubular epithelial cells are damaged due to ATP depletion caused by oxygen deprivation. As a result, they lose their characteristic brush border and detach from the basement membrane, causing tubular dilation. In response these cells express TLR2 and TLR4, which bind to the DAMPs released to the extracellular compartment and enhance the inflammatory response by recruiting inflammatory cells and producing pro-inflammatory cytokines. Additionally, the complement system is activated, further promoting inflammation. **B.** Endothelial cell injury leads to vasoconstriction of small arterioles in post-ischaemic kidney due to increased levels of vasoconstrictor agents (endothelin1 and angiotensin-II) and decreased production of vasodilators (NO). Furthermore, vascular permeability is disturbed causing leucocyte activation and migration into the vessels, facilitated by the upregulation of ICAM and VCAM. The first wave of cells are neutrophils, whose main mechanism of injury is ROS production. Secondly, macrophages infiltrate the tissue and differentiate into M1 (pro-inflammatory cytokine producing) or M2 (inflammation resolution) subtypes. Finally, T cells are activated in antigen independent (by cytokines produced by macrophages or DCs, or through complement activation) or antigen dependent fashion (through the action of antigen-presenting cells).

DAMPs: Danger-associated molecular patterns; **TLR**: Toll-like receptor; **NO**: Nitric oxide; **ICAM:** Intracellular adhesion molecule; **VCAM**: Vascular cell adhesion protein; **ROS**: Reactive oxygen species; **MIP-1**: Macrophage inflammatory protein 1; **APC**: Antigen-presenting cell; **TCR:** T-cell receptor; **MHC-II**: Major histocompatibility complex II.

The mechanisms involved in the progression from AKI to CKD are not yet fully understood; however, it is believed that they are associated with incomplete or abnormal repair[37,38].During the normal repair proximal tubular epithelial cells first undergo dedifferentiation, then migrate along the basement membrane, proliferate and finally differentiate to replace the injured cells. If however IRI causes severe damage, cells become senescent resulting in maladaptive repair[38,39].This repair leads to incomplete restoration of

kidney tissue integrity, persistent inflammation, activation of pericytes, accumulation of myofibroblasts and ECM deposition[40,41]. If cell damage includes DNA strand breaks this will hamper cell proliferation due to a G1 cell cycle arrest required for the DNA damage response. All these events collectively may lead to epigenetic changes in fibroblasts that persist long after the initial injury[42,43]. It is believed that these alterations create a fundament for the progression to CKD[38].

1.1.4. Animal models of warm ischaemia

Animal models of warm ischaemia have been crucial to understand the mechanisms involved in kidney IRI. They are by far the most commonly used AKI models reported in literature[44].Transient renal ischaemia is produced by clamping the renal pedicle for a variable amount of time (usually between 30 and 90 minutes)[45]. Bilateral ischaemia is one of the oldest models studied. It has the advantage of resembling the clinical scenario, as both kidneys are usually equally affected during ischaemia or hypoperfusion and it allows following the function of two ischaemic kidneys. However, due to its severity, longer ischaemia times are not permitted, as higher mortalities will follow[46]. Unilateral kidney ischaemia models are either performed with or without contralateral nephrectomy. Unilateral kidney ischaemia with contralateral nephrectomy is the most frequently used model to induce ischaemic AKI and allows renal function monitoring of the damaged kidney. Yet also this model does not permit longer ischaemia periods for similar reasons as mentioned above[47,48].In recent times, unilateral ischaemia without contralateral nephrectomy has gained relevance. This model allows longer ischaemia periods, as loss of renal function will be compensated by the non-ischaemic kidney. Hence, renal function monitoring of the ischaemic kidney cannot be performed in the acute phase, but can be assessed at later time points when the non-ischaemic contralateral kidney is removed [46,49].

1.2. Kidney transplantation: An overview

The first successful kidney transplant in humans was performed in 1954 by Joseph Murray, using identical twins as donor-recipient combination. Because of the lack of powerful immune suppressive drugs, renal transplantation was not an effective treatment for patients with end-stage renal disease. Although the work of Sir Roy Calne in the 1960s marked the beginning of the immunosuppressive therapy in renal transplantation, graft survival was still poor because the use of steroids alone was not adequately preventing graft rejection. It was in the mid-1980s, with the implementation of calcineurin inhibitors when transplantation medicine grew exponentially, leading to graft survival of approximately 80% after one year at that time[50,51].

Since then, kidney transplantation has become the treatment of choice in patients with end-stage renal disease (ESRD), providing improved quality of life and increasing life expectancy and quality[52]. Nevertheless, despite huge advances in immunosuppressive therapies, organ matching, preservation and donor management, chronic graft loss has not significantly changed over time and remains a scientific and clinical challenge. Consequently, 50% of renal recipients return to dialysis within 10 years[53]. Furthermore, the demand for organ transplantation has increased worldwide, while the supply of suitable organs to cover this demand has not been able to be met. Specifically, in Europe, patients in need of a kidney transplant are around 120-140 million, whereas organ availability is 14-21 million. Therefore,

patients spend approximately 5-10 years on the waiting list. In the meantime they have to rely on dialysis, which is associated with a high mortality, meaning that patients might die before a suitable organ is available.[54-56]

1.2.1. Alloantigen-dependent factors affecting transplantation outcome

Transplantation outcome is greatly determined by humoral and cellular immune responses against the foreign donor MHC molecules. This explains the benefit of HLA matching on graft survival. Humoral and cellular immune responses give rise to distinct types of rejection. Also the target cell that is being attacked by these responses as well as the time frame of occurrence is important for the classification/diagnosis of the different types of rejection. In general, rejection can be antibody-mediated (AMR) or T-cell-mediated (TMR) and in turn, acute or chronic[57].

Antibody-mediated rejection is primarily directed against the vasculature. Based on the time frame of occurrence AMR is defined as hyperacute, acute or chronic. Hereunder these types of rejection will be discussed:

Hyperacute rejection takes place almost immediately after reperfusion and it is the result of the antibody deposition on the endothelium leading to complement activation through the classic pathway. These antibodies may be directed against HLA antigens, blood group antigens or against unknown endothelial antigens. Apart from complement activation, coagulation pathways are activated leading to thrombus formation, occlusion of the microvasculature and finally to irreversible graft loss. With the improvement of pre-transplantation diagnostics, hyperacute rejection nowadays is very rare[58].

Acute antibody-mediated rejection begins within days or months after kidney transplantation and it is clinically manifested by a rapid increase in serum creatinine and non-responsiveness to treatment with steroids or drugs targeting T-cell activity[59]. Recipient antibodies against donor MHC antigens that are displayed on the endothelial cells and glomerular capillaries bind. Thereafter, endothelial cells release deleterious molecules like Von Willebrand factor and P-selectin, which cause platelet aggregation, thrombus formation and production of IL-1α, IL-8, CCL2. This leads to leukocyte migration to the glomeruli and tubules. Additionally, complement activation takes place, and C4d component is deposited in peritubular capillaries.[57,60]

Chronic antibody-mediated rejection is the major cause kidney graft failure. It occurs months to years after kidney transplantation as a response to pre-existing donor-specific antibodies or antibodies generated after transplantation. These antibodies are deposited on the endothelium of glomerular and peritubular capillaries, leading to endothelial injury manifested in the form of endothelial cell hypertrophy, subendothelial deposition of fibrilar material and duplication of the glomerular basement membrane (transplant glomerulopathy)[57].

T-cell-mediated rejection is mostly mediated by alloreactive T-cells that recognize the foreign HLA on tubular epithelial or on endothelial cells of the vasculature. It can occur in an acute or chronic manner:

Acute T-cell mediated rejection is diagnostically defined as infiltration of mononuclear cells in the tubules (tubulitis). T-cells may also infiltrate the vasculature (vasculitis/arteritis,

i.e. T-cell mediated vascular rejection). The incidence of acute T-cell-mediated rejection with the current therapies targeting T cell activity is relatively low (5-10% in the first year in unsensitised patients). The interstitial infiltrate is composed mostly of CD4+ and CD8+ T cells, whereas epithelial tubular cells upregulate ICAM-1, CD80 and CD86 and therefore, recruit macrophages as well as T cells. Endarteritis is detected in 25-40% of renal biopsies, and it is characterized by subendothelial accumulation of mononuclear cells and apoptosis of endothelial cells[59,61].

Chronic T-cell-mediated rejection is the result of failure to maintain sufficient immunosuppression in order to avoid a sustained infiltration of T-cells and macrophages over time. It is characterized by transplant vasculopathy, which is a progressive narrowing of the lumen of the vessels that eventually compromises the blood flow to the graft and leads to its failure[62]. One of the most accepted theories to explain this phenomenon is an "inside out" hypothesis. According to it, the chronic allogeneic response targets first the endothelium (tunica intima). The injured endothelial cells and macrophages (that migrated in response of pro-inflammatory cytokines and adhesion molecules) produce growth factors (VEGF) and IFN-γ, which stimulate phenotypic changes in the smooth muscle cells of the tunica media. As a result, the smooth muscle cells migrate to the intima, causing its thickening and occluding the vessels.[63]

1.2.2. Alloantigen-independent factors affecting transplantation outcome

The benefit of HLA matching on graft survival has underscored the relevance of the HLA system for transplantation outcome. Yet, recipients that receive a mismatched renal allograft from a living donor in general have a better transplantation outcome compared that of recipients with a well matched renal allograft from a deceased donor[64]. This argues against the importance of HLA and suggests that additional factors likely are playing pivotal roles in transplantation outcome. These alloantigen-independent factors include amongst others donor type, warm and cold ischaemia times and ischaemia-reperfusion injury.[65]

Renal allografts can be obtained from deceased brain dead donors (BDD), deceased circulatory dead donors (CDD) or living donors (LD). Due to organ shortage and increased time on the waiting list, the use of renal allografts from LD has gained prominence. In the last years, 27000 related and unrelated living-donor transplantations were performed in the developed countries. Recipients of living-donor kidneys have lower risk of rejection and better allograft survival (87,2% survival after 5 years). This is partly due to the much shorter cold ischaemia time (organ explantation and implantation take place in the same transplantation centre), but also to the fact that the donor did not suffer from brain or circulatory death[66,67]. Because cold ischaemia favours intracellular calcium accumulation, cellular acidosis and mitochondrial dysfunction the short cold ischaemia time in LD clearly will contribute to a better organ quality compared to renal allografts that are allocated to distant transplantation centres.[68]

Brain death (BD) initiates a cascade of hemodynamic instability ('catecholamine storm'), hormonal, metabolic, and inflammatory events (release of pro-inflammatory cytokines, complement activation) that affect the quality of the organs and increases their immunogenicity. Compared to LD grafts from BDD have significantly more delayed graft function and decreased allograft survival (71,1% survival after 5 years) [69-71]. On the other hand, circulatory death (CD) can happen under uncontrolled circumstances (death out of hospital, unsuccessful resuscitation) or controlled conditions (patients in the ICU, patients who arrest in the operating theatre or who suffer cardiac arrest while brain dead). Because of

the lack of circulation, CD is associated with prolonged warm ischaemia times. These organs suffer significantly more from delayed graft function and have increased rejection rates, although this is subject of ongoing debate[72,73].

Transplanted kidneys are subjected to ischaemia and ischaemia-reperfusion injury at different moments. The first warm ischaemia occurs at the time of cross-clamping before perfusions with cold preservation solution. The organ remains ischaemic (cold ischaemia) while in transit to the transplantation centre after having been flushed with a preserving solution. The second warm ischaemia occurs during anastomosis, where the organ warms up to reach the body temperature of the recipient[74]. If the kidney is not adequately perfused after anastomoses this may further increase regional ischaemia, also referred to as the no-reflow phenomenon[75]. Reperfusion injury takes place, when the organ is ultimately perfused with the blood of the recipient at 37°C. Therefore, ischaemia-reperfusion injury is an unavoidable event in solid organ transplantation, and is a major cause of early graft dysfunction and rejection[76]. Its role in triggering the innate and adaptive immune responses has already been discussed in section 1.1.2.

1.2.3. Fischer to Lewis model of chronic renal allograft rejection

The Fischer to Lewis model was the first chronic kidney allograft rejection model in rats reported in literature in 1969[74]. Ever since, it has been extensively used to elucidate mechanisms of rejection as well as to test the efficiency of a number of treatment modalities[77,78] .In this model, the Fischer rat (F344/ $RT1^{1u1}$) acts as a donor and the Lewis rat (Lew/$RT1^{l}$) as the recipient. Initially it was believed that these strains differed at weak histocompatibility loci, but now it is known that they differ at two expressed MHC class I-like genes (RT1.C) and various non-MHC genes (RT6). IgM and IgG alloantibody production has been described in this model, although their circulating levels may decline after 2-4 weeks, and are only present sporadically thereafter[79]. It is reported that progression to chronic rejection starts at 4 weeks, when mild mononuclear cell infiltration, minor proliferation of mesangial cells and occasional thickening of the glomerular basement membrane is observed. At 8-12 weeks, there is significantly more mononuclear cell infiltration of vessels and glomerular changes, leading to proteinuria. At 28 weeks, extensive interstitial fibrosis and vascular intimal thickening with mononuclear cell infiltration is observed, and complete rejection of the graft is reported at 48 weeks if no immunosuppression is administered[80].

1.3. Rationale of the use of mesenchymal stromal cells in kidney injuries

Multipotent mesenchymal stromal cells (MSC) were first described by Friedenstein *et.al* in 1970, when they isolated fibroblast-like colonies from the bone marrow of Guinea pigs[81]. They are mesoderm-derived cells with self-renewal capacity that can be isolated from different adult or foetal sources: bone marrow, adipose tissue, periosteum, synovium, dental pulp, umbilical cord tissue and blood, placenta and amniotic fluid, among others.[82] To date, there is no specific marker to identify MSC, and thus, their in vivo functions are not fully known. However, they are believed to sustain homeostasis in hematopoietic niches as well as to support the *in vivo* homeostasis of other progenitor cells through the secretion of trophic factors like stem cell factor, platelet-derived growth factor, macrophage-colony stimulating factor (M-CSF), erythropoietin (EPO) and angiopoietin-1(Ang-1)[83].

Due to the lack of specific markers, the International Society for Cellular Therapy determined the minimal criteria to define MSC:

1. Plastic adherence under standard culture conditions and a fibroblastoid phenotype
2. More than 95% of the cell population must be positive for antigens absent in haematopoietic cells: CD105, CD73 and CD90. Besides, up to 2% can express CD45 (leucocytes), CD34 (haematopoietic progenitor), CD14 or CD11b (monocytes and macrophages), CD79α or CD19 (B-cells), and HLA-DR (antigen presenting cells and lymphocytes) surface molecules
3. Potential to differentiate into adipocytes, chondrocytes and osteoblasts. [84]

The use of MSC as a potential therapeutic modality in different fields of regenerative medicine has been a subject of study for decades. In those studies it has been shown that MSC are able to modulate the immune response, show anti-inflammatory, anti-apoptotic, anti-oxidative, and anti-fibrotic capacity, as well as angiogenic properties[85] (**Fig.2**).

1.3.1. Immunomodulation

From different *in vitro* and *in vitro* studies it is known that MSC are able to induce an effect in all types of cells of the immune system, although all the exact mechanisms involved are not yet fully known. One of the main interactions studied are those between MSC and macrophages, and the general consensus is that MSC are able to induce polarization of macrophages from M1 (pro-inflammatory) to M2 (anti-inflammatory) phenotype. This switch has been shown to be promoted by the secretion of prostaglandin E2 (PGE2)[86] by MSC as well as by the secretion of IL-1 receptor antagonist (IL1-RA)[87].Moreover, polarization of M2 macrophages can also take place through cytokine-independent mechanisms, as it has been reported that when MSC are phagocytosed by monocytes/macrophages it causes a polarization toward CD14++, CD16+ and CD206+ regulatory subtypes, with anti-inflammatory properties, like production of IL-10 and increased expression of PD-L1[88]. MSC have been proven to interfere in DC maturation by downregulation of maturation markers and costimulatory molecules (CD80/CD86)[89]. In the presence of MSC, DC are less efficiently supporting T cell proliferation and display reduced amounts of MHC class II molecules[90].

Independent of their effect on DC, MSC can directly suppress T-cell activation. One of the postulated mechanisms accountable for this is IDO (indoleamine 2,3-dioxygenase) secretion, which catalyses the conversion of tryptophan, essential to T cell activation. In CD4+ Th1 cells, MSC induce the downregulation of the IFN-γ receptor, thus reducing their IFN-γ mediated susceptibility[91]. Similarly, in CD4+ Th2 cells, MSC have been shown to inhibit IL-4 and IL-5 production. In addition to that, their effect inhibiting CD8+ T cells seem to be mediated by downregulation of the CD8 surface marker, making them less active and acquiring regulatory functions[92,93].

MSC also have the capacity to induce regulatory T cells (Tregs). This is partly mediated by TGF-β1 production but seem to require the presence of monocytes. It is believed that MSC favour M2 macrophage differentiation which leads to CCL18 production. The latter chemokine plays a pivotal role in the induction of Tregs[92,94]. Tregs are part of the peripheral tolerance mechanisms and have important roles in shaping the immune response.

MSC interactions with B cells are much less researched. Some studies have highlighted the ability of MSC to induce regulatory B-cells (Bregs) that like Tregs modulate immune responses[95,96]. Finally, NK cells are also powerfully inhibited by MSC, impairing their cytotoxic cytokine production potential. These effects are mediated by MSC production of PGE2, IDO, TGF-β1, IL-6 and NO.[97,98]

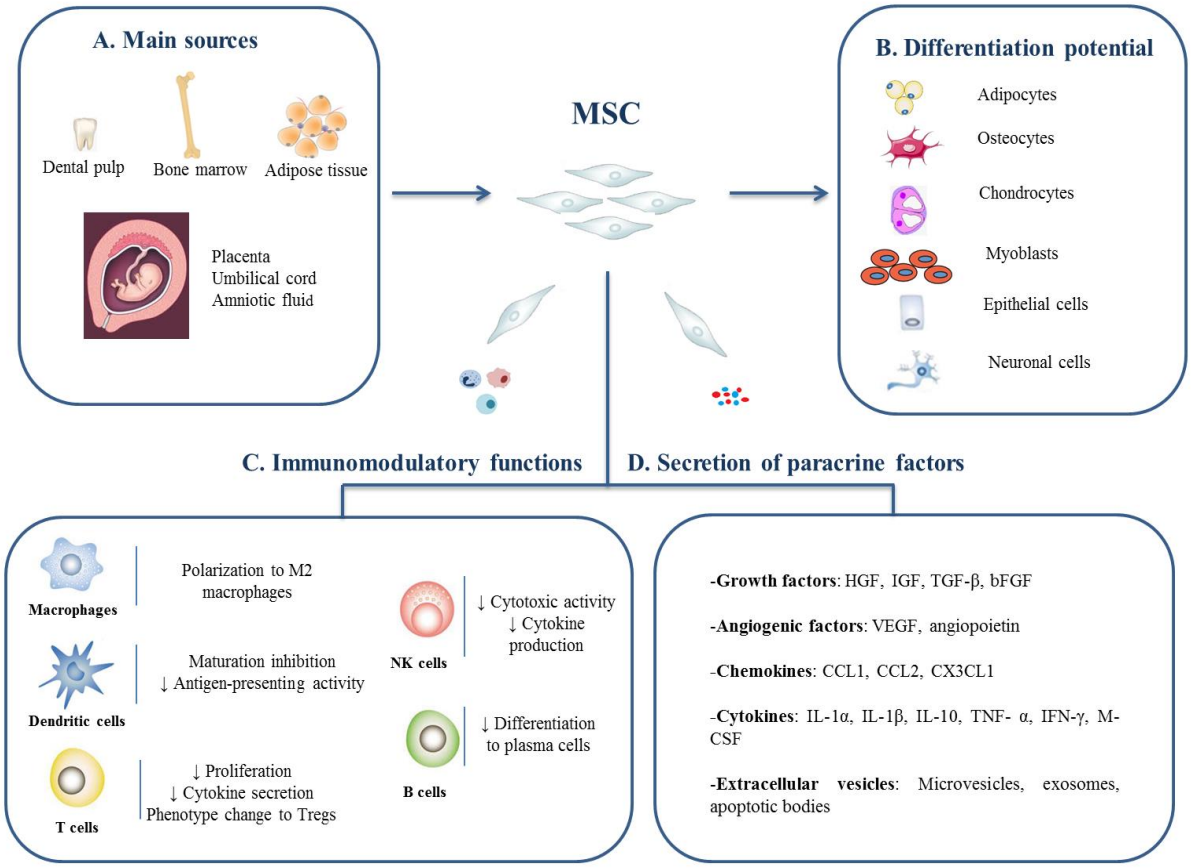

Figure 2: Mechanisms of action of MSC supporting their therapeutic potential. A. MSC are mesoderm-derived, fibroblast-like cells than can be isolated from adult or foetal sources. **B**. One of the mechanisms supporting MSC therapeutic capacities is their ability to differentiate into different cell types of mesoderm origin, *in vitro* and *in vivo*. **C.** Immunomodulation is one of the most widely studied properties attributed to MSC, as they can exert effects on all cell types of the immune system mainly by inhibiting their pro-inflammatory potential, and helping inflammation resolution. **D**. Secretion of paracrine factors is recognised as the main mechanism of action of MSC. These factors comprise the MSC secretome, constituted of different kind of proteins (growth factors, angiogenic factors, chemokines, cytokines) and extracellular vesicles, all of which have been shown to present anti-inflammatory, angiogenic and regenerative potential.

HGF: Hepatic growth factor; **IGF:** Insulin-like growth factor; **TGF-β**: Transforming growth factor beta; **bFGF**: Basic fibroblast growth factor; **VEGF**: Vascular endothelial growth factor; **M-CSF**: Macrophage colony stimulating factor.

1.3.2. Role in fibrosis, angiogenesis and apoptosis

MSC are also reported to reduce tissue fibrosis, not only by decreasing overall inflammation, but also by favouring ECM degradation through suppression of tissue inhibitor of metalloproteinase (TIMP) activity[99]. Furthermore, MSC treatment has been shown to reduce the expression of TGF-β1 and α-SMA in several pre-clinical models [100]. Some of these actions have been mediated by TNF-stimulated gene 6 (TSG-6), released by MSC when in co-culture with activated macrophages[101]. It seems that MSC also mediate anti-oxidative processes through secretion of soluble factors or exosomes[102,103].

The role of MSC in angiogenesis is known to be mediated by enhancement of different growth factors like VEGF, bFGF and HGF, but also by the action of MSC-derived extracellular vesicles (MSC-EV)[104,105].The secretion of growth factors seems to be also involved in their anti-apoptotic properties, together with the upregulation of anti-apoptotic molecules, like Bcl-2 and Bcl-xl[104].

All of these properties together, make MSC eligible candidates for cell based treatment of AKI or to prevent the progression to CKD. Because currently used immunosuppressive therapies in renal transplantation mostly include calcineurin inhibitors that by themselves have adverse effects for the kidney[85,106], the use of MSC in kidney transplantation may not only diminish allogeneic immune responses but also may help in establishing calcineurin inhibitor free or nearly free immunosuppressive regimens.

1.3.3. MSC secretome: conditioned media

In vivo studies using MSC have shown that intravenously injected MSC are preferentially trapped into the lung circulatory system and only a minor fraction of cells reach other organs, including secondary lymph nodes[107]. In addition to that, it has also been reported that MSC are no longer detectable 24-72 hours post-injection, even though a beneficial effect is observed [108]. In keeping with this, the question that needs to be addressed is how MSC exert their therapeutic activity if they don't reach the target organ? Some authors suggest that MSC can differentiate into glomerular mesangial cells and tubular epithelial cells,[109,110] whereas more recent studies suggest that the beneficial effects occur through secretion of autocrine and paracrine factors [111]. The latter explanation has been reported in at least 80% of preclinical studies, being the most accepted hypothesis on how MSC mediated therapeutic effects[112]. The paracrine factors are mostly referred as stem cell secretome, containing different types of proteins, mRNAs, miRNAs, antioxidants wrapped in extracellular vesicles. The cell culture that comprises this secretome is referred to as conditioned media (CM)[113].

Several preclinical studies have shown the efficacy and safety of MSC-derived CM (MSC-CM), even when used in xenogeneic combinations of stem cell donor and recipient. In a porcine model of myocardial infarction, human MSC-CM was able to reduce myocardial nuclear oxidative stress and decrease de phospho-Smad2 and active caspase 3, resulting in a 60% reduction of infarct size and enhancement of systolic and diastolic heart performance [114]. Also, in an antigen-induced arthritis model in mice, it was found that when treated with CM-MSC, CD4+T cells showed increased FOXP3 and IL-4 expression leading to decreased knee swelling and histopathological signs of cartilage loss[115]. Furthermore, ASC-CM has also been used in a mice ischaemic stroke model, ensuing reduction of infarct volume and brain swelling[116].

Additionally, the use of extracellular vesicles (EVs) derived from MSC (MSC-EVs) as a therapeutic strategy has gained relevance in the last few years. Depending on their origin and size, EVs can be classified as microvesicles, exosomes and apoptotic bodies. Microvesicles (100-1000 nm) originate from direct budding of the plasma membrane. They contain surface receptors and biologically active molecules like proteins and lipids as well as mRNA and miRNA. Exosomes (40-100nm) are secreted by multivesicular bodies and play an important role in immunomodulation and cell-to-cell communication. Apoptotic bodies (1-5µm) on the other hand, are released from the plasma membrane when cells undergo apoptosis and contain intracellular fragments, organelles and fragmented DNA; nevertheless, their specific role is not fully known[117].

EVs have been used in some preclinical studies with promising results. For instance, when used in a fully MHC mismatched transplantation model in rats, MSC-MV ameliorated outcome by reducing the number of NK cells and the expression of TNF-α[118]. Likewise, MSC-MV enhanced tubular cell proliferation, reduced apoptosis and leukocyte infiltration in an ischaemia-induced AKI model in rats. Interestingly, the protective effect was lost when RNase treatment was implemented; suggesting that miRNA transfer from MV to the injured cells is one of the mechanisms involved[119]. Thus, since MSC-CM and MSC-EVs use in preclinical models has been reported to show promising preliminary results, their use as a prospective replacement to MSC therapy seems feasible. Compared to the use of MSC, cell-free therapy presents several advantages, like cheaper production and lower immunogenicity and carcinogenic potential[113].

1.4. Aims of the thesis

Epidemiological studies have revealed that AKI is a risk factor for progression to CKD.[32,33] Murine models of AKI are mostly based on renal ischaemia, and are less susceptible to chronic renal function deterioration in long-term observation studies. The different models of ischaemia-induced AKI are controversially discussed, with no consensus as to whether chronic renal function deterioration is influenced by removal of the contralateral kidney at the time of ischaemia[46]. The main option for the treatment of patients with AKI remains the provision of supportive care and renal replacement therapy. Hence the lack of treatment modalities underscores the unmet need for better translational models for testing potential new treatment options.[120]

Stem cells, as well as stem cell secretome-based therapies have emerged as potential candidates for improving the clinical outcome of patients suffering from AKI. Nevertheless, their exact mechanisms of actions are not fully understood, emphasizing the need for animal models that more closely resemble the clinical sequel that underlies the progression to CKD. Since human MSC and ABCB5+ stromal cells are currently tested in clinical trials, these cells in particular should be tested in such models[121,122].

This study underlies the hypothesis that human MSC and MSC-CM can mitigate long-term renal function deterioration following AKI in rodent models. These models need to be sufficiently strong, displaying significant chronic histopathological changes in renal tissue.

To this end, the following questions are addressed:

1. Is a single severe episode of unilateral kidney ischaemia without contralateral nephrectomy able to induce sufficient long-term injury? What are the main histopathological features of this injury? Does it lead to long-term renal function impairment?

2. What is the difference in terms of long-term functional and morphological outcomes between removal and non-removal of the contralateral kidney at the time of ischaemic injury?

3. Can human adipose-derived MSC improve major structural and functional parameters in this model?

4. Can chronification of injury be increased by implementing cold ischaemia and minor MHC disparity? Is this reflected by GFR deterioration?

5. What is the influence of human ABCB5+ cells and its derived conditioned media on the major functional and histopathological features of this model?

2. Material and Methods

2.1. Experimental designs

2.1.1. Assessment of long-term renal outcomes in a model of ischaemia-induced acute kidney injury without contralateral nephrectomy

Acute kidney injury was induced by clamping the left renal pedicle of non-uninephrectomised Lewis rats for 60 minutes.

Prior to the beginning of the experiments, animals were randomly allocated in two different groups, as follows:

Group 1: *AKI Nx170 (n=6)*
AKI-induced animals, right nephrectomy at day 170 after injury
Group 2: *Control Nx170 (n=6)*
Non AKI-induced animals, right nephrectomy at day 170

The day of AKI induction surgery was considered day 0. One day before injury animals were placed into metabolic cages, to monitor their weight and to collect and quantify the urine produced in 24 hours. Thereafter, blood sampling was performed by retrobulbar plexus puncture, and the transcutaneous measurement of kidney function was also assessed. These procedures were repeated at day 1, 3, 150, 166 and 177 after AKI induction.

Animals in both groups underwent right nephrectomy at day 170. In the case of the control group, nephrectomy was performed taking as a reference the day that age-matched animals were AKI-induced. All animals were sacrificed 180 days after ischaemic injury (**Fig.3**)

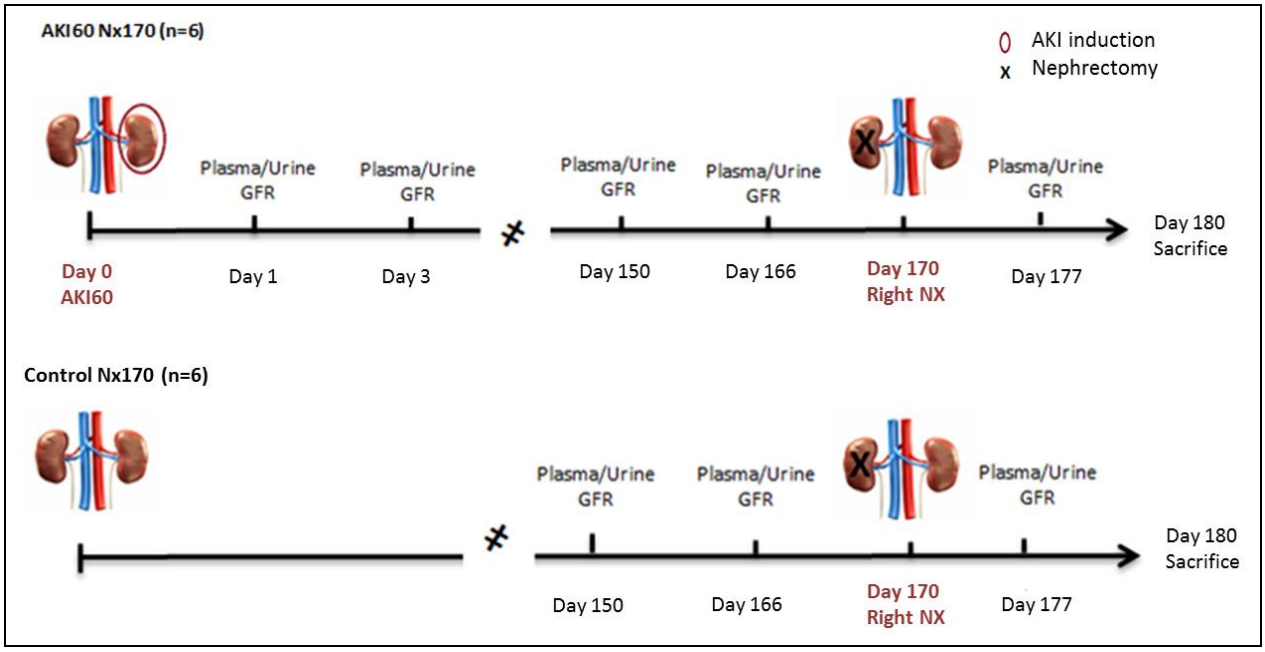

Fig.3: Experimental plan followed for the assessment of long-term renal outcomes in a model of unilateral kidney ischaemia without contralateral nephrectomy at the time of injury.

2.1.2. Assessment of long-term renal outcomes using two different models of ischaemia-induced acute kidney injury

Acute kidney injury was induced in Lewis rats that had been either uninephrectomised or not at the time of injury. Prior to the beginning of the experiments, animals were randomly allocated in different groups, as follows:

Group 1: *AKI Nx170 (n=6)*
AKI-induced animals, right nephrectomy at day 170 after injury
Group 2: *Control Nx170 (n=6)*
Non AKI-induced animals, right nephrectomy at day 170
Group 3: *AKI Nx0 (n=9)*
AKI-induced animals, right nephrectomy at the time of injury (day 0)

The same experimental plan as described in section 2.1.1 was followed, with the addition of one new group, as depicted in **Fig.4.**

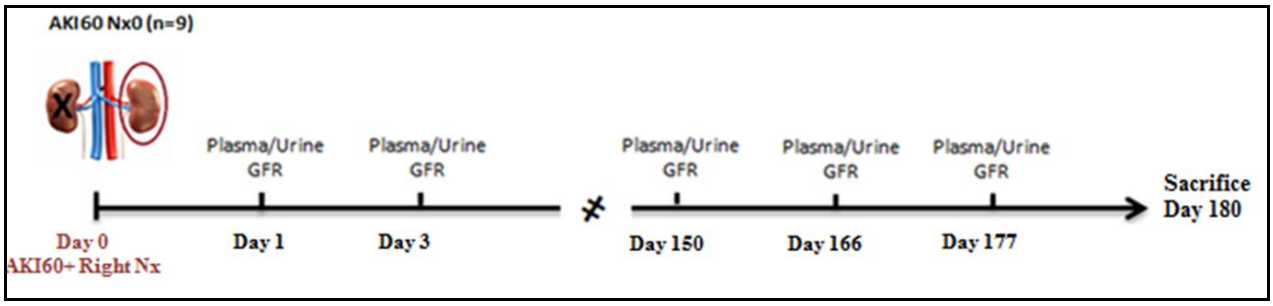

Fig.4: Experimental plan followed for the assessment of long-term renal outcomes in a model of unilateral kidney ischaemia with contralateral nephrectomy at the time of injury.

2.1.3. Assessment of the therapeutic efficacy of human adipose-derived mesenchymal stromal cells (hASC) in an ischaemia-induced AKI model

For this set of experiments, the same plan as described in section 2.1.1 was followed, with the addition of the treatment with $1x10^6$ of hASC or 500 µL of vehicle (NaCl, 0,9%) 14 days after AKI induction (**Fig.5**).

Animals were randomly assigned into different groups, as follows:

Group 1: *AKI Nx170 (n=6)*
AKI-induced animals, right nephrectomy at day 170 after injury
Group 2: *Control Nx170 (n=6)*
Non AKI-induced animals, right nephrectomy at day 170
Group 3: *AKI Nx170+hASC (n=10)*
AKI-induced animals, hASC-treated 14 days after AKI induction (IV)

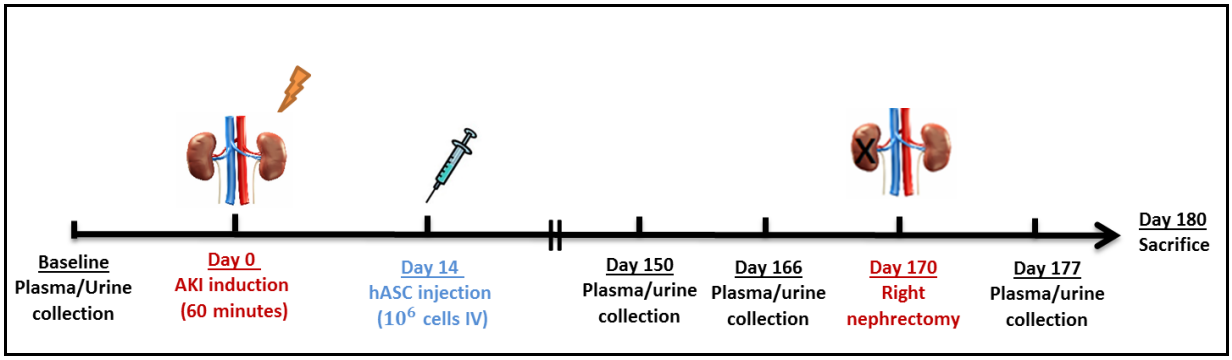

Fig.5: Experimental design followed to assess the efficacy of hASC in an ischaemia-induced AKI model without contralateral nephrectomy at the time of injury.

2.1.4. Assessment of therapeutic efficacy of human ABCB5+ cells and its derived CM in a chronic kidney allograft rejection model

In these experiments, the left kidney of Fischer 344 rats was explanted, in order to be implanted orthotopically 8 hours later, after cold storage, in an age-matched Lewis rat. Histidine-tryptophan-ketoglutarate-solution (HTK solution) was used for organ perfusion and as preservation solution during cold storage.

One day before transplantation, recipients were treated with either $1x10^6$ hABCB5+ cells or 500 µL of hABCB5-derived CM intravenously (tail vein). To assess the function of the transplanted graft, the right kidney of the recipients was removed 10 days after surgery. A second injection of either $1x10^6$ hABCB5+ cells or 500 µL of hABCB5-derived CM was performed 17 days after kidney transplantation.

Follow up of general condition, weight, and kidney function was assessed every two weeks by collecting plasma samples and urine, placing the animals in metabolic cages for 24 hours.

An end-point transcutaneous kidney function measurement was performed, one day before sacrifice, which took place 98 days after kidney transplantation (**Fig.6**).

Animals were randomly allocated in different groups, as follows:

Group 1: *KTx control (n=7)*
Transplanted animals, untreated
Group 2: *KTx+hABCB5 (n=7)*
Transplanted animals treated with hABCB5+ cells (IV)
Group 3: *KTx+CM- (n=5)*
Transplanted animals treated with hABCB5+ derived CM (IV)

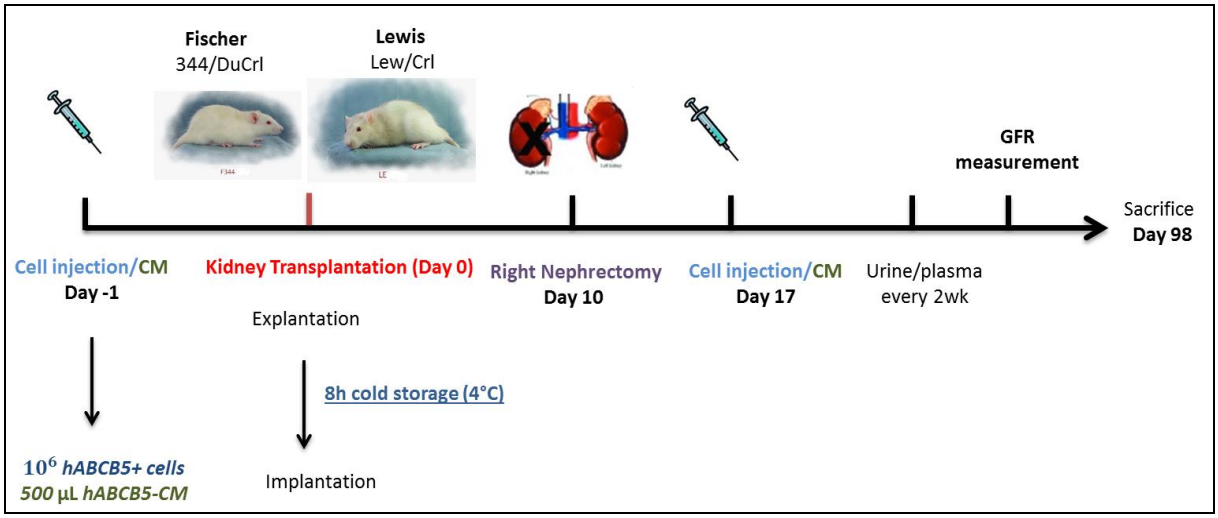

Fig. 6: Experimental design followed to study the efficacy of hABCB5+ cells and CM in a Fischer to Lewis chronic allograft rejection model.

2.2. Surgical methods

Every procedure was performed according to the Guide for Care and Use of Laboratory Animals published by the National Academy of Sciences and were approved by the local authorities (RP Karlsruhe AZ 35-9185.81/G-240/16 and AZ35-9185.81/G-153/14).

All the operations that will be described utilised micro surgical techniques. For that reason, a binocular cold-light microscope with 6-40x objectives was used (Leica MZ6, Leica Microsystems Wetzlar, Germany) as well as an anaesthetic vaporizer (SurgiVet®, Smith Medicals PM, Massachusetts, USA) for anaesthetic maintenance. The core temperature of the animals was kept at 37°C by placing them on a heating table (MEDAX GmbH Neumünster, Germany) during the whole duration of the procedures.

2.2.1. Warm ischaemia model (acute kidney injury induction)

Inbred male Lewis (LEW/Crl) rats weighing 200-250g were obtained from Charles River (Sulzfeld, Germany). Animals were kept in standard conditions and fed standard rodent food and tap water *ad libitum*.

To induce anaesthesia, animals were placed into a sliding-top induction chamber (Kent Scientific, Torrington, CT, USA) connected to the anaesthetic vaporizer, delivering isoflurane (CP-pharma, Burgdof, Germany) (3-4% 1L/min 0_2). Afterwards, a mixture of Ketamin (100 mg/mL; Ketamin® Wirtschaftsgenossenschaft deutscher Tierärtze eG, Garbsen, Germany) and xylazin (6 mg/mL; Serumwerk Bernburg, Bernburg, Gerrmany) was administered IP .To maintain anaesthesia, isoflurane was delivered to the animals (1,5-2% 1L/min 0_2) through a mask connected to the vaporizer.

Next, and after checking the onset of anaesthesia by toe pinch and corneal reflex, the hair from the abdomen was shaved and the skin disinfected (Softasept ®, B.Braun, Melsungen, Germany). To protect the cornea from drying, an eye ointment was used (Bepanthen®, Bayer GmbH, Leverkusen, Germany). Afterwards, 100 IU/animal of heparin (Heparin-Natrium-25000®, Rathiopharm ,Ulm, Germany) were injected into the caudal vein (tail vein) to avoid clot formation.

Then, a midline incision was performed, first on the skin, separating it from the subcutaneous tissue, and then through the *linea alba*, from the xiphoid process to the pelvis. To better visualize the left kidney, the caecum and the small intestine were placed to the right abdominal side with the help of metal retractors (**Fig.7**).

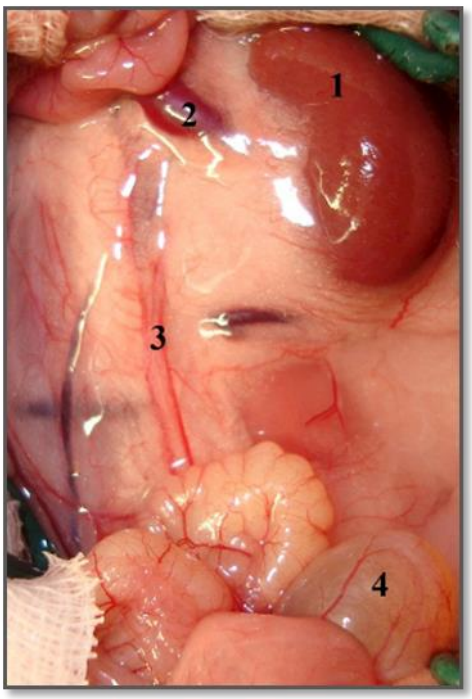

Fig.7: Overview of the abdomen of a rat after laparotomy. **1.** Left kidney, **2**. *V.renalis*, **3.** Left ureter, **4**.Urinary bladder

Once the left kidney was clearly visible and the renal artery and vein were accessible, two holes were open with the help of curved forceps (S&T Vessel Dilating Forceps angled 45°, Fine Science Tools, Heidelberg, Germany), one cranial to the renal artery and the other caudal to the renal vein. In these holes the atraumatic vascular clamps were placed, first the one occluding the renal artery (Micro Serrefines 4x 0,75 mm, Fine Science Tools, Heidelberg, Germany) and then the one obstructing the blood flow to the renal vein (Micro Serrefines 8x2mm,Fine Science Tools, Heidelberg, Germany). Success of the procedure was confirmed when the kidney turned from pale pink to dark purple due to the complete lack of blood circulation (**Fig.8**).

Ischaemia time was set to 60 minutes. In this period, the abdomen was covered with a damp swab to avoid dryness and the temperature of the animals was checked every 10 minutes. When the 60 minutes had passed, the clamps were released, first the venous clamp and then the arterial clamp. The kidney turned back to its physiological colour within a few seconds. To compensate for possible fluid loss, 2mL of NaCl 0,9% (Fresenius Kabi, Bad Homburg, Germany) were infused into the abdominal cavity. The abdominal wall and skin were closed using a continuous suture (3/0 Surgicryl PGA, SMI, Steinerberg, Belgium) and the wound was disinfected with Braunol® (B.Braun, Melsungen, Germany).

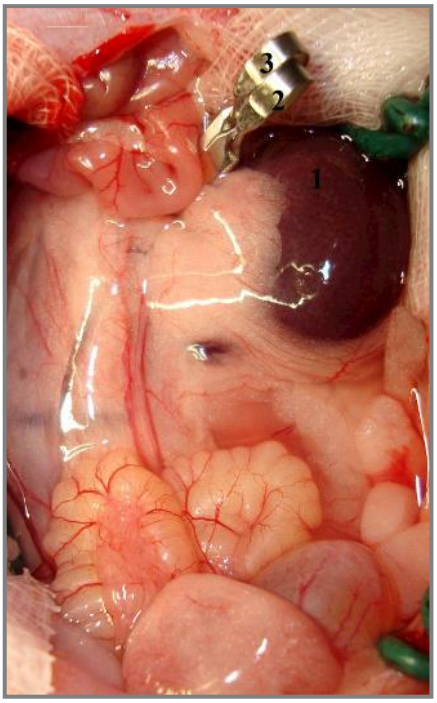

Fig.8: Overview of the operation field during warm ischaemia. **1**. Ischaemic left kidney, *2*. Venous clamp, **3.** Arterial clamp

Animals were then placed into a separate cage under a red light lamp to allow them to recover from the anaesthesia. To provide analgesia, 0,05mg/kg of buprenorphine hydrochloride (Buprenovet® Bayer GmbH, Leverkusen, Germany) was administered SC. Once animals were awake, they were placed into a separate cage with free access to food and water until the wound was completely closed.

2.2.2. Kidney transplantation

Male Fischer rats (F344/DuCrl) were used as donors and male Lewis rats (LEW/Crl) as recipients. All rats weighed around 200-250g and were obtained from Charles River (Sulzfeld, Germany). Animals were kept in standard conditions and fed standard rodent food and tap water *ad libitum*.

Anaesthesia was induced by placing the animals into a sliding-top induction chamber (Kent Scientific, Torrington, CT, USA) connected to the anaesthetic vaporizer, delivering isoflurane (CP-pharma, Burgdof, Germany) (3-4% 1L/min 0_2). To provide analgesia during the procedure, 0,05mg/kg of buprenorphine hydrochloride (Buprenovet® Bayer GmbH, Leverkusen, Germany) were administered SC. Once the onset of anaesthesia was ensured, animals were fixed on the heating table and isoflurane (1,5-2% 1L/min 0_2) was further delivered through a mask connected to the vaporizer.

Explantation of the kidney from the donor: Preparation of the animals and of the surgical field was the same as previously described. The display and name of the surgical instruments needed for this procedure are shown in **Fig.9.**

Left hand side

Electric cauteriser

Tissue forceps (1x2 teeth)

Pierse fixation forceps

Right hand side

Student Surgical Scissors (12,5 cm)

S&T Vessel dilating forceps angled 45°

Clamp holder: Micro-Serrefines clamp applicator with lock

Arterial clamp: Micro-serrefines 4x0,75 mm

Extra Fine Bonn Scissors (8,5cm)

Metal retractors

Fig. 9: List and display of surgical instruments used in the explantation procedure.

First, midline incision through the *linea alba* was performed from the xiphoid process to the pubis symphysis, having previously separated the skin from the subcutaneous tissue. Next, a damp swab was positioned on the thorax of the animals, and the intestines were carefully placed on top, wrapped into the damp swab, creating a package and making sure that the intestines were not subjected to torsion.

After that, and with the help of cotton buds (Rotilabo®, Carl Roth GmbH, Karlsruhe, Germany) the descending mesocolon was dissected, allowing the descending colon to be placed on the left side of the abdominal cavity. Using metal retractors (Bowman retractors, Fine Science Tools, Heidelberg, Germany) the operation field was made fully visible.

Afterwards, using cotton buds, the fat tissue covering the big abdominal vessels (abdominal aorta and vena cava caudalis) was carefully removed, and the left ureter was separated together with its surrounding fat. Next, the testicular veins were cauterised (ERBE cauteriser, Erbe Elektromedizin GmbH,Winsen, Germany) as well as the little vessels entering the vena cava caudalis approximately 1 cm cranially and 2 cm caudally of the left renal artery and vein (**Fig. 10A and 8B**).

Then, the adrenal vein was cauterised, as well as the fat tissue surrounding the left kidney, taking special care of preserving the integrity of the left ureter. After this step, the kidney was placed in the right abdomen and the vessels connecting the vena cava caudalis to the retroperitoneum were also cauterised and the remaining fat tissue removed, resulting in a complete separation of the aforementioned vessels.

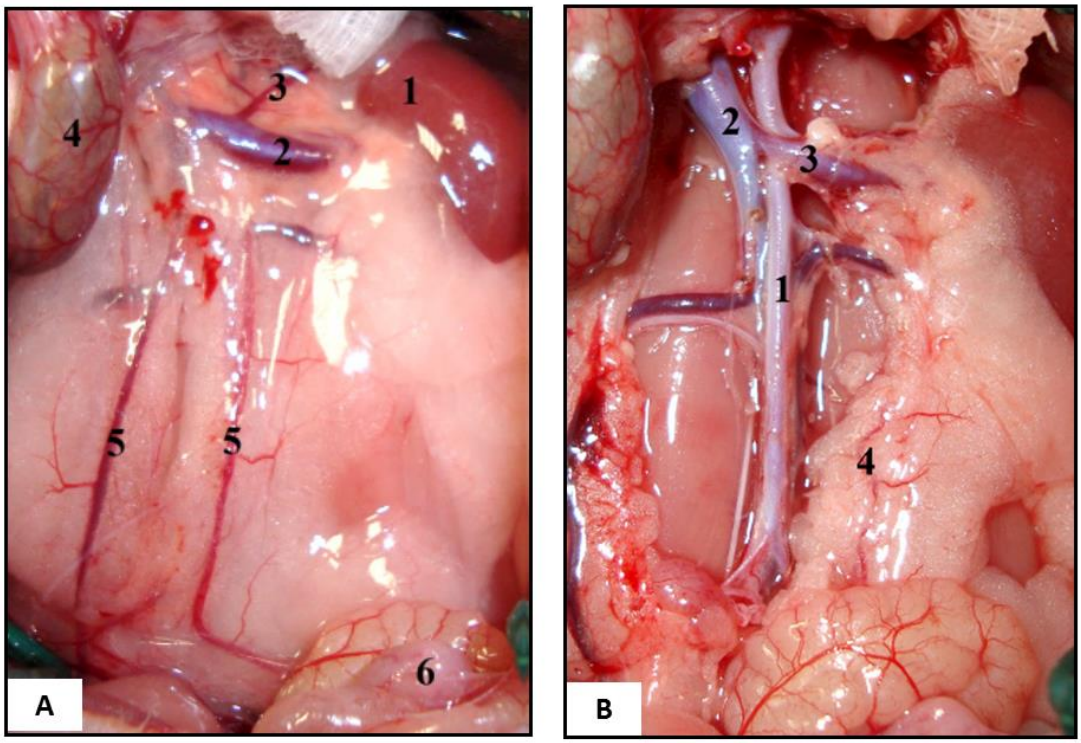

Fig. 10: **A.** Overview of the operation field after laparotomy. **1**. Left kidney, **2**. Renal vein, **3**.Adrenal vein, **4**.Descending colon, **5**. Testicular veins, **6**. Urinary bladder. **B.** Operation field after preparation of the big abdominal vessels. The abdominal aorta and the v.*cava caudalis* are fully separated and the venous patch completely cleaned. **1**. Abdominal aorta, **2**. V. *cava caudalis*, **3.** Renal vein, **4.** Left ureter in periureteral fat.

Of special importance was removing all the fat and connective tissue from the arch connecting the cava caudalis to the renal vein, as this constituted the venous patch for the venous anastomosis between donor and recipient. Once all the vessels were clean and the vena cava and the aorta were fully separated, the left ureter was cut, as caudally as possible, with its protective fat. Next, a double ligation was done around the vena cava and the aorta, approximately 2cm caudally to the renal artery (**Fig.11)**.

The next step had to be done in less than 30 seconds in order to avoid thrombotic complications. An atraumatic clamp was placed on the aorta, cranially to the renal artery, leaving enough space to dissect the vascular stump for arterial anastomosis. Right after, the venous patch was cut with sharp scissors using a glass spatula, pulling carefully to the left side, with a single movement.

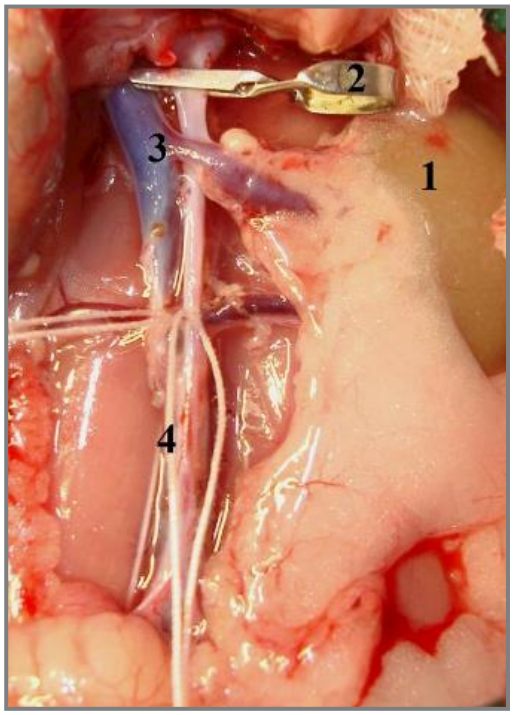

Fig.11: Operation field before kidney graft retrieval. **1.** Unperfused left kidney, **2.** Arterial clamp, **3.**Cutting point for the venous patch,**4.** Injection point for HTK solution.

For flushing, 1mL of HTK solution (Histidine-tryptophan-ketoglutarate solution, Custiodiol®, Dr.Franz Köhler Chemie GmbH, Bensheim, Germany) at 4°C was injected cranially to the ligation into the aorta, using a curved 27G needle. Well performed, flushing resulted in fast colour change of the kidney from pink to pale brown. Afterwards, the lower aorta was excised under the ligation and, lastly, the upper aorta was cut right below to the clamp. The kidney was then kept in HTK at 4°C for 8 hours.

The duration of this procedure was around 25-30 minutes.

Implantation of the kidney from the donor into the recipient was performed 8 hours after the kidney was collected from the donor. Animal preparation and laparotomy procedure was the same as for the explantation. The surgical instruments needed for this procedure as well as their setup, is shown in **Fig.12**.

The implantation step started with a left nephrectomy by decapsulation of the left kidney and hilar ligation of the renal artery and vein. Then, once the surgical field was completely clear, excess fat and connective tissue was removed from the surface of the abdominal aorta and *vena cava caudalis* (**Fig.13A**). Then, using forceps, the aorta and the cava were separated cranially and caudally of the recipients renal vessels in order to place clamps for anastomosis.

Using two threads, the abdominal aorta and *vena cava caudalis* were moved to the right side in order to better visualize the vessels from the back side. All these little vessels were cauterised, taking special care of not disturbing the muscular fascia underneath them.

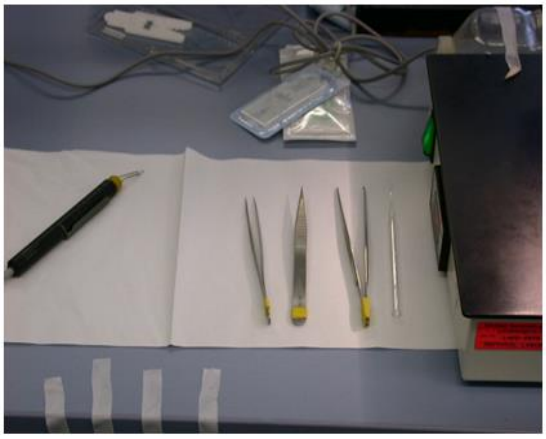

Left hand side
Electric cauteriser
Tissue forceps (1x2 teeth)
Pierse fixation forceps
Dumont SS forceps

Right hand side
Student Surgical Scissors (12,5 cm)
S&T Vessel dilating forceps angled 45°
Dumont vessel cannulation forceps
Clamp holder: Micro-Serrefines clamp applicator with lock
Arterial clamp (2x): Micro-serrefines 4x0,75 mm
Venous clamp (2x): Micro-serrefines 8x2mm
Extra Fine Bonn scissors (8,5cm)
Round handled needle holder

Fig.12: List and display of the surgical instruments and materials needed in the implantation procedure

Next, the arterial and venous clamps were placed following the direction of blood circulation: cranial arterial clamp, caudal arterial clamp, caudal venous clamp, cranial venous clamp **(Fig.13B).** Afterwards, aorta and vena cava were punctured using a 25G needle at the site of the latter anastomosis and dissected using microsurgery vascular scissors (Bone Cutting Spring Scissors, Fine Science Tools, Heidelberg, Germany). Thereafter, the vessels were thoroughly flushed with saline (NaCl 0,9%, Fresenius Kabi, Bad Homburg, Germany) until they were completely free of residual blood clots.

The following step was the ventral aortic anastomosis, where the aortic stump from the donor was sutured to the abdominal aorta of the recipient, using a 9/0 suture (Ethilon 9/0, Ethicon, Livingston, Scotland) and continuous stitches.

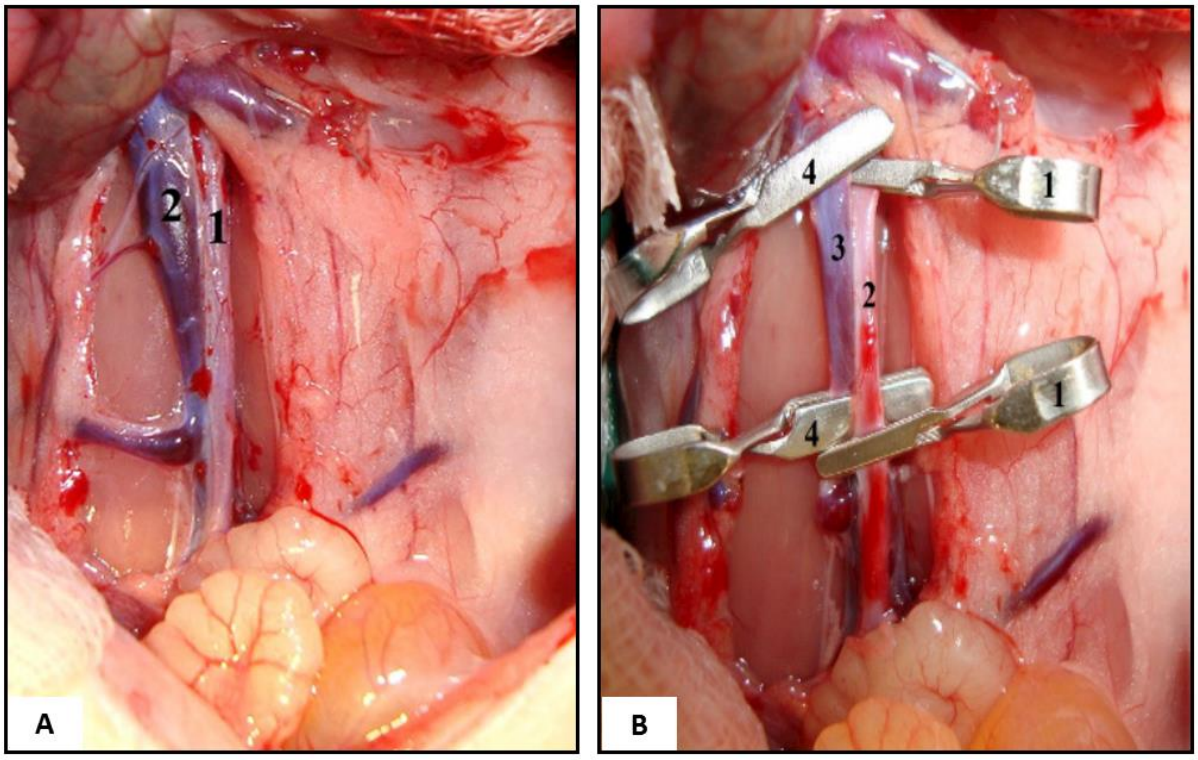

Fig.13: **A**. Overview of the operation field after left nephrectomy and preparation of the main vessels.**1.** Abdominal aorta, **2**. *V. cava caudalis***. B.** Operation field after positioning the clamps in clockwise direction: **1.** Arterial clamps, **2.** Abdominal aorta, **3**. *V.cava caudalis*, **4.** Venous clamps.

Afterwards, the ventral venous anastomosis was performed using a 9/0 suture (Ethilon 9/0, Ethicon, Livingston, Scotland) and continuous stitches. For that purpose, the venous patch (which has a funnel shape) had to be stretched from the sides, making sure that when the blood would enter later it would be sufficiently open. Then, the kidney was flipped to the right in order to stitch the dorsal anastomosis of the venous patch. Before knotting the anastomosis, the open venous system had to be flushed with saline thoroughly in order to make sure that there was no air in it. After completion of the dorsal arterial anastomosis, the arterial system was flushed and the caudal aortic stump of the donor kidney was ligated using a 3/0 non-absorbable suture (3/0 Polyester green, SMI, Steinerberg, Belgium)(**Fig.14**).

Once both anastomoses had been performed, the clamps were removed, this time in anti-clockwise direction. As a result, the kidney blood flow was established and turned back to its physiological colour. Then, the kidney was placed and fixed in the retroperitoneum by forming a pocket behind the retroperitoneal fat.

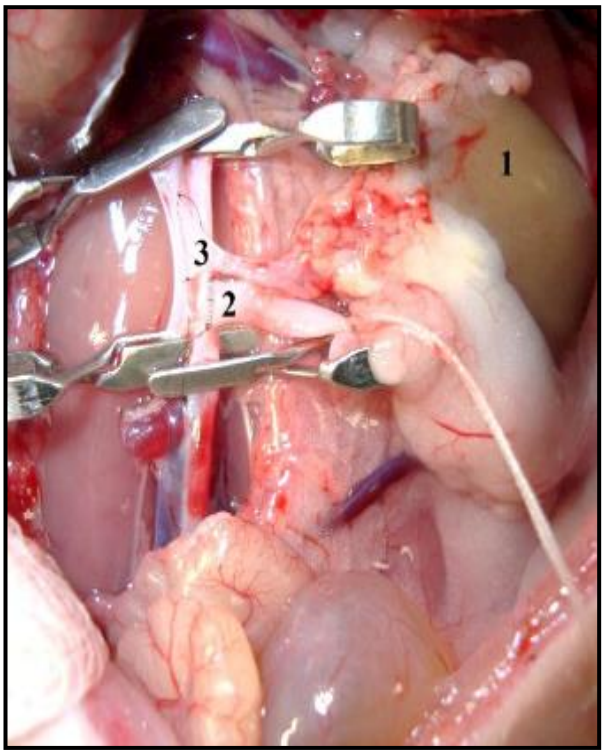

Fig.14: Operation field after aortic and venous anastomoses. **1**. Unperfused kidney graft, **2.** Aortic anastomosis,**3**. Venous anastomosis

The final step of this procedure is the insertion of the ureter into the urinary bladder. For this purpose, the ureter was carefully dissected at the very distal end and freed from surrounding fat, then it was cut diagonally and a ligation was performed using a 10/0 suture (Ethilon 10/0, Ethicon, Livingston, Scotland). Next, the peritoneal cover and vesical muscle were separated at the apex of the urinary bladder, without destroying the mucosa. In this area a puncture was performed with a 25G needle. Afterwards, the needle attached to the suture holding the distal end of the ureter was pulled through this mucosal hole and fixed within the bladder by knotting the suture to the ventral bladder wall. That way the ureter was inserted into the bladder without tension. Then, the periureteral fat tissue was stitched to the bladder with 4 single stitches using a 10/0 suture (Ethilon 10/0, Ethicon, Livingston, Scotland) (**Fig. 15A and 15 B**).

To compensate from possible fluid loss, 2mL of NaCl 0,9% (Fresenius Kabi, Bad Homburg, Germany) were flushed into the abdominal cavity ; then, the abdominal wall was closed by layers (3/0 Surgicryl PGA, SMI, Steinerberg, Belgium) and the wound was disinfected with Braunol® (B.Braun, Melsungen, Germany).

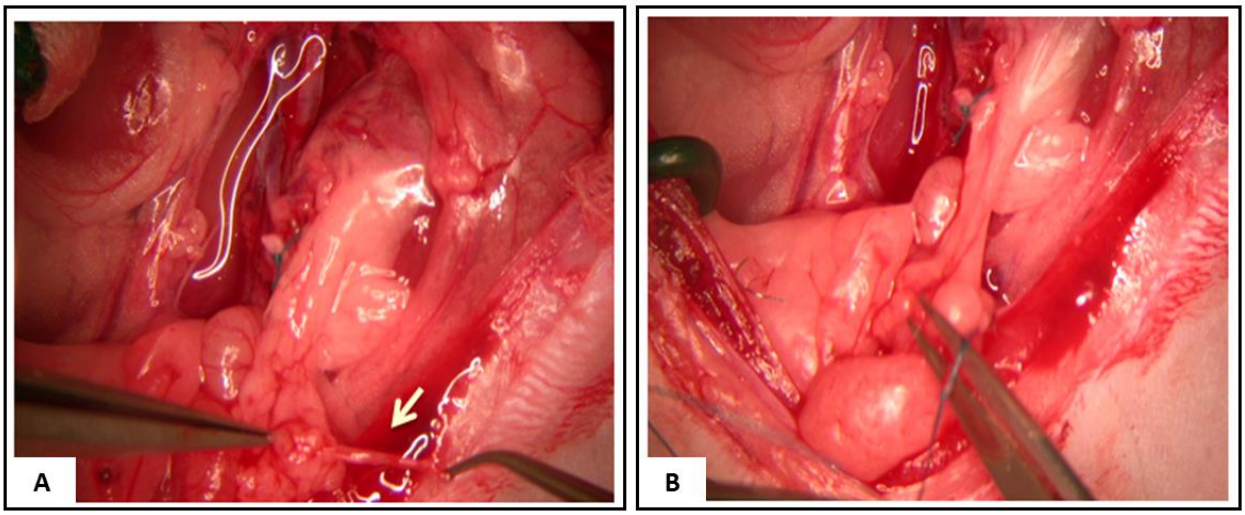

Fig.15: Ureter insertion into the bladder **A**. Ureter after removing removing periureteral fat. **B.** The ureter is inserted into the bladder with a 10/0 needle and suture

Lastly, animals were placed in a cage under a red light to help them recover from the anaesthesia.

The duration of the whole procedure was approximately 90 minutes[123].

2.3. Blood and urine collection and analysis

Blood samples were obtained through retrobulbar plexus puncture using haematocrit capillaries (Hirschmann GmbH & Co. KG, Eberstadt, Germany) and were put into EDTA-KE tubes (Sarstedt, Nümbrecht, Germany). Afterwards, samples were centrifuged to obtain plasma (Centrifuge 5415R, Eppendorf, Hamburg, Germany) for 15 min at 5000g and 4°C. Plasma samples were transferred into 1,5 mL Eppendorf tubes (Eppendorf, Hamburg, Germany) and stored at -20°C until analysis.

To obtain the urine samples, animals were placed into metabolic cages, with free access to food and water, for 24 hours. After this time, urine production was measured, samples were put into 1,5 mL Eppendorf tubes and kept at -20°C until analysis.

Routine plasma and urine parameters (***plasma***: creatinine, urea, sodium, potassium, calcium, total protein, cholesterol, triglycerides, phosphate and glucose; ***urine***: creatinine, urea, proteinuria, sodium, potassium, phosphate, calcium and glucose) were measured using a cobas c311 analyzer (Roche Diagnostics GmbH, Mannheim, Germany). Albumin content in urine was determined by ELISA and osmolarity was measured using an osmometer (2020 Multi-Sample Osmometer, Advanced Instruments Inc., Norwood, MA).

2.4. Transcutaneous assessment of renal function

FITC-sinistrin (Fluorescein isothiocynate, Fresenius Kabi, Linz, Austria) was the fluorescent dye chosen to measure kidney function. It constitutes a suitable candidate because it is highly soluble in water, and fully excreted by the kidneys[124]. To obtain the final concentration of 40mg/mL, 1g of dye was diluted in 25 mL of NaCl 0,9% (Fresenius Kabi, Bad Homburg, Germany) and injected intravenously in the animals through the tail vein .

The transcutaneous measurement was possible thanks to a small device attached to the back of the animals, constituted by two light-emitting diodes (LEDs), with an emission maximum for FITC-S at 470 nm and a photodiode detecting the fluorescence emitted with maximum sensitivity at 525 nm. The device was configured to perform a measurement every 1757 milliseconds. The recorded data was stored in the internal memory of the device, and using a micro-USB cable, it was transferred into a PC. The software used to read the data and to obtain the clearance curves was MPD studio (Medibeacon GmbH, Mannheim, Germany).

To perform the measurement, animals were placed into a sliding-top induction chamber (Kent Scientific, Torrington, CT, USA) connected to the anaesthetic vaporizer, delivering isoflurane (CP-pharma, Burgdof, Germany) (4-5% 1L/min 0_2). The induction chamber was at all times on top a heating table, set at 37°C (MEDAX GmbH Neumünster, Germany).

To make sure the signal was recorded correctly, animals were shaved from the scapula to the last rib, and the remaining hair was further removed using a shaving cream (Veet®, Reckitt Benckiser, Hull, United Kingdom). Afterwards, the device and its corresponding battery were attached into a double-sided adhesive patch (Lohmann GmbH&Co. KG, Neuwied, Germany), containing a small window where the LEDs were placed. Next, the patch was attached to the shaved back of the animals, and the battery was connected to the device, letting a background signal be measured for 4 minutes. The adhesive patch was further secured to the animal with an elastic net bandage (Askina 2A, Braun, Hessen, Germany) and a strip of adhesive tape. Then, FITC-S was injected into the tail vein (4-5 mg/100g BW) using an intravenous cannula (26G, Terumo Deutschland GmbH, Eschborn, Germany). Afterwards, animals recovered from anaesthesia and were placed into a separate cage, allowing free movement and free access to food, but not water for at least 2 hours, which is the minimum time for the measurement to take place in rats (**Fig 16**.).

When the FITC-sinistrin is injected intravenously, the fluorescent signal recorded by the device starts to rise until it reaches a peak. Hereafter, the signal decreases until completely fading, due to the excretion of the marker (**Fig.17**). Once the measurement was finished, the device was removed from the animal, and the battery disconnected.

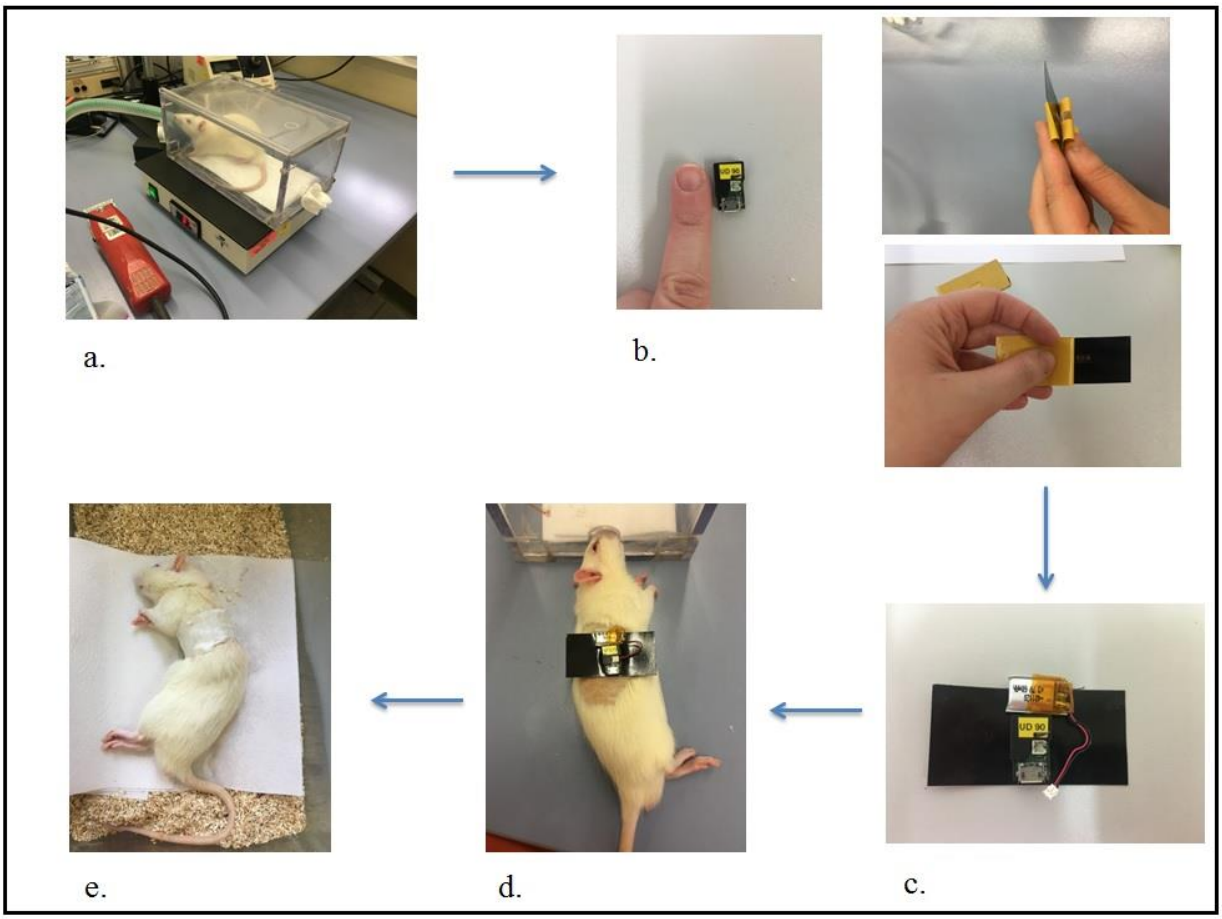

Fig.16: Transcutaneous measurement of renal function in conscious rats:

a) Animals were placed into a chamber to induce mild anaesthesia using isoflurane.

b) Device for transcutaneous measurement of renal function. Its optical part is composed by two LEDs on the side and one photodiode in the middle. It was placed into a double-sided adhesive patch with a small window to allow the signal to be recorded.

c) The lithium battery was attached to the patch, connected to the device and the background signal was measured.

d) The patch was fixed to the shaved back of the animal.

e) The device was secured with an elastic band and leukosilk, taking care of not over compressing the thorax.

The half- life (t½) of FITC-sinistrin was calculated by the software using a 3-compartment model. In a 3-compartment pharmacokinetic model, the system is divided into one central compartment and two peripheral compartments. Compartment one is constituted by plasma and tissues where the dye is distributed instantaneously, whereas peripheral compartments consist of tissues where the dye distribution is slower[125,126]. The use of the 3-compartment model allows fitting the clearance curve of animals with severely impaired kidney function, in contrast with the 1-compartment model, which fails to do so due to the lack of decay of the curve.

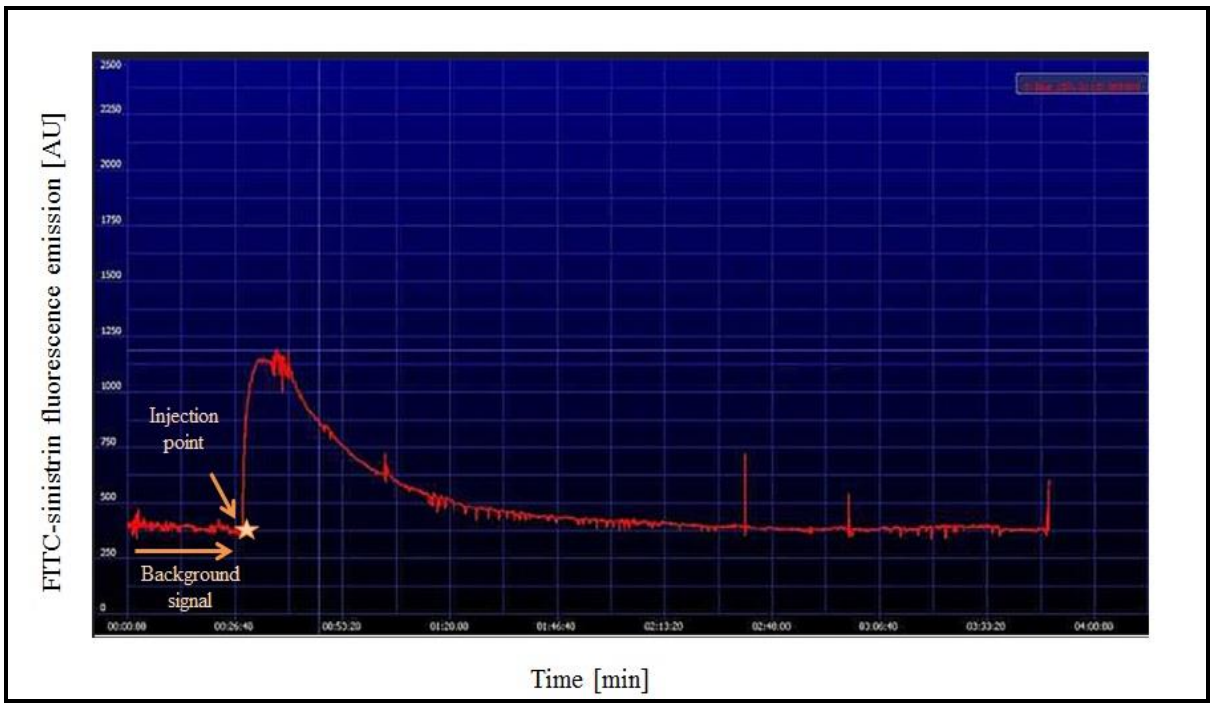

Fig.17: Excretion kinetics of FITC-sinistrin measured in a healthy rat [127]. Before the injection, the background signal was measured. After the intravenous injection of the dye, the signal increases until it reaches a peak, and then, due to the clearance of the marker, the signal decreases until complete excretion.

2.5. Cells and conditioned media

2.5.1 Human adipose-derived mesenchymal stromal cells (hASC)

hASC were isolated and cultured by Professor Karen Bieback´s group, from the Institute of Transfusion Medicine and Immunology (Medical Faculty Mannheim, Heidelberg University).

Cells were isolated from human lipoaspirates obtained from healthy donors who underwent liposuction surgery. First, the raw lipoaspirate was thoroughly washed with sterile PBS to remove cellular debris and red blood cells. Then, the washed aspirates were treated with 0,15% w/v collagenase type I (Sigma-Aldrich, Munich, Germany), for 45-60 min at 37°C, with gentle agitation, adding the same amount of collagenase as lipoaspirate volume (1:1 dilution). Inactivation of the collagenase was achieved by addition of an equal volume of DMEM/10% FBS (Thermo Fischer Scientific, Darmstadt, Germany) and was centrifuged (1200g, 10 min). The obtained stromal vascular fraction (SVF) pellet was resuspended in medium (DMEM low glucose, 10% FBS) and filtered through a 100µm nylon mesh filter (Falcon® 100 µm cell strainer, Sigma-Aldrich, Munich, Germany) to remove cellular debris. The filtrate was then centrifuged (1200g, 10 min) and resuspended in medium (DMEM+10% FBS) and plated in a T25 or T75 culture flasks (dependent of pellet size) and was incubated overnight at 37°C, 5% CO_2. On the following day, extensive washings were performed to remove non-adherent cells and red blood cells, prior to media change. Cell morphology was constantly monitored by microscope observation.

After cells had started to form colonies, they were tested to assess if the criteria for defining multipotent MSC was met. At passage 2 cells were seeded to assess *in vitro* differentiation into osteoblasts and adipocytes during a minimum of 14 days after which a differentiation assay was performed. Furthermore, an extensive cell marker panel was tested and measure by flow cytometry to assess the expression of CD90, CD73, CD105, and lack of expression of CD34 and HLA-DR.[84]

On the day the injections were scheduled, hASC were washed and suspended in PBS at a concentration of $1x10^7$/1mL.

2.5.2. Human ABCB5 positive mesenchymal stromal cells (hABCB5+)

ABCB5+ cells were obtained in collaboration with the company Ticeba-REHACELL GmbH&Co (Heidelberg, Germany).

Cell isolation, culture and characterization were performed in their facility as described by Tappenbeck *et al.* and Vander Beken *et al*[122,128].

Briefly, human ABCB5+ cells were obtained from healthy patients undergoing any medical intervention resulting in leftover skin tissue. Afterwards, skin tissue was separated from subcutaneous adipose tissue, disinfected, washed, dissected and enzymatically digested. Then, cells were centrifuged and expanded in stem cell-selecting growth media. ABCB5+ cells were isolated by antibody-coupled magnetic bead sorting, using a mouse-anti-human ABCB5 monoclonal antibody. Purity of the isolated cells was determined by flow cytometry. A content of 90% of ABCB5+ cells was set as optimal. After purity was checked, cells were cryo-preserved in liquid nitrogen.

The same day the injections were scheduled, cells were thawed, washed and suspended in HRG solution (Ringer´s lactate solution containing 2,5% human serum albumin and 0,4% glucose) at a concentration of $1x10^7$/1mL.

2.5.3.ABCB5-derived Conditioned media (CM)

Conditioned media was provided by Ticeba-REHACELL GmbH&Co (Heidelberg, Germany), according to their own manufacturing protocols. It was obtained by collecting the supernatant of the ABCB5+ cell culture.

2.6. Organ collection

At the day of right nephrectomy, the kidney was excised and weighed. Afterwards, the kidney poles were cut into small pieces with a disposable sterile scalpel (B.Braun, Melsungen, Germany), snap frozen in liquid nitrogen, and placed into CryoTube NUNC™ vials (Thermo Scientific, Schwerte, Germany). The frozen tissue was kept at -80°C.

The remaining organ was cut in half and kept in a 4% formalin solution for at least 24 hours. Afterwards, the tissue was processed with an automatic tissue processor (Leica

TP1020, Leica microsystems Nussloch GmbH, Nussloch, Germany) to be later embedded in paraffin.

The same procedure was performed at the sacrifice point, when the left kidney was collected. All animals were sacrificed by cutting the heart under isoflurane anaesthesia (5% 1L/min 0_2).

2.7. Histology methods

Once the tissue was processed and embedded in paraffin, it was cut (3µm thickness) using a rotary microtome (Richert-Jung Biocut 2030, Leica microsystems, Wetzlar, Germany) and left in an incubator at 37°C overnight.

2.7.1. Haematoxylin-eosin staining (H&E)

Haematoxylin-eosin is the most common staining technique used in histology for medical diagnosis. Haematoxylin is a deep blue-purple dye that stains nucleic acids and eosin, which has a pink colour, non-specifically stains proteins. Once the tissue was cut, the slides were placed into an autostainer (Leica ST5010 Autostainer XL, Leica microsystems Nussloch GmbH, Nussloch, Germany) and the staining was performed automatically, during the routine pathological staining.

2.7.2. Masson-Goldner staining

Masson-Goldner or Masson trichrome Goldner staining demonstrates the presence of connective tissue, which can be visualized by the combination of three different staining solutions: Azophloxine, Tungstophosphoric acid Orange G (muscle, cytoplasm and erythrocytes) and Light green SF (connective tissue counter-staining). Using this technique, the nuclei are stained in dark brown-black, cytoplasm and muscle appear in red and connective tissue acquires green colour.

The staining was performed by the Pathology department of the University Hospital in Mannheim, using an automated system during the routine pathological staining.

2.7.3. Periodic Acid-Schiff staining (PAS)

PAS staining shows mucins, basement membranes, glycogen and mycelial spores. When treated with periodic acid, glycols are oxidized to aldehydes. After reaction with Schiff reagent, the aldehydes show a purple-magenta colour. In this study, PAS staining was used to visualize glomerular basement membranes and tubular basement membranes, in order to assess glomerular and tubular abnormalities in transplanted kidneys. The staining was performed by the Pathology department of the University Hospital in Mannheim, using an automated system during the routine pathological staining.

2.8. Immune histology

2.8.1. ED1staining

ED1 is an antibody directed against the CD68 protein. It is used to identify macrophages, Kupffer cells, osteoclasts and monocytes. The ED1 antigen is expressed predominantly in the cell cytoplasm[129,130].

In the present study, ED1 staining was performed to quantify the macrophage/monocytes present in AKI and transplanted kidney sections and thus, the degree of inflammation in the different kidney compartments.

2.8.2. CD3 staining

CD3 consists of a protein complex composed by four different chains. It is involved in signal transduction to the T-cell after antigen recognition.

The CD3 antibody recognizes T-cells in thymus, bone marrow, peripheral lymphoid tissue and blood, and it also detects normal and neoplastic T-cells. It bounds to the membrane of all mature T-cells, and no other cell type, which makes it a very specific marker[131,132].

In the present study, CD3 staining was used to analyse the presence of T-cells in the kidney allografts, in order to assess T-cell mediated rejection between treated and untreated groups.

The following protocol was followed:

1. **Deparaffinization and hydration**:
   - Xylene (3x5 min)
   - Ethanol 100% (1min)
   - Ethanol 96% (1min)
   - Ethanol 80% (1min)

2. **Washing**: Tris Buffered Saline (TBS) (2x5min)

3. **Antigen retrieval**: Antigen retrieval reverses the protein modifications caused by fixation with formalin, optimizing the sntigen-antibody reaction. In this case, the antigen retrieval was produced using heat and a citrate buffer solution for **20 minutes**.
   - Citrate buffer (pH 6-6,3)
   - 10 min 800 Watts
   - 10 min 360 Watts

4. **Cooling and washing**: 20 min cooling at room temperature and washing in TBS

5. **Blocking of endogenous peroxidase**: H_2O_2 (2%) in methanol (**30 min.**)

6. **Washing**: TBS(2x5min)

7. **Blocking of unspecific background**:
   - **ED1**:Horse serum 10% (**20 min.** in humidified chamber)
   - **CD3**: Goat serum 10% (**20 min** in humidified chamber)

8. **Blocking of endogenous biotin**:
   - Incubation with Avidin (**15 min.**)
   - Incubation with Biotin (**15 min.**)

9. **Washing**: TBS (2x5 min)

10. **Incubation with first antibody**:
    - **ED1**: Mouse-anti-rat CD68 antibody (Linaris Biologische Produkte, Dossenheim, Germany) diluted 1:200 in 2% TBS/BSA (**Overnight, 4°C**)
    - **CD3**: Anti-CD3-antibody (Abcam, Berlin, Germany) diluted 1:400 in 1% goat serum (**Overnight, 4°C**)

11. **Washing:** TBS (2x5 min)

12. **Incubation with second antibody**:
    - **ED1**: Horse-anti-mouse antibody (Linaris Biologische Produkte, Dossenheim, Germany) diluted 1:200 in 2% TBS/BSA (**45 min.**)
    - **CD3**: Goat-anti-rabbit antibody (Linaris Biologische Produkte, Dossenheim, Germany) diluted 1:400 in 1% goat serum (**45min.**)

13. **Washing:** TBS (2x5 min)

14. **Incubation with avidin-biotin complex**: Incubation with ABC solution (Vector Laboratories, Burlingame, CA/USA) (30 min.)

15. **Washing:** TBS (2x5 min)

16. **Incubation with DAB solution**: DAB solution (Vector Laboratories, Burlingame, CA/USA) (**1-5 min.**)

17. **Counterstaining:** Haematoxylin (3-5 min)

18. **Dehydration**:
    - Ethanol 80% (rinse)
    - Ethanol 96% (rinse)
    - Ethanol 100% (2x1min)
    - Xylene (3x5 min)

2.9. Quantification of ED1 and CD3 positive cells

ED1+ and CD3+ cells were quantified using a light microscope (BX51TF, Olympus Germany GmbH, Hamburg, Germany) coupled to a camera (XC10, Olympus Germany GmbH, Hamburg, Germany) and the Cell F software (Cell F 5.2, Olympus Germany GmbH, Hamburg, Germany).

For ED1+ count, sections from both warm ischaemia models and hASC treated animals were taken into the analysis. Right (non-ischaemic) and left (ischaemic) kidneys were analysed, counting the positive cells in 20 fields each: 10 fields in the interstitium and 10 in the periglomerular region, using a 20x objective lens (Olympus Germany GmbH, Hamburg, Germany). Sections from all groups in the transplantation experiments were also analysed, counting the number of ED1+ cells in 10 random fields, using the same magnification.

The number of positive cells was calculated by the software (expressed in positive cells/μm^2 or in % of positive cells in the selected field), after optimal intensity was manually selected for each field.

For the CD3+ cell count, sections from transplanted kidneys (treated or untreated) were analysed. Ten random fields per section were chosen, and the positive cells were manually selected and counted using the 20x objective lens (Olympus Germany GmbH, Hamburg, Germany).

2.10. Quantification of kidney fibrosis

Kidney fibrosis was quantified in both warm ischaemia models, as well as in kidneys from hASC treated animals.

Kidney sections were stained using the Masson-Goldner protocol and scanned with the automated slide scanner Axioscan Z1 (Carl Zeiss, Oberkochen, Germany), obtaining digitalized high-resolution images of the cuts (40x magnification). The images produced were stored in an external high storage capacity drive for further analysis.

In these models, most of the fibrotic lesions are located between the cortico-medullary junctions and the outer cortex, and that constituted the areas of interest, which were manually selected using ImageJ software. Once the regions of interest were defined, their total area was quantified.

Next, the fibrotic areas (those stained positive for collagen I deposition, thus showing a green colour) were manually selected for each cut. Then, the total area of these fibrotic selections was also quantified by the software **(Fig.16 a and b).** The sum of all these areas was performed and a percentage of fibrosis in total kidney cortex was obtained.

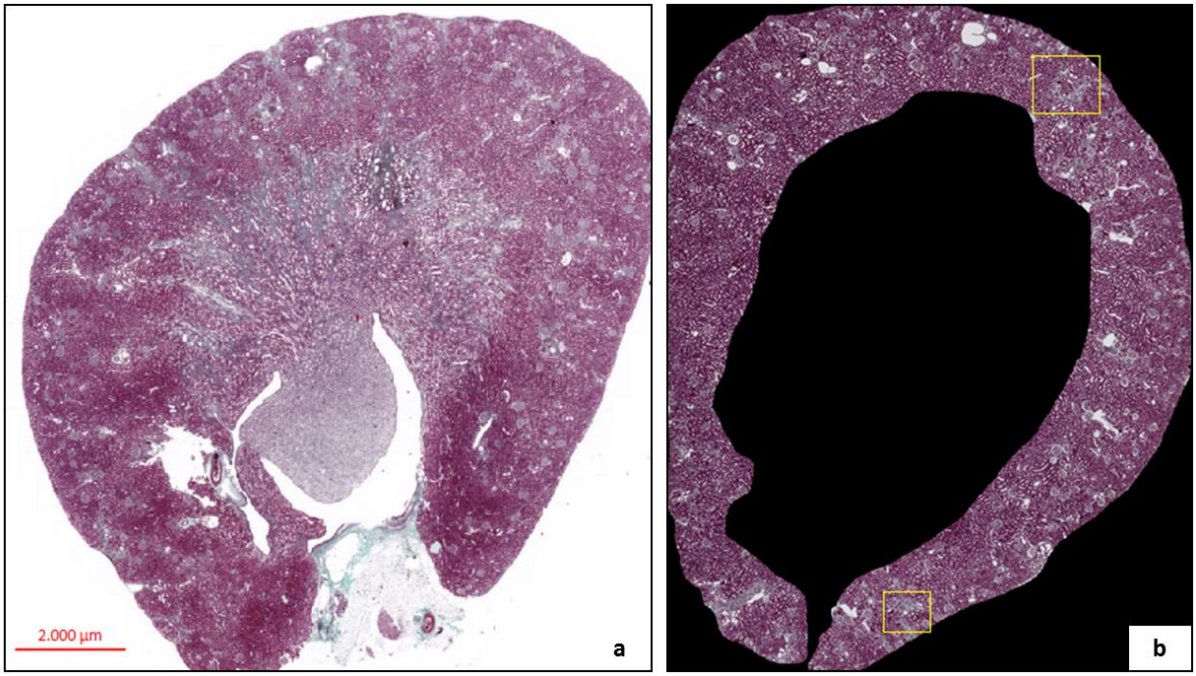

Fig.18: **a.** Kidney section scanned with Axioscan Z1 (40x objective lens). **b**. Region of interest (cortex) was selected and quantified. Fibrotic areas (yellow square) were manually selected and also quantified to obtain a percentage of fibrosis out of total cortex.

2. 11. Banff classification

The Banff classification was conceived in 1991 by a group of pathologists to develop an international scheme for standardization of criteria to diagnose renal allograft rejection, based on histologic analysis.

The original Banff classification was divided into different categories: hyperacute rejection, borderline changes, acute rejection, chronic transplant nephropathy and other changes. Acute rejection and chronic transplant nephropathy are, in turn, classified in three different grades according to severity. In acute rejection, the main focus is interstitial infiltration, tubulitis and intimal arteritis; whereas in chronic allograft nephropathy, the defining features are interstitial fibrosis and tubular atrophy[133].

The classification performed in the present study is a modification of the original Banff classification, following the criteria suggested by Roufosse *et al*. [134]:

Tubulitis	t0= No mononuclear cells in tubules or single focus of tubulitis only t1= Foci with 1 to 4 mononuclear cells/tubular cross section t2= Foci with 5 to 10 mononuclear cells/tubular cross section t3= Foci with >10 mononuclear cells/tubular cross section
Arteritis	**v0**—No arteritis. **v1**—Mild to moderate intimal arteritis in at least 1 arterial cross section. **v2**—Severe intimal arteritis with at least 25%luminal area lost in at least 1 arterial cross section **v3**—Transmural arteritis and/or arterial fibrinoid change and medial smooth muscle necrosis with lymphocytic infiltrate in vessel
Interstitial fibrosis	**ci0**—Interstitial fibrosis in up to 5% of cortical area. **ci1**—Interstitial fibrosis in 6 to 25% of cortical area (mild interstitial fibrosis). **ci2**—Interstitial fibrosis in 26 to 50% of cortical area (moderate interstitial fibrosis). **ci3**—Interstitial fibrosis in >50% of cortical area (severe interstitial fibrosis)
Tubular atrophy	**ct0**—No tubular atrophy. **ct1**—Tubular atrophy involving up to 25% of the area of cortical tubules. **ct2**—Tubular atrophy involving 26 to 50% of the area of cortical tubules. **ct3**—Tubular atrophy involving in >50% of the area of cortical tubules

2.12. Exclusion criteria

In both warm and cold ischaemia models a score sheet was used to determine the health status of all the animals in the experimental groups. Animals were checked every day for one week after surgery, and then every two weeks in order to assess the following criteria

Body weight (0-3)	**0.** No weight loss **1.** <10% weight loss **2.** 10-15% weight loss **3.** >20% weight loss
Breathing (0-3)	**0.** Normal **1.** Fast **2.** Superficial **3.** Dyspnoea
Faeces (0-3)	**0.** Normal **1.** Isolated soft faecal components **2.** Soft faeces **3.** Diarrhoea
General behaviour (0-3)	**0.** Normal **1.** Responsive **2.** Moderately irresponsive **3.** Non responsive, apathy, lethargy

Animals showing a score of three in one or more of the welfare criteria were euthanized and excluded from the statistical analysis.

2.13. Statistical analysis

The data are expressed as box plots. The middle line represents the median value of the respective parameter. The box delimitates the first (q1) and third (q3) quartiles of the data. Minimum and maximum values are depicted by the whiskers. One-way analysis of variance (ANOVA) followed by Tukey-Kramer test was used to evaluate differences between clinical chemistry parameters and histology-based quantitative parameters in all the groups through the different time points. In paired measurements following a parametric distribution, means were compared using a T-test. Survival analysis plots were generated according to Kaplan-Meier method. Statistical significance was defined when $p<0.05$. All the statistical analysis was performed using the software JMP® (JMP 14, SAS Institute, Cary, North Carolina, USA).

3. Results

3.1. Assessment of long-term renal outcomes in a model of unilateral kidney ischaemia without contralateral nephrectomy

3.1.1. Clinical parameters

To assess if ischaemia-induced acute kidney injury without contralateral nephrectomy leads to long-term kidney function impairment, baseline plasma creatinine (p-crea) and plasma urea (p-urea) were first measured. The left kidney was then subjected to 60 minutes of ischaemia (see materials and methods) and the right non ischaemic kidney was removed 170 days after AKI induction. Animals in which the left kidney was not subjected to ischaemia and the right kidney was also removed at day 170 served as controls. P-crea and p-urea were measured at days 150, 166 and 177. Although p-crea was significantly higher in the ischaemic group at days 150 (0,25 ± 0,02 vs. 0,3 ± 0,02 mg/dL, Control vs. AKI; *p*=0,0055;) and 160 (Control: 0,28 ± 0,02 vs. 0,31 ± 0,03mg/dL; Control vs. AKI ; *p*=0,0479), the values were within a physiologic range reported for this strain (p-Crea >0,5mg/dL; Biochemistry and haematology for Lewis rat colonies in North America, https://www.criver.com/products-services/find-model/lewis-rat). At day 177, i.e. 7 days after removal of the non-ischaemic kidney, the mean p-Crea value in the AKI group was compatible with a mild kidney function impairment and significantly higher than that of the controls (0,38 ± 0,02 vs. 0,66 ± 0,29 mg/dL, Control vs. AKI; *p*=0,0341) (**Fig.19A**). P-urea values showed a similar pattern as observed for p-crea. Statistical significant differences between the control and AKI group were achieved at days 166 (31,38 ± 1,9 vs. 35,38 ± 2,8 mg/dL, Control vs. AKI; *p*=0,012) and 177 (45,6 ±4,89 vs. 77,9 ± 37,55 mg/dL, Control vs. AKI; *p*=0,0446)(**Fig.19B**).

Like p-crea and p-urea, also proteinuria was increased in the AKI as compared to the control group. Significance between both groups was reached at day 150 (14,45 ± 2,52 vs. 27,91 ± 14,51 mg/24h, Control vs. AKI *p*=0,0362) and at day 177 (16,492 ± 3,78 vs. 33,11 ±15,29 mg/24h, Control vs. AKI *p*=0,0139)(**Fig.19C).**

FITC-S clearance was used to assess impairment of glomerular filtration rate. No difference in half-life time ($t_{1/2}$) of FITC-S between the control and AKI groups were found at days 150 (27,42 ± 3,2 vs. 28,8 ± 4,7 min, control vs. AKI) and 166 (23,75 ± 4,1 vs. 28,1 ± 6,4 min, control vs. AKI). Importantly, none of the values were in a pathological range (i.e. $t_{1/2}$> 40min[126]) at these time-points. In contrast, 7 days after removal of the non-ischaemic kidney a significant difference between the control and AKI group was observe reaching pathological levels (27,7 ± 5,9 vs. 61,91 ± 31,38 min, Control vs. AKI *p*=0,0244) (**Fig.20).**

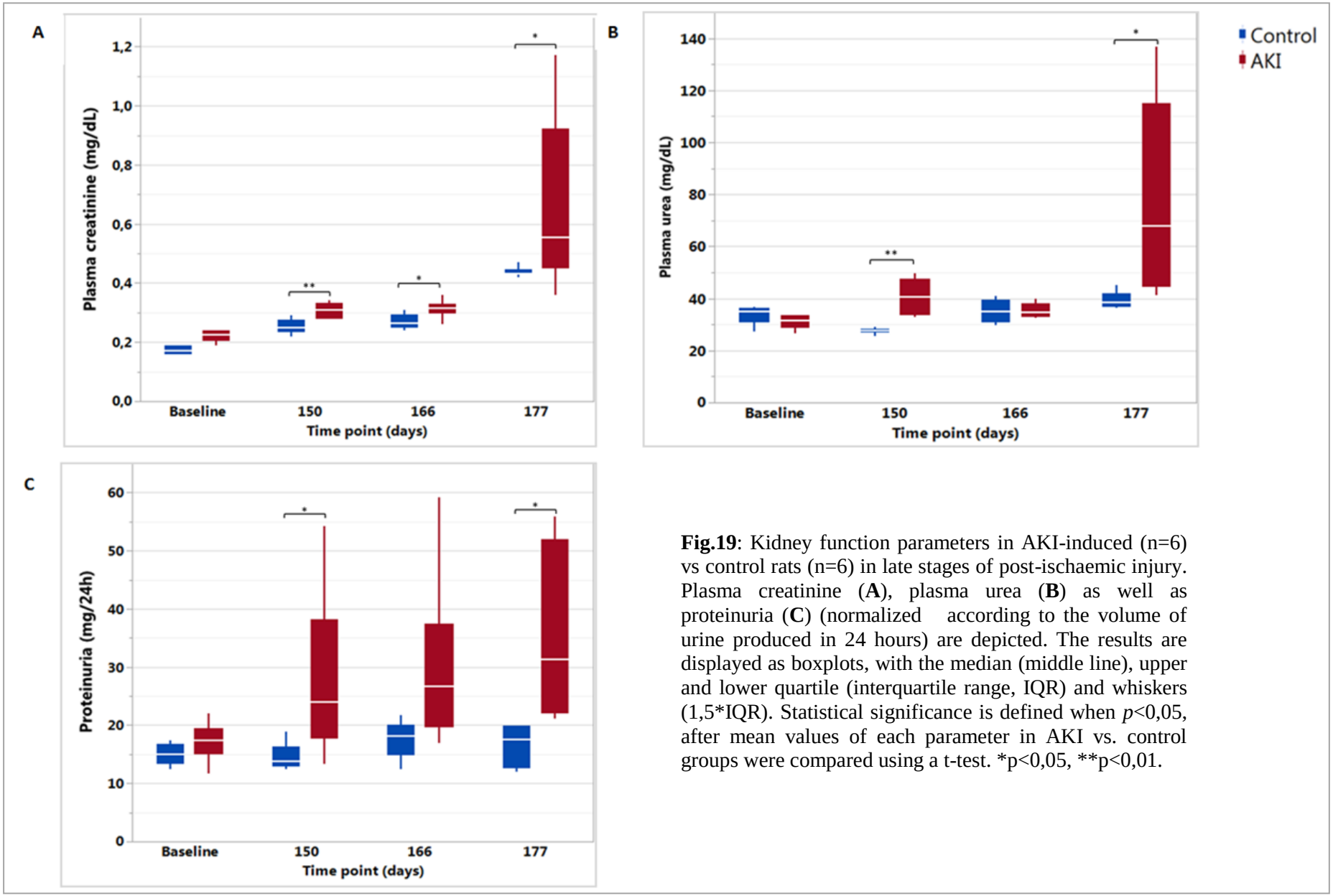

Fig.19: Kidney function parameters in AKI-induced (n=6) vs control rats (n=6) in late stages of post-ischaemic injury. Plasma creatinine (**A**), plasma urea (**B**) as well as proteinuria (**C**) (normalized according to the volume of urine produced in 24 hours) are depicted. The results are displayed as boxplots, with the median (middle line), upper and lower quartile (interquartile range, IQR) and whiskers (1,5*IQR). Statistical significance is defined when $p<0,05$, after mean values of each parameter in AKI vs. control groups were compared using a t-test. *p<0,05, **p<0,01.

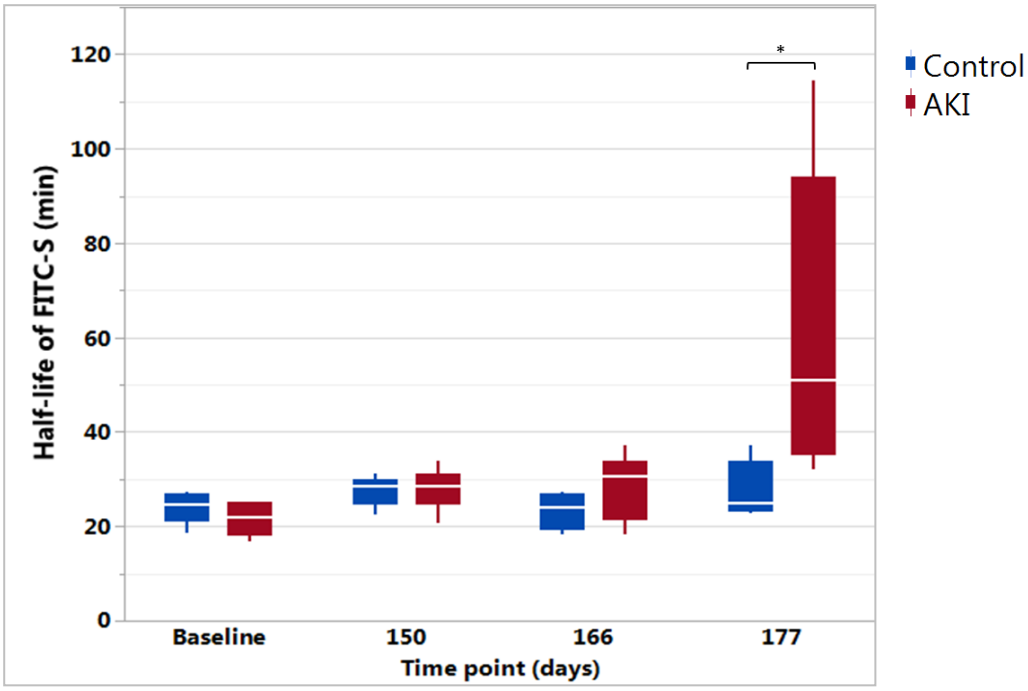

Fig.20: Half-life for FITC-S clearance in AKI-induced (n=6) vs. control group (n=6) remained similar in both groups until the contralateral kidney was removed in the AKI group, when a pathological increase in the $t_{1/2}$ of FITC-S was observed. The results are displayed as boxplots, with the median (middle line), upper and lower quartile (interquartile range, IQR) and whiskers (1,5*IQR). Significance between groups was assessed by comparing the means of this parameter in both groups using a t-test and indicated as:*p<0,05.

As a summary, values of the main kidney function parameters assessed throughout the experimental period are shown in **Table 1**.

Table 1: Kidney function parameters assessed, namely: p-crea (mg/dL), p-urea (mg/dL), proteinuria (mg/24h) and $t_{1/2}$ FITC-S (min), in control (n=6) and AKI groups (n=6), expressed as mean ± SD. Values shown in red are within the pathologic range for the Lewis strain. Statistical significance between AKI vs. control group was defined when p<0,05, by means of t-test. (*ns*: not statistically significant)

	Baseline			Day 150			Day 166			Day 177		
	Control	**AKI**	***p* value**	**Control**	**AKI**	***p* value**	**Control**	**AKI**	***p* value**	**Control**	**AKI**	***p* value**
P-crea	0,15±0,02	0,22±0,01	*ns*	0,27±0,02	0,3±0,02	0,005	0,27±0,03	0,31±0,03	0,04	0,38±0,02	**0,66±0,29**	0,03
P-urea	33,7±3,6	31±2,7	*ns*	27,5±1,2	40,6±7	0,002	31,4±3,6	35,4±2,9	*ns*	45,6±4,9	**77,9±37,5**	0,026
Proteinuria	15±1,8	17,2±3,4	*ns*	14,4±2,5	**27,9±14,5**	0,362	17,6±3,3	**30±15,2**	*ns*	16,5±3,7	**35,4±15,3**	0,013
$t_{1/2}$ FITC-S	24,1±3,4	21,5±3,6	*ns*	27,4±3,2	27,9±4,4	*ns*	23,3±4,2	28,2±7,1	*ns*	27,7±5,9	**61,9±32,4**	0,024

3.1.2. Macroscopic and histological changes

In order to assess how ischaemic injury affects kidney morphology macroscopically, both post-ischaemic and non-ischaemic kidneys were weighed. The weight of the non-ischaemic kidneys in the AKI-induced animals was significantly higher than the non-ischaemic kidney of the control animals (0,39 ± 0,04 vs. 0,58 ± 0,08 g/100g BW, Control vs. AKI p=0,0001). In contrast, the weight of the left (ischaemic) kidneys in the AKI group was significantly lower than the left (non-ischaemic) kidneys in the control group (0,5 ± 0,027 vs. 0,35 ± 0,03g/100g BW, control vs. AKI; *p*<0,001) (**Fig.21A**). In all cases the post-ischaemic kidneys showed an irregular and wrinkly surface and in about 33% of the animals a dramatic decrease in kidney size was evident. Furthermore, cyst formation occurred in 50% of the animals in the AKI group and was only observed in the left ischaemic - but not in the right non-ischaemic kidney (**Fig. 21B)**.

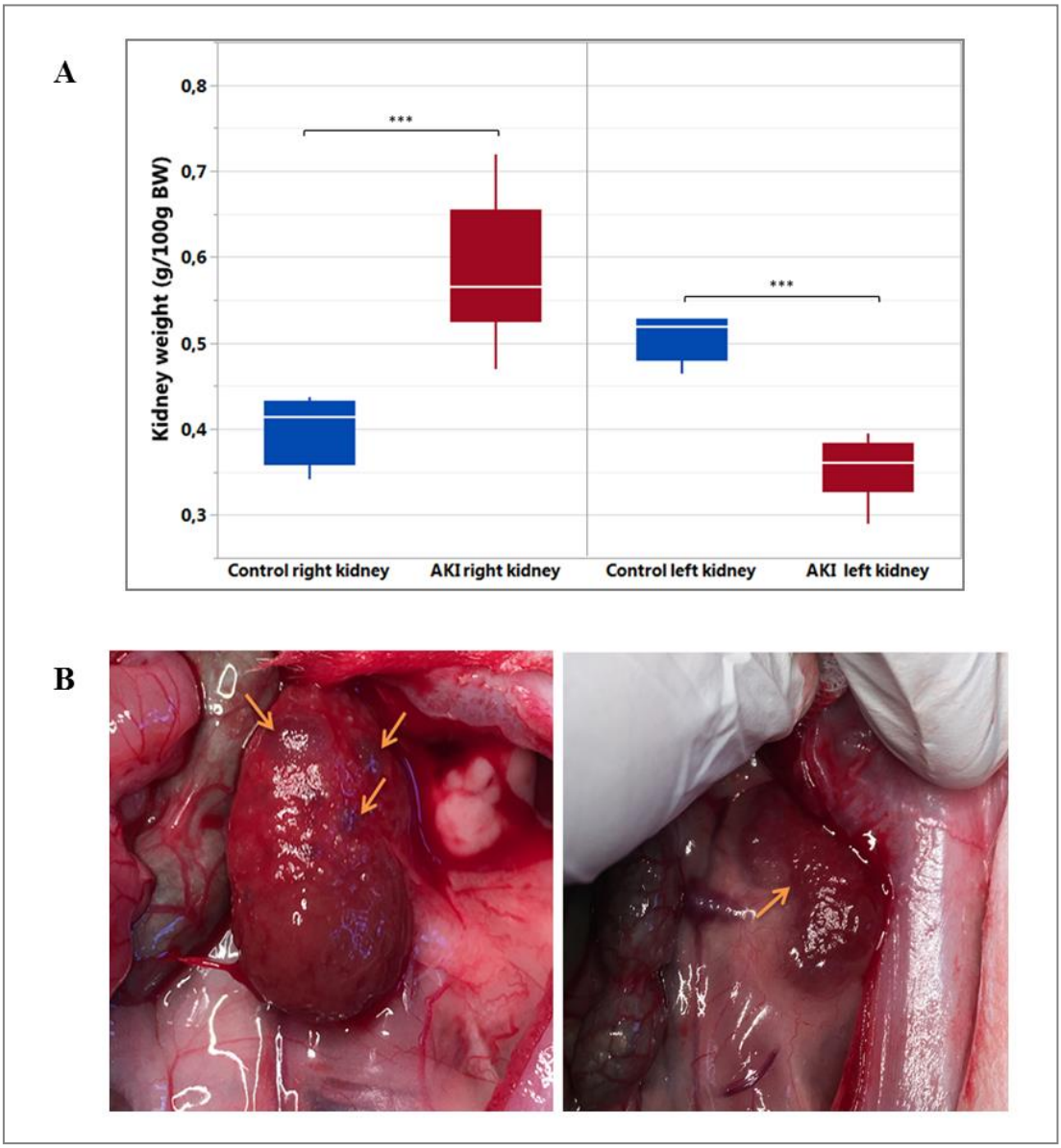

Fig.21: Macroscopic changes in the ischaemic and non-ischaemic contralateral kidney. (**A)** The right non-ischaemic kidneys in both groups as well as the left ischaemic kidney and left non ischaemic kidney

in the AKI (n=6) and control (n=6) group respectively were weighed. The results are displayed as boxplots, with the median (middle line), upper and lower quartile (interquartile range, IQR) and whiskers (1,5*IQR). Statistical significance is defined when $p<0,05$, after means in AKI vs. control groups were compared using a t-test. *$p<0,05$, **$p<0,01$, ***$p<0,001$. **(B)** Macroscopic findings in the post-ischaemic kidneys in the AKI-group. Several cysts of different sizes (arrows) are visible throughout the kidney surface (picture to the left). Severe size reduction and wrinkling together with the presence of cysts in one of the poles (picture to the right)

Microscopic analysis was next performed using light microscopy (general histology, haematoxylin-eosin (HE) staining), immune histology (for macrophage infiltration using ED1 antibody) and Masson-Goldner staining (fibrosis).

Haematoxylin-eosin staining in the post-ischaemic kidneys revealed lesions typically seen after ischaemic injury mostly gathered in the outer cortex. These include tubular dilations and tubular atrophy with foci of interstitial infiltration (**Fig 22 A and B)**. Although cyst formation is not a classic histopathological feature of ischaemic injury, but rather of progressive renal failure, renal histology confirmed cyst formation (**Fig.22 C**).

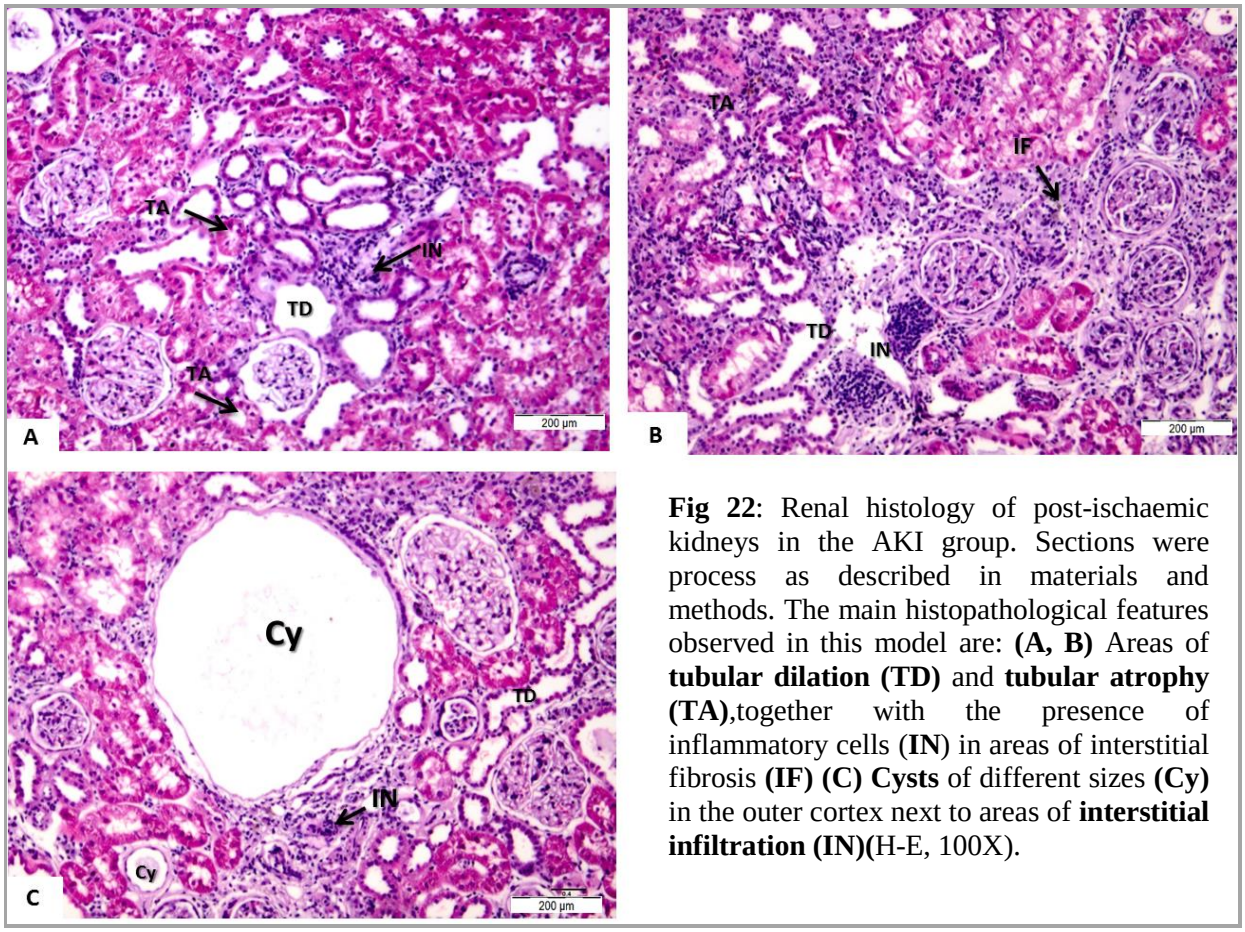

Fig 22: Renal histology of post-ischaemic kidneys in the AKI group. Sections were process as described in materials and methods. The main histopathological features observed in this model are: **(A, B)** Areas of **tubular dilation (TD)** and **tubular atrophy (TA)**,together with the presence of inflammatory cells (**IN**) in areas of interstitial fibrosis **(IF) (C) Cysts** of different sizes **(Cy)** in the outer cortex next to areas of **interstitial infiltration (IN)(**H-E, 100X).

Although the right non –ischaemic kidneys in the AKI group presented with a significantly increased weight, no signs of histo-morphologic abnormalities or signs of ongoing inflammation or scarring were observed (**Fig. 23 A and B**). Renal histology of these animals was comparable to that of the right non-ischaemic kidney in the control group (**Fig. 23 C and D**).

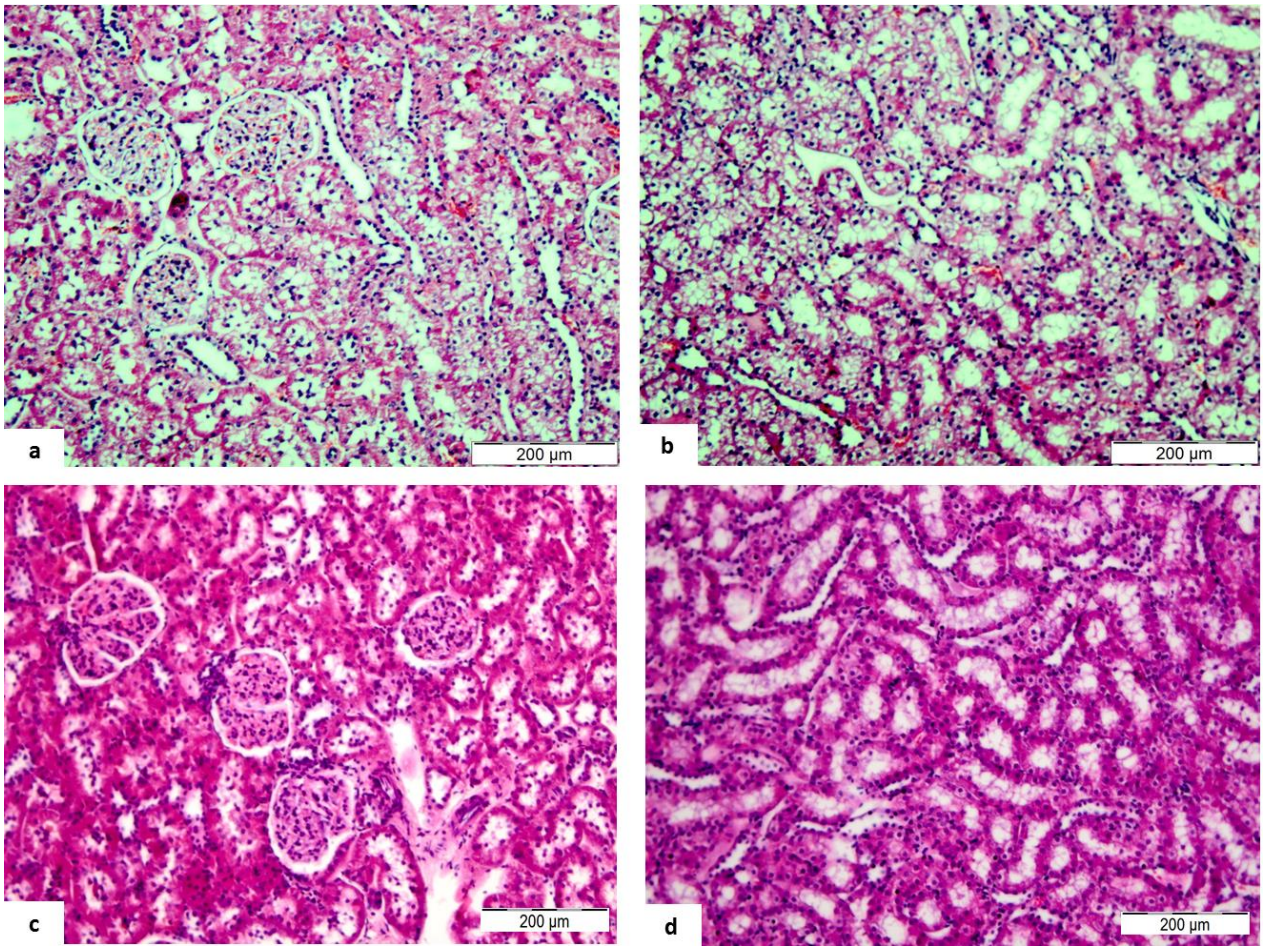

Fig.23: (A, B) Sections of non-ischaemic kidneys of AKI-induced animals show no glomerular or tubular abnormalities 180 days after AKI induction. (**C, D)** Similar findings are observed in the kidneys of control animals, where the normal renal architecture is preserved. (H-E, 100X)

Immune histology using ED1 antibody was performed to assess the degree of macrophage infiltration. The post-ischaemic kidneys showed significantly increased numbers of ED1+ macrophages compared to the control group (162,38 ± 47,39 vs. 7105 ± 4940,45 cells/µm² control vs. AKI; *p*= 0,0092) (**Fig. 24A**). ED1+ cells were found most predominantly in the outer cortex and cortico-medullary junction, in areas of extensive interstitial fibrosis (**Fig. 24 B and E**), as well as in areas of tubular atrophy (**Fig. 24C**) and dilation (**Fig. 24D**).

ED1+ macrophages were seldom in sections of the right non-ischaemic kidneys from the control or AKI animals (data not shown).

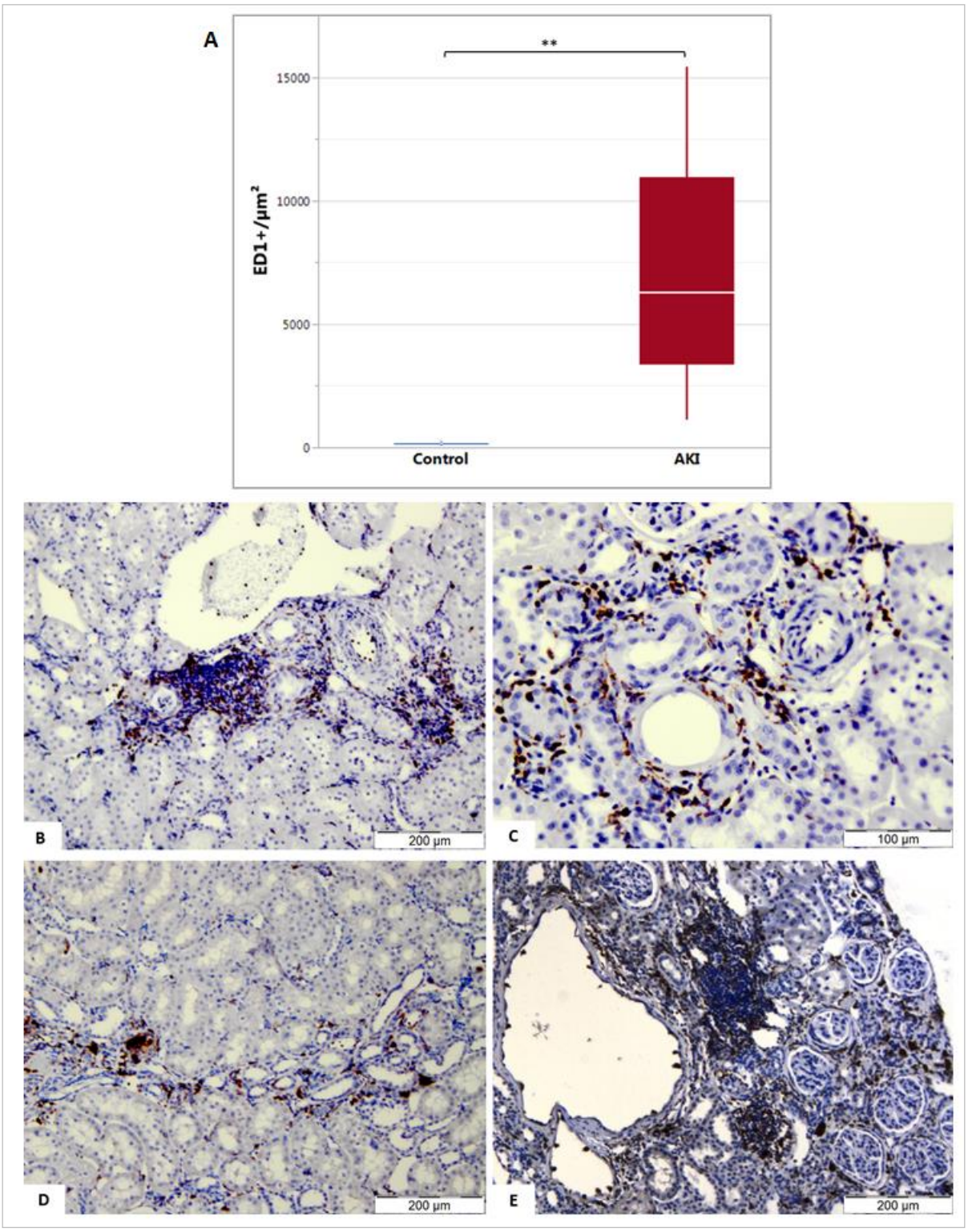

Fig.24 (A): AKI induction leads to a significant increase in ED1+ cells in the post-ischaemic kidney (AKI, n=6), compared to control group (n=6). The results are expressed in box plots. Statistical significance is defined when $p<0{,}05$, after mean values in AKI vs. control groups were compared

using a t-test. *p<0,05, **p<0,01, ***p<0,001. (**B)** Macrophage infiltrate in areas of interstitial fibrosis (ED1, 100X), **(C)** ED1+ cells surrounding atrophic tubules (ED1, 200X), **(D)** ED1+ cells in areas of tubular dilation (ED1, 100X), **(E)** Large ED1+ infiltrate in an area of severe interstitial fibrosis (ED1, 100X).

Masson-Goldner staining was used for the assessment of kidney fibrosis, a characteristic of progressive chronic kidney disease. Post- ischaemic kidneys in the AKI group showed areas of interstitial fibrosis scattered mostly through the outer cortex (**Fig.25 A**). Interstitial fibrosis was accompanied by tubular atrophy, characterized by thickening of the basement membrane causing reduction of the tubular lumen. This feature, together with the presence of hyaline casts evidenced tubular injury (**Fig.25B**). Moreover, some of the AKI-induced animals presented different sized cysts surrounded by large amounts of connective tissue and atrophic tubules (**Fig. 25C**). Glomerular abnormalities, e.g. enlargement of the Bowman space, were also observed in the animals displaying the severest degrees of tissue fibrosis (**Fig. 25D**). Kidney fibrosis was quantified on the basis of connective tissue deposition in the renal cortex as described in section 2.10. The percentage of connective tissue deposition in the AKI group was significantly higher than in the control group, where the presence of pathologic deposition of connective tissue was almost non-existent (0,02 ± 0,008 vs. 0,37 ± 0,19%; control vs. AKI ; p=0,003) (**Fig.26**).

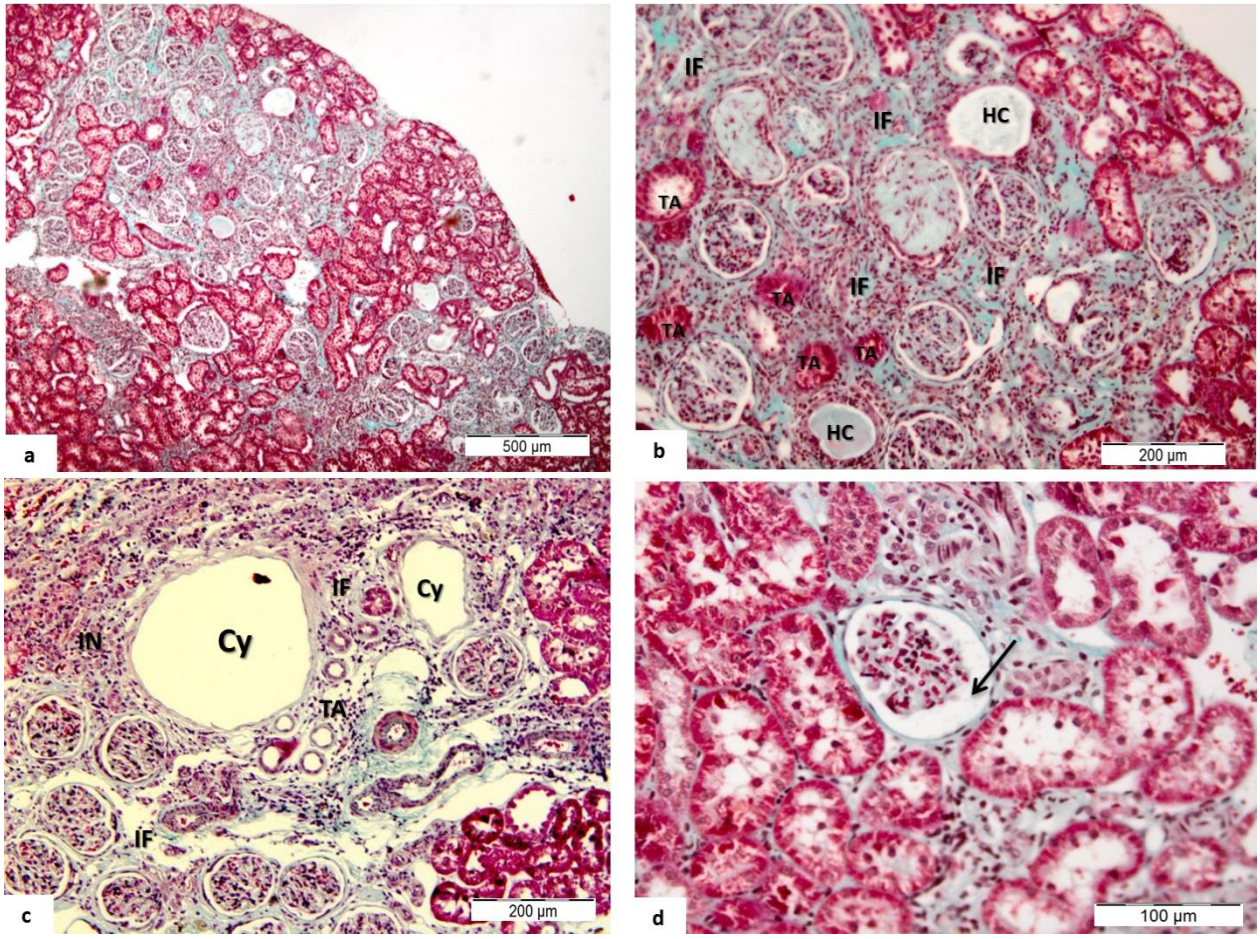

Fig.25: Masson-Goldner staining demonstrates the presence of connective tissue (green) in the post-ischaemic kidneys of AKI-induced animals: **(A)** Areas of interstitial fibrosis are scattered through the outer cortex (M-G, 40X), **(B)** Severe degree of interstitial fibrosis (IF) is observed accompanied with tubular atrophy (TA) and hyaline casts (HC)(M-G, 100X), **(C)** Cysts of different sizes (Cy) are observed in the outer cortex, surrounded by areas of interstitial fibrosis and tubular atrophy (M-G, 100X), **(D)** Glomerular abnormalities like enlargement of the Bowman space (arrow) due the presence of fibrotic tissue surrounding the glomerulus (M-G, 200X)

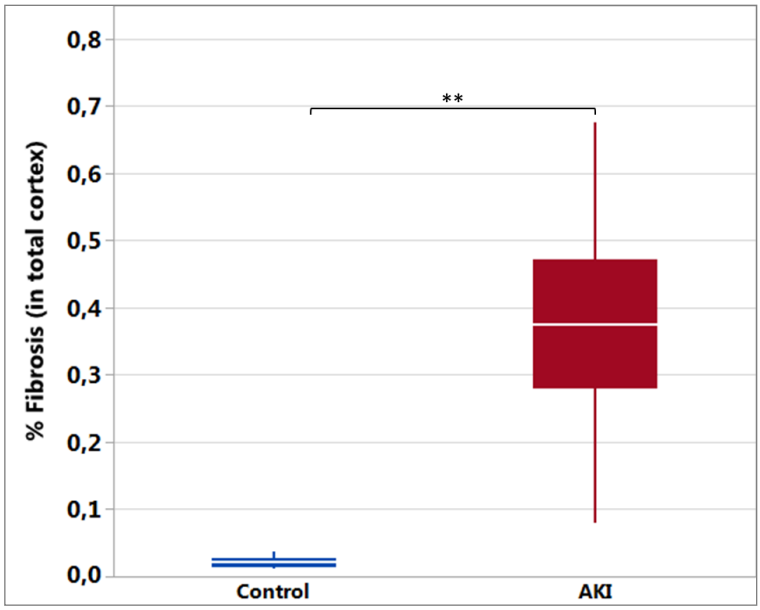

Fig.26: AKI-induced animals (n=6) show significantly higher percentage of fibrosis in the cortex of the post-ischaemic kidney compared to control animals (n=6) when assessed 180 days after initial injury. The results are displayed as boxplots, with the median (middle line), upper and lower quartile (interquartile range, IQR) and whiskers (1,5*IQR). Statistical significance is defined when $p<0,05$, after mean values of this parameter in AKI vs. control groups were compared using a t-test. *$p<0,05$, **$p<0,01$, ***$p<0,001$

3.2. Assessment of long-term renal outcomes using two different models of ischaemia-induced acute kidney injury

3.2.1. Clinical parameters

Changes in the acute phase: To better understand the long-term effects of ischaemia induced AKI on kidney function, we first assessed kidney function in the acute phase in two models of AKI. To this end, plasma creatinine and plasma urea were determined before, and 1 and 3 days after the onset of AKI. Two groups of rats were studied, i.e. rats in which the contralateral kidney was removed immediately after AKI induction (AKI Nx0) and rats in which the contralateral kidney was maintained until day 170 (AKI Nx170).

One day after AKI-induction, animals in the AKI Nx0 group displayed a significant rise in p-crea as compared to animals in the AKI Nx170 group (2,7 ± 0,37 vs. 0,41 ± 0,05 mg/dL AKI Nx0 vs. AKI Nx170; p<0,001). Three days after the onset of AKI p-crea remained in a pathologic range in animals of the former group, while p-crea of animals in the AKI Nx170 was still in a normal range (2,89 ±1,39 vs. 0,34 ± 0,03 mg/dL, AKI Nx0 vs. AKI Nx170; p=0,0003) (**Fig.27A**). Similar as observed for p-crea, p-urea increased only in animals of the AKI Nx0 group (at day 1: 248,62 ± 22,37 vs. 40,31 ± 5,6 mg/dL, AKI Nx0 vs. AKI Nx170; p<0,001; at day 3: 407,02 ± 148,08 vs. 45,81 ± 5,46 mg/dL, AKI Nx0 vs. AKI Nx170; p<0,001))(**Fig.27B**) Hence, only animals of the AKI Nx0 group displayed severe kidney function impairment in the acute phase. This was in line with an increased $t_{1/2}$ for FITC-S clearance in these animals (at day 1: 682,87 ± 528,72 vs. 31,78 ± 12,95 min, AKI Nx0 vs. AKI Nx170; p=0,019; at day 3: 189,69 ± 172,26 vs. 34,68 ± 7,26 min, AKI Nx0 vs. AKI Nx170; p=0,019)(**Fig.27C**). Renal function parameters in the AKI Nx0 group returned to baseline values 7 days after AKI induction in 85% of the animals. Due to the severity of this model, 15% mortality was observed in the AKI Nx0 group. In contrast, in the AKI Nx170 group animals showed no kidney function deterioration at any of the time points tested in the acute phase, and, accordingly 100% survival was found.

Changes in the chronic phase: At later stages, p-crea increased to a similar degree in both ischaemic groups and at all points was slightly higher compared to the no-AKI controls. Except for day 150 in the AKI Nx0 the differences did not reach statistical significance. Since in the AKI Nx170 group the contralateral non-ischaemic kidney was not removed until day 170, kidney function deterioration of the ischaemic kidney could not be assessed. One week after removal of the contralateral kidney p-crea increased to pathological levels and was significantly higher compared to the AKI Nx0 and control groups. (0,66 ± 0,29 vs. 0,35 ±0,04 mg/dL, AKI Nx170 vs. AKI Nx0; p=0,0084) (**Fig.28A**). Likewise p-urea increased much stronger in the AKI Nx170 group at day 177 (77,9 ± 37,55 vs. 49,47 ± 8,97 mg/dL, AKI Nx170 vs. AKI Nx0, p=0,05), albeit that significant differences between the control group were also found for the AKI Nx0 group at earlier time-points (day 150: 47,7 ± 8,67 vs. 34,84 ±3,09 mg/dL, AKI Nx0 vs. Control, p=0,013; day 166: 46,52 ±7,18 vs. 31,38 ± 1,96 mg/dL, AKI Nx0 vs. Control, p=0,0002)(**Fig.28B**). At early time-points the $t_{1/2}$ of FITC-S clearance was significantly increased only in the AKI Nx0 group (day 150: 44,46 ± 10,07 vs. 27,42 ±3,27 min., AKI Nx0 vs. Control; p=0,0019; day 166: 41,1 ±7,16 vs. 23,37 ± 4,16 min, AKI Nx0 vs. Control, p=0,0018), while in the AKI Nx170 group significance was only reached one week after removal of the contralateral kidney (61,91 ± 32,3 vs. 27,78 ± 5,99 min, AKI Nx170 vs. Control, p=0,024) (**Fig.28C**).

3.2.2. Histopathology findings

Haematoxylin-eosin staining AKI Nx0 kidney sections were compatible with ischaemic injury and similar to those found in AKI Nx170 post-ischaemic kidneys. However, the location as well as the severity of some lesions, e.g. tubular dilations hyaline casts where different. In AKI Nx0 animals, large areas of severe tubular dilation were found in the inner cortex of the kidney, while in AKI Nx170 animals sections tubular dilation were more abundant in the outer cortex. In the former groups of animals, the number and severity of the tubular dilations was much higher than in the latter group of animals. This was accompanied by hyaline casts in the AKI Nx0 animals (**Fig.29**).

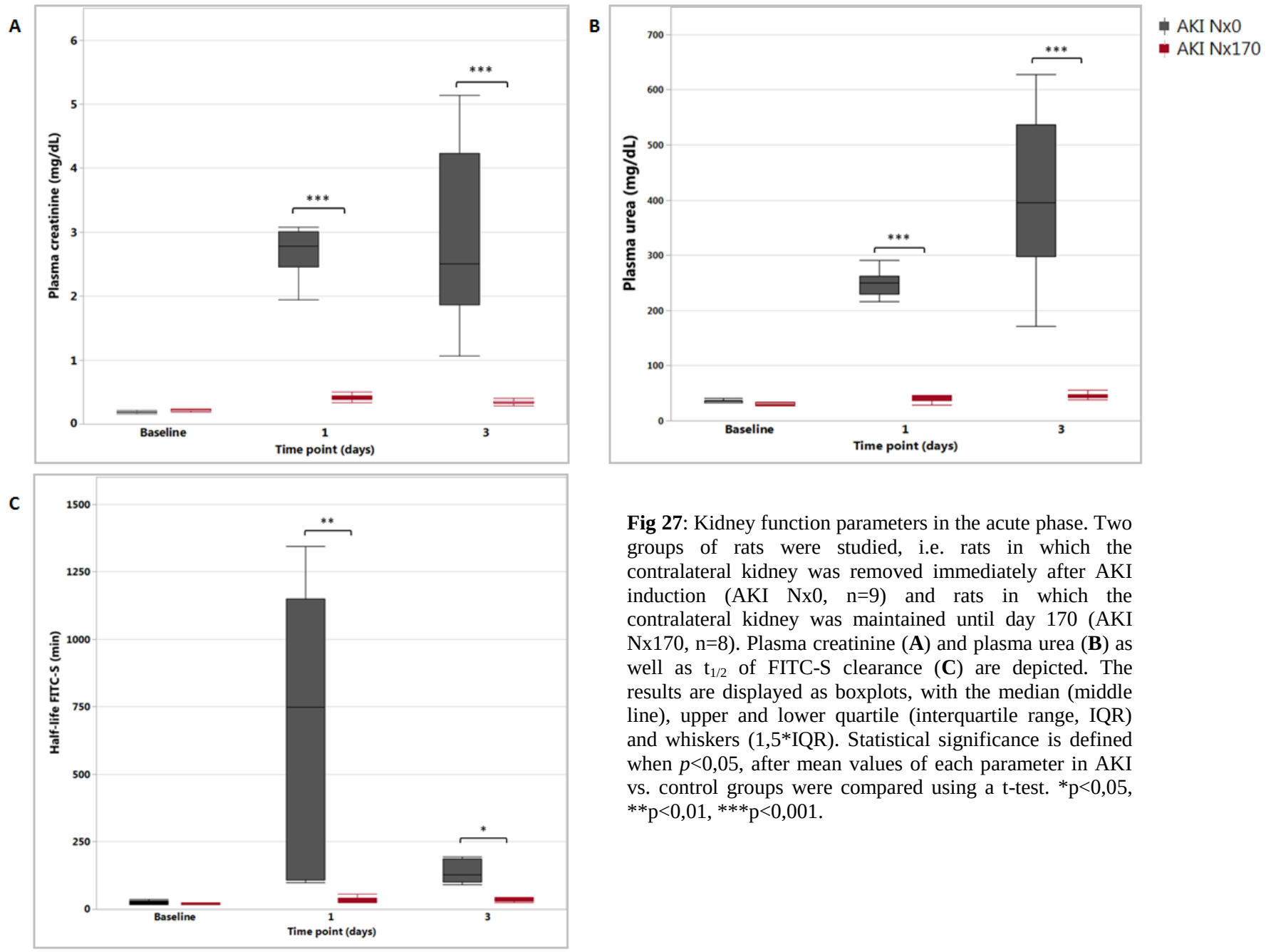

Fig 27: Kidney function parameters in the acute phase. Two groups of rats were studied, i.e. rats in which the contralateral kidney was removed immediately after AKI induction (AKI Nx0, n=9) and rats in which the contralateral kidney was maintained until day 170 (AKI Nx170, n=8). Plasma creatinine (**A**) and plasma urea (**B**) as well as $t_{1/2}$ of FITC-S clearance (**C**) are depicted. The results are displayed as boxplots, with the median (middle line), upper and lower quartile (interquartile range, IQR) and whiskers (1,5*IQR). Statistical significance is defined when $p<0{,}05$, after mean values of each parameter in AKI vs. control groups were compared using a t-test. *p<0,05, **p<0,01, ***p<0,001.

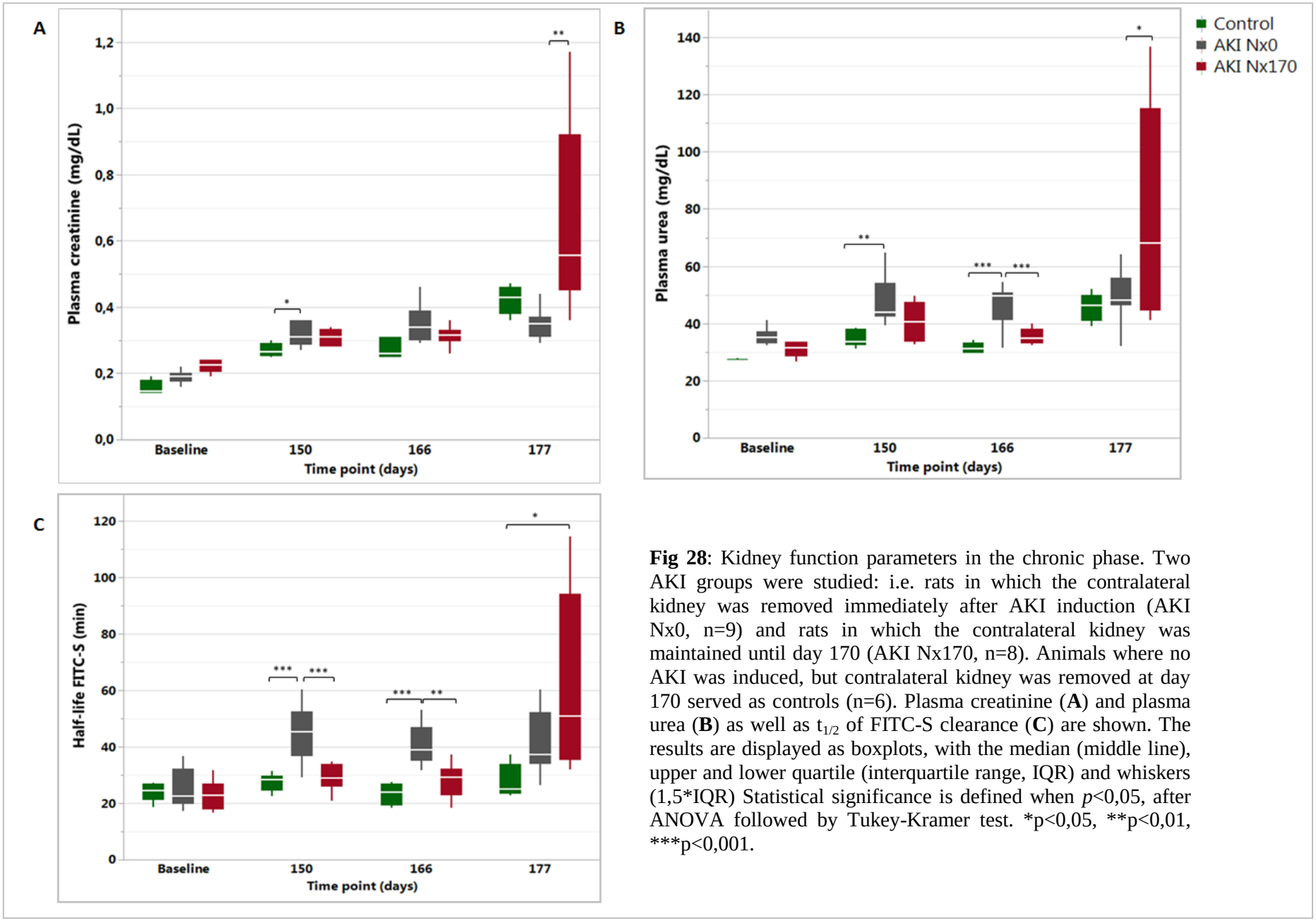

Fig 28: Kidney function parameters in the chronic phase. Two AKI groups were studied: i.e. rats in which the contralateral kidney was removed immediately after AKI induction (AKI Nx0, n=9) and rats in which the contralateral kidney was maintained until day 170 (AKI Nx170, n=8). Animals where no AKI was induced, but contralateral kidney was removed at day 170 served as controls (n=6). Plasma creatinine (**A**) and plasma urea (**B**) as well as $t_{1/2}$ of FITC-S clearance (**C**) are shown. The results are displayed as boxplots, with the median (middle line), upper and lower quartile (interquartile range, IQR) and whiskers (1,5*IQR) Statistical significance is defined when *p*<0,05, after ANOVA followed by Tukey-Kramer test. *p<0,05, **p<0,01, ***p<0,001.

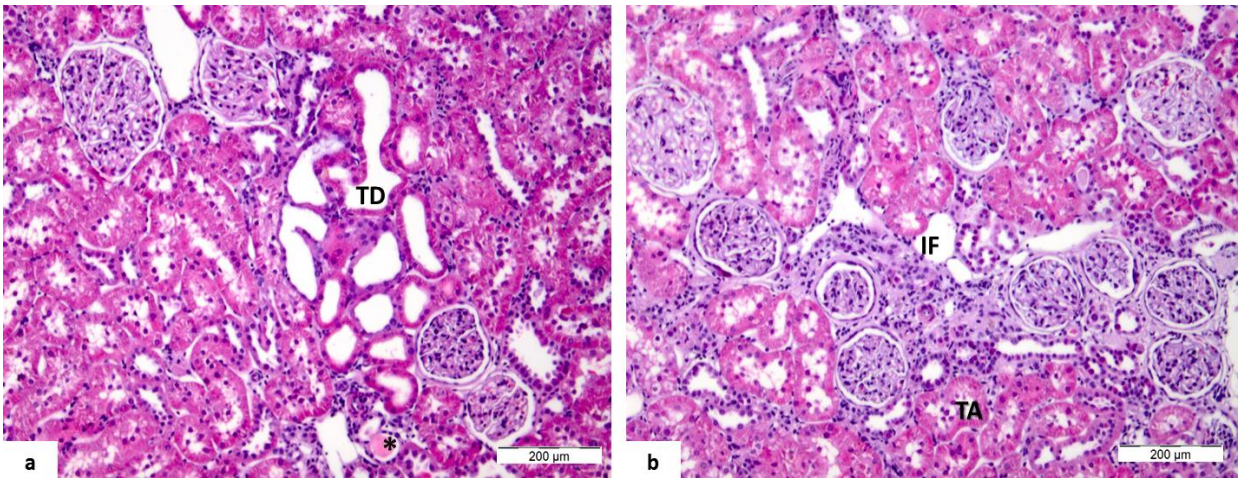

Fig.29: Post-ischaemic kidney sections of AKI Nx0 (**A**) and AKI Nx170 animals (**B**), 180 days after AKI induction. AKI Nx0 rats present areas of severe tubular dilation (**TD**) scattered through the inner cortex, accompanied with the presence of hyaline casts (asterisk) (H-E, 100X); whereas AKI Nx170 animals show scattered foci of interstitial fibrosis (**IF**) and tubular atrophy (**TA**), present mostly in the outer cortex, as well as a milder degree of tubular dilation compared to AKI Nx0 (H-E, 100X).

Immune histology of the post-ischaemic kidneys showed significantly increased number of ED1+ macrophages in both groups as compared to the control group (5370 ± 3431 vs. 162 ±47 cells/µm², AKI Nx0 vs. Control, *p*=0,033; 7105 ± 4940 vs. 162 ±47 cells/µm²:AKI Nx170 vs. Control, p=0,033) (**Fig.30A**). Although the mean number of infiltrated ED1+ cells was larger in the AKI Nx170 group the difference did not reach statistical significance. Scattered foci of ED1+inflammatory cells were found around the glomerulus or in areas of tubular dilation in the AKI Nx0 group of animals (**Fig.30B**), whereas ED1+ macrophages were mostly located within the fibrotic areas or surrounding the atrophic tubules (**Fig.30C**) in kidneys of AKI Nx170 animals.

Masson-Goldner staining revealed more severe kidney fibrosis in AKI Nx170 post-ischaemic kidneys (**Fig. 31 A and B**), with larger areas of interstitial fibrosis and tubular atrophy located in the outer cortex. In contrast, AKI Nx0 post-ischaemic kidney sections showed smaller areas of interstitial fibrosis, much more scattered and predominantly in the inner cortex (**Fig. 31 C and D**). Quantification of fibrosis demonstrated that the degree of fibrosis for each of the AKI groups was only significant when compared to controls, but not was significant between both AKI groups (0,02 ± 0,008 vs. 0,375 ± 0,18% control vs. AKI Nx0, *p*=0,002; 0,3 ± 0,11 vs. 0,02 ± 0,008% AKI Nx170 vs. control ; *p*=0,0005) (**Fig 31E**).

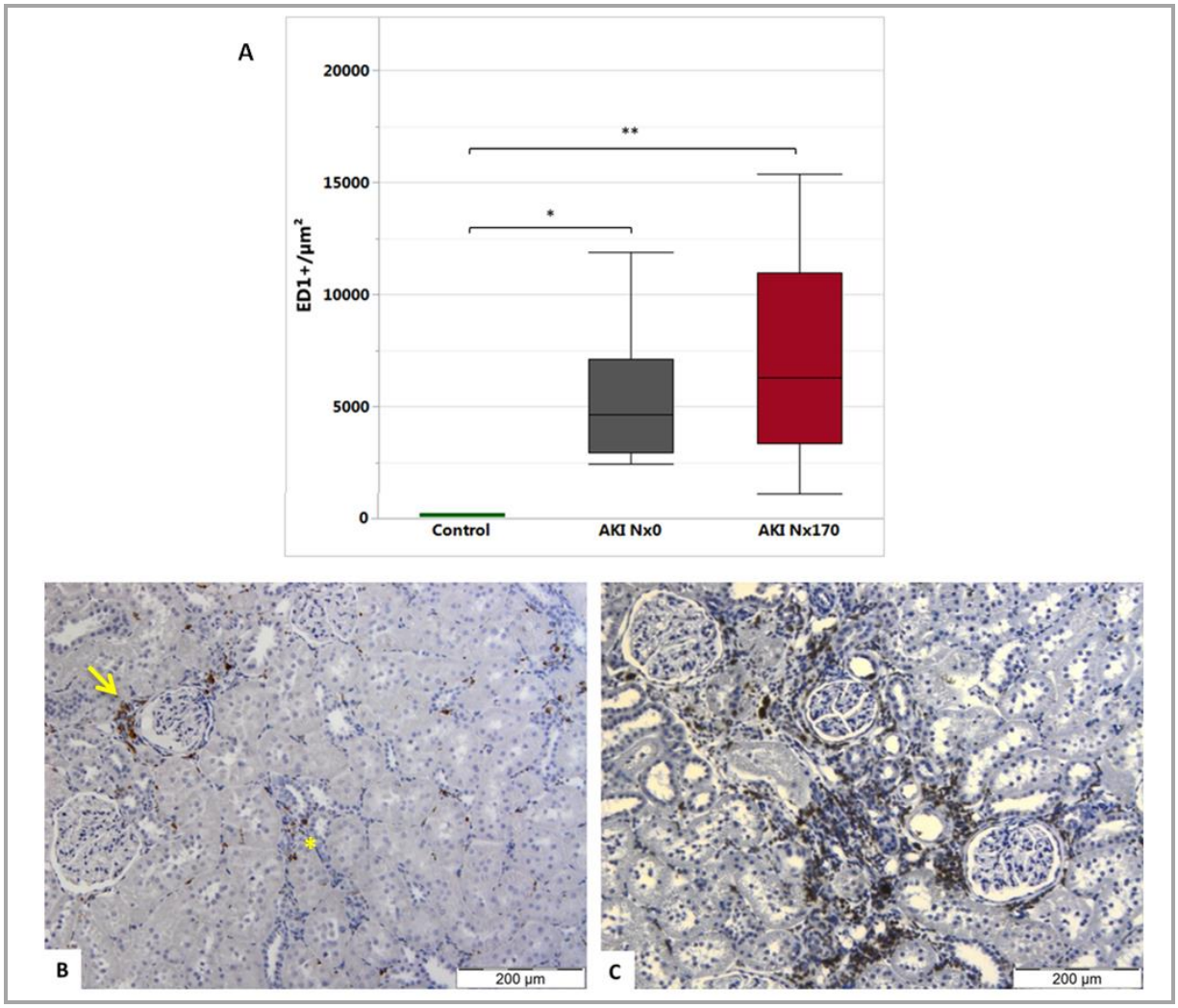

Fig. 30: **(A)** ED1+ cell infiltration (positivity/µm²) was assessed in sections of the post-ischaemic kidneys in Control (n=7), AKI Nx0 (n=6) and AKI Nx170 (n=6) groups. Quantification of ED1+ cells was performed by quantitative morphometric analysis, and showed that AKI induction in either conditions leads to a significant increase in ED1+ macrophages compared to the control group, albeit no significant differences amongst both ischaemic groups was observed. The results are displayed as boxplots, with the median (middle line), upper and lower quartile (interquartile range, IQR) and whiskers (1,5*IQR). Statistical significance is defined when $p<0,05$, after ANOVA followed by Tukey-Kramer test. *p<0,05, **p<0,01. **(B)** ED1 staining in the post-ischaemic kidney of AKI Nx0 animal shows scattered foci of ED1+ macrophages around the glomerulus (arrow) and in areas of tubular atrophy (asterisk), **(C)** ED1 staining in the post-ischaemic kidney of Nx170 animal demonstrates the presence of ED1+ macrophages in in areas of interstitial fibrosis and tubular atrophy of the outer cortex (ED1, 100X).

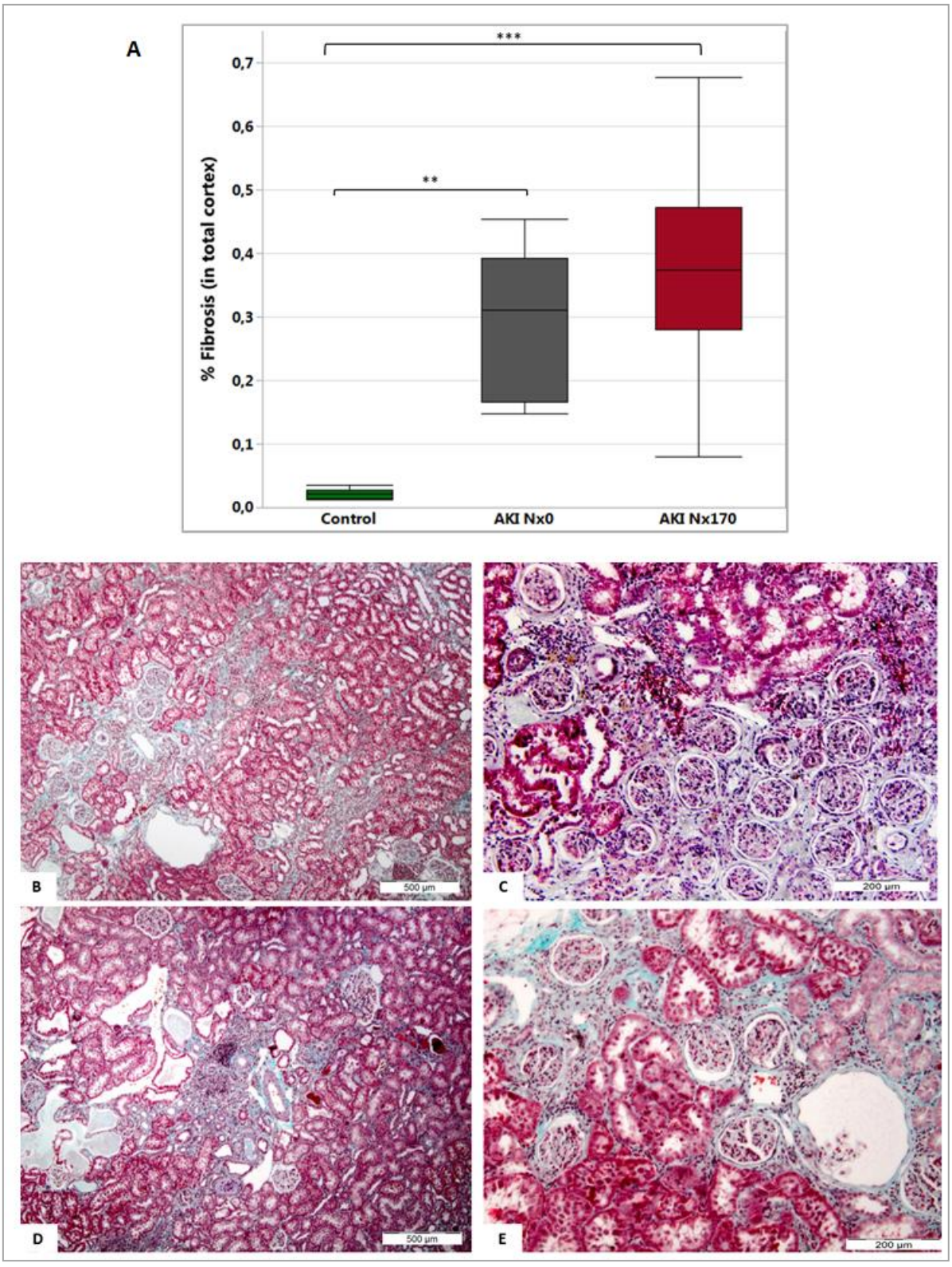

Fig.31: **(A)** Quantification of kidney fibrosis using Masson-Goldner staining revealed a higher percentage of connective tissue deposition in the cortex of both AKI-induced groups (AKI Nx0 n=7, AKI Nx170 n=6) compared to the control group (n=6). AKI Nx170 presented higher degree of fibrosis compared to AKI Nx0, although no statistical significance was found among the ischaemia-induced groups .The results are displayed as boxplots. Statistical significance is defined when $p<0{,}05$, after ANOVA followed by Tukey-Kramer test. $^{**}p<0{,}01$, $^{***}p<0{,}001$. AKI Nx170 animals **(B and C)** show higher severity of interstitial fibrosis and tubular atrophy gathered in the outer cortex (MG, 40X-

100X, respectively); on the other hand, AKI Nx0 animals (**D and E**) present milder degree of interstitial fibrosis and tubular atrophy, with small, scattered lesions in the inner cortex (MG, 40X-100X, respectively).

3.3. Assessment of the therapeutic efficacy of human adipose-derived mesenchymal stromal cells (hASC) in an ischaemia-induced AKI model

3.3.1. Clinical parameters

In order to assess whether hASC treatment is able to ameliorate long-term kidney function deterioration, animals were subjected to ischaemia induced AKI without immediate removal of the non-ischaemic contralateral kidney. Renal function parameters p-crea and p-urea were measured at similar time intervals as described in sections **3.2** and **3.1**.

In animals treated with hASC p-crea levels were at all post-ischaemic time points slightly lower compared to animals that were vehicle treated (NaCl 0,9%) or compared to animals that were not subjected to AKI. Statistical significance was found at day 150 (0,3 ±0,02 vs. 0,27 ± 0,02 mg/dL, AKI vs. AKI+hASC; *p*=0,025). Due to the presence of the contralateral kidney all p-crea values remained in the normal range. One week after removal of the contralateral kidney the mean p-crea level became pathologic only in the vehicle treated animals but not in animals that received hASC, where treatment was able to significantly reduce p-crea to a non-pathologic range (0,66 ± 0,29 vs. 0,49 ± 0,06 mg/dL, AKI vs. AKI+hASC; *p*=0,049) (**Fig.32A**). Compared to vehicle treated AKI animals, hASC treatment also decreased p-urea values at all post-ischaemic time points with statistical significance observed at day 150 (40,65 ± 7,09 vs. 30,72 ± 2,21 mg/dL, AKI vs. AKI+hASC; *p*=0,0003) and day 177 (77,9 ± 37,55 vs. 49,65 ± 6,8 mg/dL AKI vs. AKI+hASC; *p*=0,032) (**Fig.32B**).

3.3.2. Renal histology

<u>Haematoxylin-eosin staining</u> renal sections did not differ outstandingly between vehicle and hASC-treated AKI induced animals, presenting a similar degree of tubular dilation mostly found in the outer cortex, (**Fig. 33 A and B**) as well as comparable amount of hyaline cast formation.

<u>Immune histology</u> using ED1 antibody was performed to assess if inhibition of macrophage infiltration might be held accountable for the beneficial effect of hASC. Indeed hASC treatment significantly decreased the infiltration of ED1+ macrophages as compared to vehicle treated animals (7105 ± 4940 vs. 828 ± 398 cells/ µm², vehicle vs. hASC; *p*=0,0001)(**Fig.34**). In vehicle treated animals, macrophage infiltration was particularly observed in the outer cortex, in areas of tubular atrophy and interstitial fibrosis (**Fig.35A**), and less frequently in glomeruli of the post-ischaemic kidneys (**Fig.35B**). In hASC treated animals a few scattered foci of macrophage infiltration mostly surrounding the glomeruli or between the tubuli were visible (**Fig. 35 C and D**)

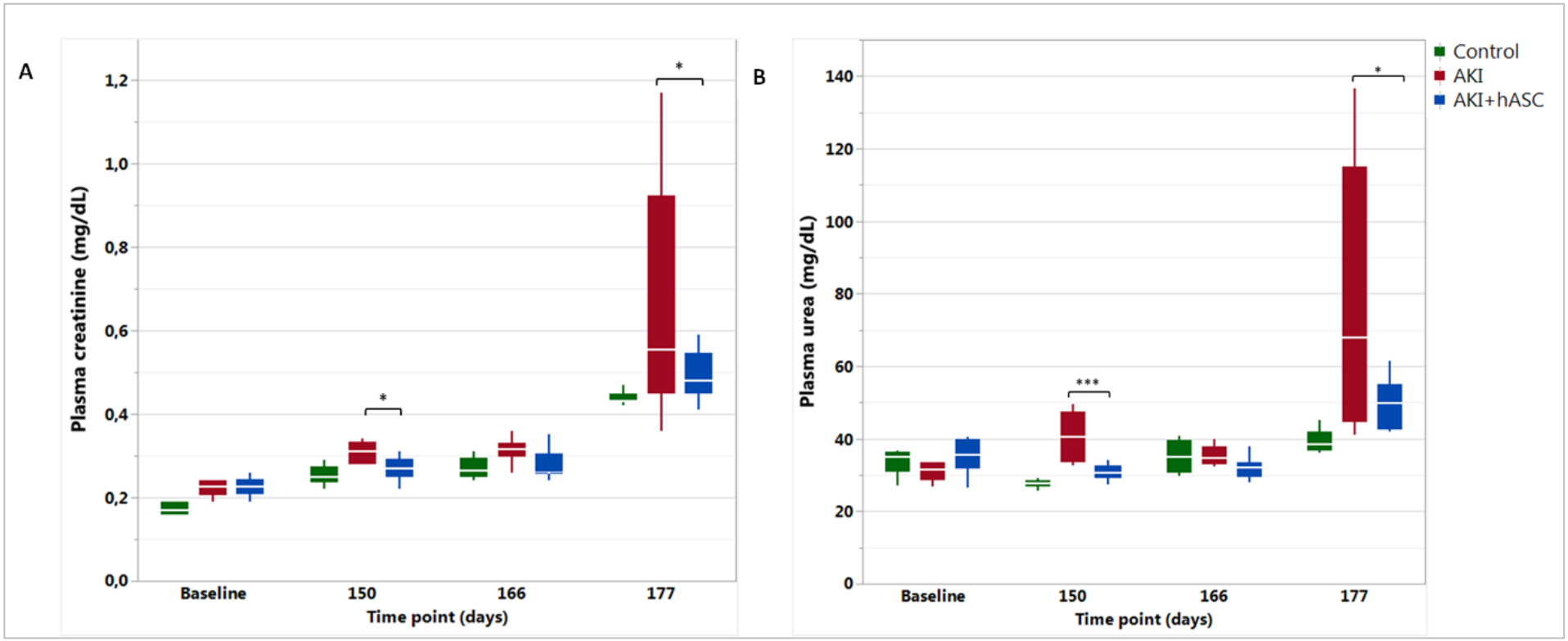

Fig.32: Kidney function parameters assessed to determine the efficacy of hASC treatment in AKI-induced animals. **(A) Plasma creatinine** is decreased at all post-ischaemic time points in cell-treated animals (n=10) compared to vehicle treated ones (n=6). After contralateral nephrectomy (day 177), a pathologic increase in p-crea is observed in the vehicle treated group, which is able to be significantly reduced by cell-treatment. A same trend is observed for **plasma urea (B)** where hASC treated animals also present lower values compared to vehicle-treated at all post-ischaemic time points. Likewise, after the contralateral nephrectomy is performed, a pathologic increase in p-urea in vehicle-treated animals is significantly reduced to non-pathologic levels in hASC-treated. The results are displayed as boxplots, with the median (middle line), upper and lower quartile (interquartile range, IQR) and whiskers (1,5*IQR). Statistical significance is defined when $p<0,05$, after ANOVA followed by Tukey-Kramer test. *p<0,05, ***p<0,001

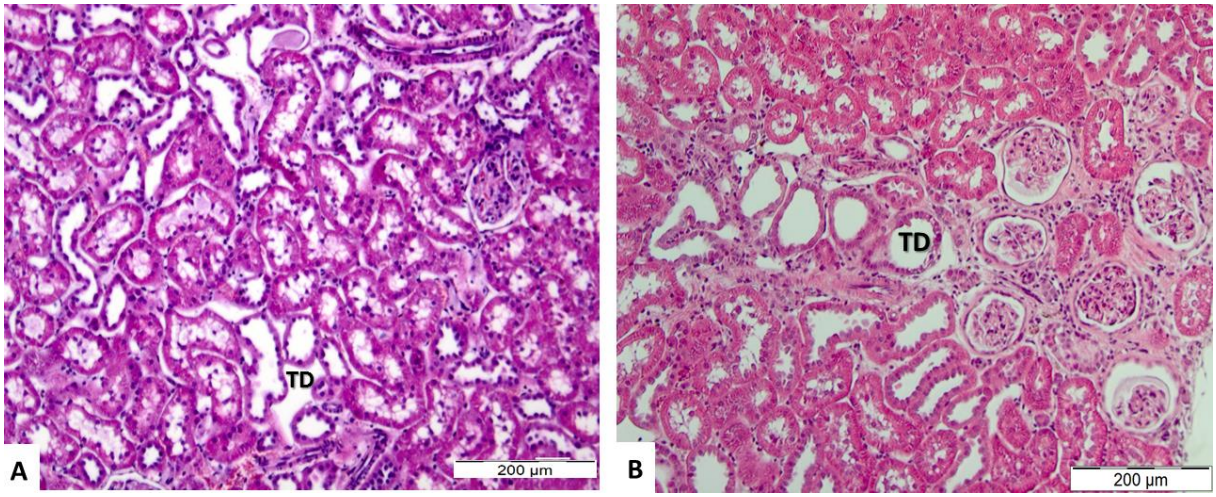

Fig. 33: Hematoxylin-eosin stained sections of the post-ischaemic kidneys of vehicle- treated **(A)** and hASC- treated **(B)** AKI-induced animals showed a comparable degree and pattern of tubular dilation (outer cortex) amongst the two groups. (H-E, 100X)

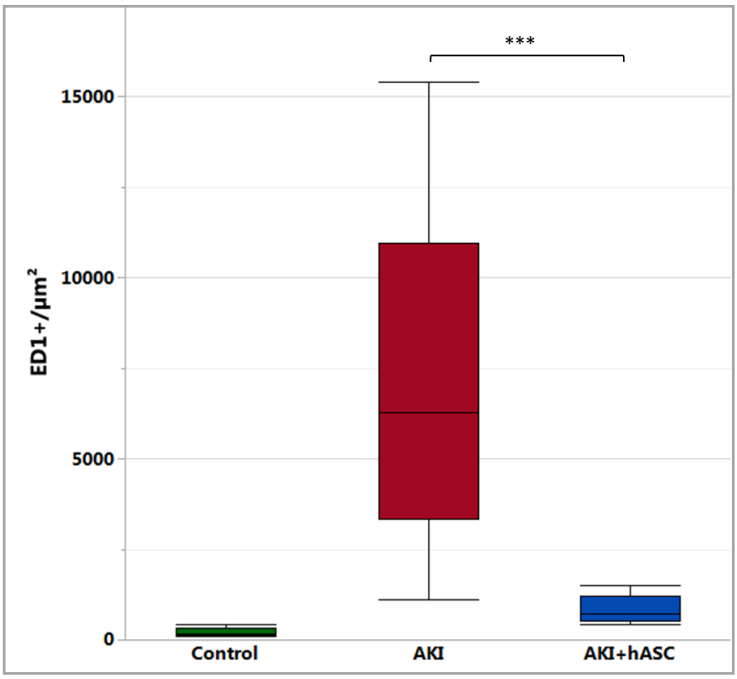

Fig.34: ED1+ cell infiltration (positivity/µm²) was assessed in control (n=8), AKI (vehicle-treated, n=6) and AKI+hASC (n=10) groups by a quantitative morphometric analysis, showing that hASC treatment is able to highly significantly reduce the number of ED1 positive macrophages in the post-ischaemic kidneys compared to the AKI-vehicle treated group. The results are displayed as boxplots, with the median (middle line), upper and lower quartile (interquartile range, IQR) and whiskers (1,5*IQR). Statistical significance is defined when $p<0{,}05$, after ANOVA followed by Tukey-Kramer test. ***$p<0{,}001$.

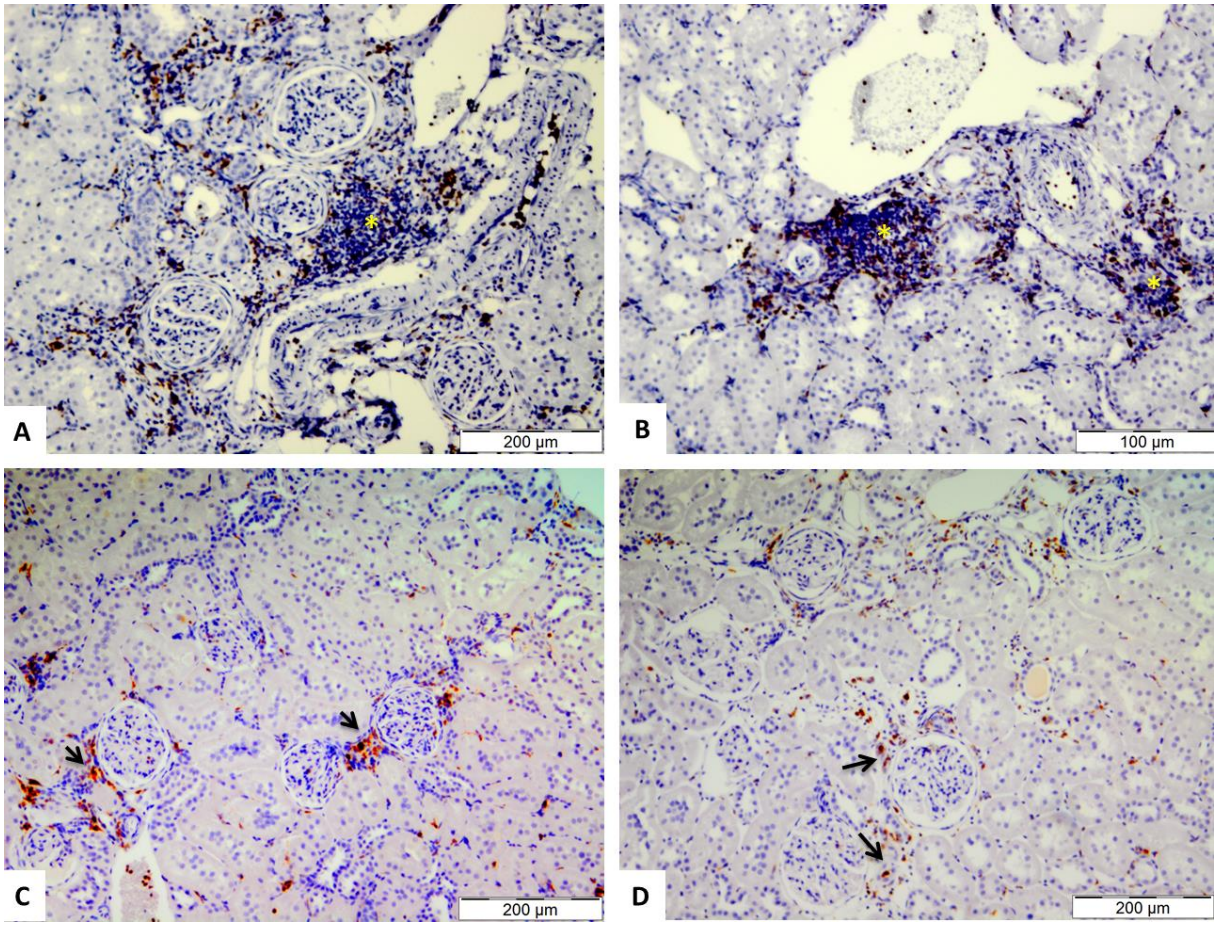

Fig.35: ED1 staining of post-ischaemic kidney sections of vehicle-treated and hASC-treated group. Vehicle-treated group presents areas of extensive ED1+ infiltration (asterisks) in areas of tubular atrophy and interstitial fibrosis (**A and B**); whereas hASC-treated animals (**C and D**) show fewer foci of ED1+ cells, located mostly around the glomeruli (arrows) (ED1, 100X).

Masson-Goldner staining revealed a subtle reduction of tissue fibrosis in the hASC treated animals (**Fig.36A and B**), albeit that the difference in the extent of fibrosis did not reach statistical significance (0,37 ± 0,189 vs. 0,271 ± 0,1 %; vehicle vs. hASC; $p>0,05$ (**Fig.36C)**.

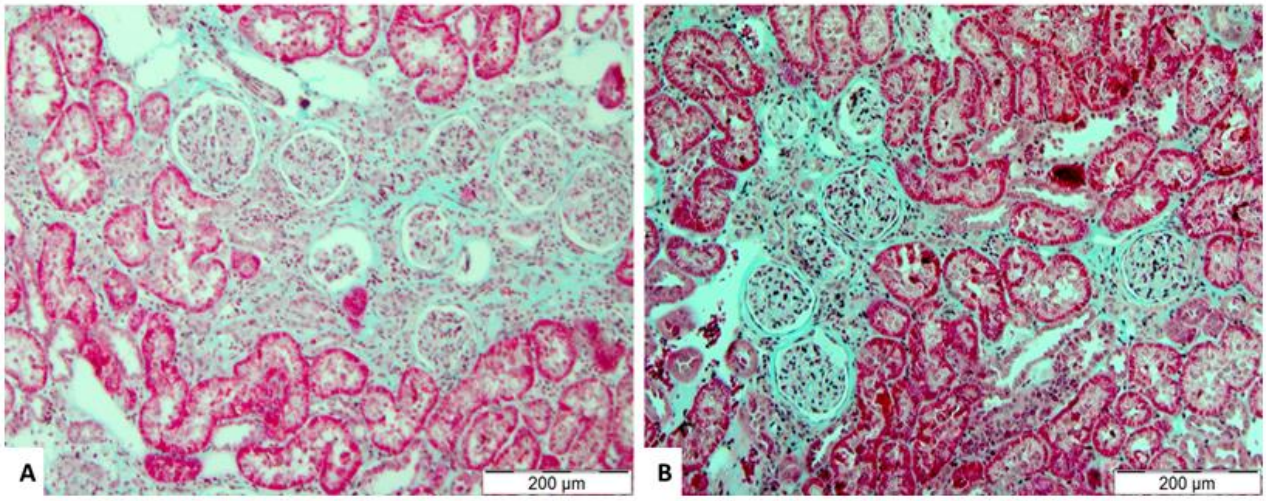

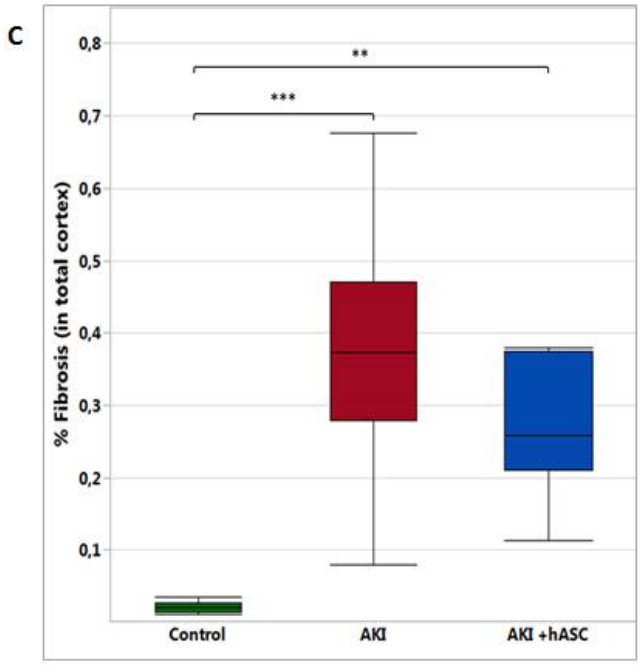

Fig.36: Kidney fibrosis shown with Masson-Goldner staining in post-ischaemic kidneys of AKI (**A**) and AKI+hASC (**B**) groups 180 days after injury. Similar location pattern as well as degree of interstitial fibrosis is observed in both groups. **(C)** Quantification of kidney fibrosis revealed a lesser degree of fibrosis in the cortex of hASC-treated animals (n=6) compared to the vehicle-treated group (n=6), although no statistical significance was found between the two ischaemic groups. The results are displayed as boxplots, with the median (middle line), upper and lower quartile (interquartile range, IQR) and whiskers (1,5*IQR). Statistical significance is defined when $p<0,05$, after ANOVA followed by Tukey-Kramer test. **$p<0.01$, ***$p<0.001$

3.4. Therapeutic efficacy of human ABCB5+ and its derived CM in a chronic kidney allograft rejection model

3.4.1. Animal general condition

Since hASC seem to be effective in the aforementioned AKI model, but the model itself did not result in severe renal function impairment, we questioned if the beneficial effect of MSC would still be found in a model that leads to severe chronic renal function deterioration.

Within the first week of transplantation animals were evaluated every day and thereafter every other week until completion of the experiment at day 98 after kidney transplantation. The evaluation consisted of assessing animals' weight and behaviour.

Animals showing signs of lethargy, unresponsiveness to external stimuli, or signs of neurologic disorders were euthanized. These signs were, in most cases, found soon after transplantation, and were the result of hydronephrosis or paralytic ileus. Neurologic signs were found in a few cases at later time points possibly as a result of increased p-crea/p-urea values due to failure of graft function. If none of the above mentioned complications occurred leading to pre-defined euthanasia, a 100 % of the animals (n=7) survived. For the treated study arms this was 83,3 % (n=7) and 77,7 % (n=5) in the CM and ABCB5 cell-treated groups respectively.

3.4.2. Clinical parameters

In all three groups and at all time points tested, plasma creatinine values were within a pathologic range, reaching the highest values at day 84 and day 98 after transplantation (**Fig.37A**). At these two last time points, ABCB5 cell-treated animals showed higher p-crea values compared to CM-treated and controls animals (day 84: 1,09 ± 0,47 vs. 0,8±0,26 mg/dL ABCB5 vs. control, *p*=0,27 and 1,09 ± 0,47 vs 0,81± 0,2 mg/dL ABCB5 vs CM-treated, *p*=0,35; day 98: 1,34 ± 0,76 vs. 0,82 ± 0,35 mg/dL ABCB5 vs. control, *p*=0,19 and 1,34 ± 0,76 vs. 0,89 ± 0,26 mg/dL ABCB5 vs. CM-treated, *p*=0,35). P-crea in CM-treated animals showed a similar progression as in the control group. Like p-crea, p-urea was pathologically increased at all time points tested in the three experimental groups, reaching the highest values at day 28 (114,88 ± 37,5 vs. 98,14± 28,53 mg/dL ABCB5 vs. control; *p*=0,54 , 92,26±82,26 vs. 98,14±28,53 mg/dL CM-treated vs. control, p=0,93 and 114,88 ± 37,5 vs. 92,26 ± 82,26 mg/dL ABCB5 vs. CM-treated, *p*=0,4) and at days 84 (120,14 ± 45,43 vs. 95,25±30,19 mg/dL ABCB5 vs. control *p*=0,34; 95,25 ± 30,19 vs. 95,25±30,19 mg/dL, *p*=0,99 and 120,14 ± 45,43 vs. 92,26 ± 82,26 mg/dL ABCB5 vs.CM-treated , *p*=0,46) and 98 after kidney transplantation (156,25 ±106,7 vs. 98,24 ±37,02 mg/dL ABCB5 vs. control *p*=0,28; 101,64 ± 7,96 vs. 98,24 ± 37,02 mg/dL CM-treated vs. control, *p*= 0,99 and 156,25 ±106,7 vs. 98,24 ± 37,02 mg/dL ABCB5 vs. CM-treated, *p*=0,39) . P-urea displayed a similar hierarchy as p-crea, i.e. being the highest in the ABCB5 cell-treated animals and no difference between CM treated and vehicle treated control animals (**Fig.37B)**. The increased p-crea and p-urea values were accompanied by an increased proteinuria, which was also much higher in the ABCB5 cell-treated group compared to the CM-treated and control groups, predominantly at day 98 after transplantation (223,58 ± 121,3 vs. 132,31±61 mg/24h ABCB5 vs. control, *p*=0,15; 223,58 ± 121,3 vs. 192,7 ± 54,57 mg/24h ABCB5 vs. CM-treated *p*=0,82)(**Fig.37C**). Polyuria, i.e. urine volume >3,3mL/100g BW/24h, was observed in all groups and was neither affected by the ABCB5 cell - nor by the CM treatment (**Fig.38A**). Polyuria was accompanied by low osmolarity (osmolarity ≤1400 mosmol/L), which was similar in all the three groups (**Fig.38B**) Transcutaneous FITC-S clearance was assessed one day before the animals were sacrificed. In the ABCB5-treated animals, the $t_{1/2}$ for clearance of the dye was longer compared to controls (99,37± 85,29 vs.77,41 ± 34,84 min; ABCB5 vs. control; *p*=0,86) and slightly longer compared to CM-treated animals (99,37± 85,29 vs. 97,1 ± 85,26 min; *p*=0,99). For all three group $t_{1/2}$ values for FITC-S clearance were compatible with severely impaired kidney function (**Fig.39**).

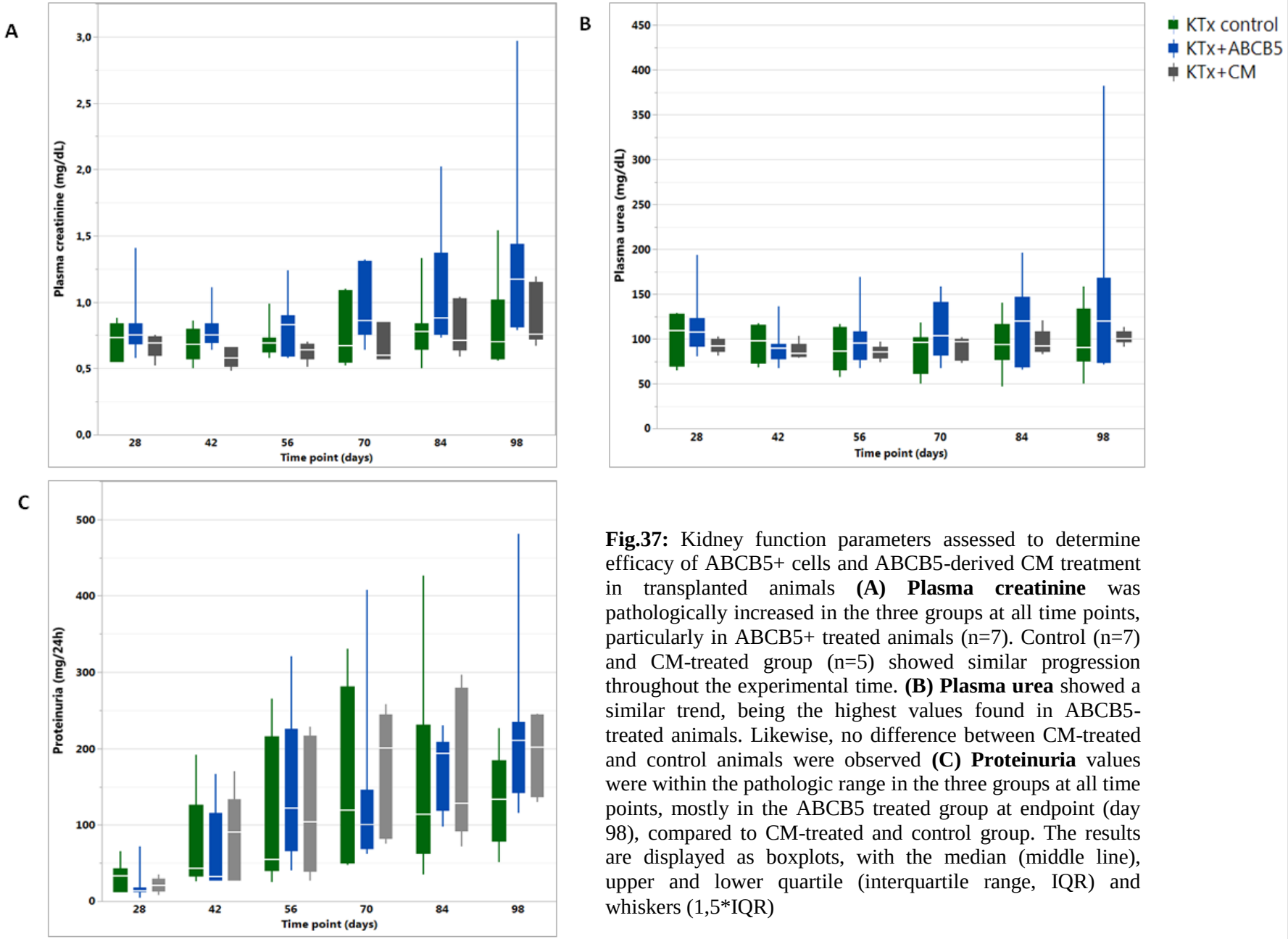

Fig.37: Kidney function parameters assessed to determine efficacy of ABCB5+ cells and ABCB5-derived CM treatment in transplanted animals **(A) Plasma creatinine** was pathologically increased in the three groups at all time points, particularly in ABCB5+ treated animals (n=7). Control (n=7) and CM-treated group (n=5) showed similar progression throughout the experimental time. **(B) Plasma urea** showed a similar trend, being the highest values found in ABCB5-treated animals. Likewise, no difference between CM-treated and control animals were observed **(C) Proteinuria** values were within the pathologic range in the three groups at all time points, mostly in the ABCB5 treated group at endpoint (day 98), compared to CM-treated and control group. The results are displayed as boxplots, with the median (middle line), upper and lower quartile (interquartile range, IQR) and whiskers (1,5*IQR)

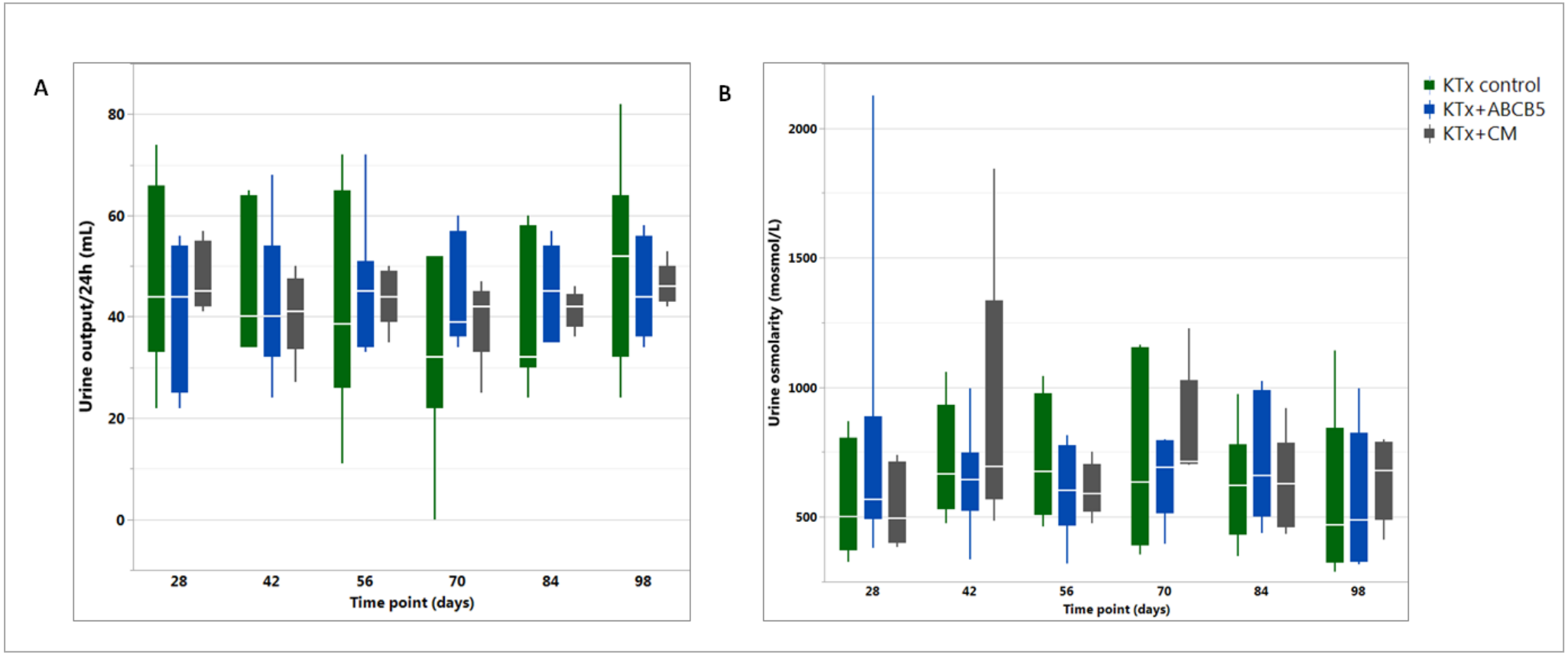

Fig.38: (A) Urine output in 24 hours was measured in control (n=7), ABCB5+ (n=7) and CM-treated animals (n=5) at different time points after kidney transplantation. Animals in all the groups presented polyuria, which was not affected by either of the treatments. This highly polyuric state was associated with low **urine osmolarity (B)**, with similar values among the groups. The results are displayed as boxplots, with the median (middle line), upper and lower quartile (interquartile range, IQR) and whiskers (1,5*IQR).

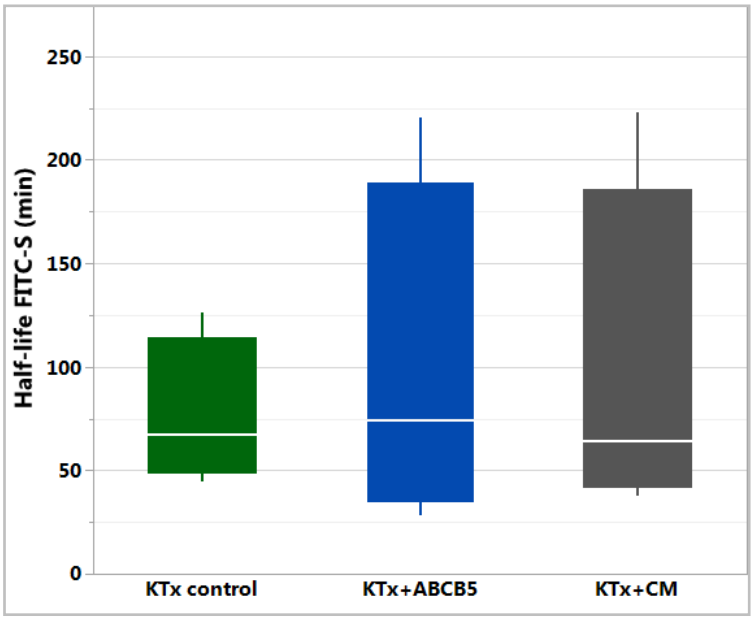

Fig.39: Transcutaneous FITC-S clearance was assessed in control (n=6), ABCB5+ (n=4) and CM-treated (n=4) animals one day before sacrifice (day 97 after transplantation). ABCB5+ treated animals presented longer $t_{1/2}$ for clearance of the dye compared to controls and slightly longer compared to CM-treated group. Clearance values found in all three groups were compatible with highly impaired kidney function. The results are displayed as boxplots, with the median (middle line), upper and lower quartile (interquartile range, IQR) and whiskers (1,5*IQR)

3.4.3. Renal histology

Chronic renal allograft rejection in the Fischer to Lewis model is mostly accompanied by features of T-cell mediated rejection, with its typical hallmark of tubulitis (**Fig.40A**); endarteritis and in severe cases, transplant vasculopathy with the presence of intimal endarteritis and intimal fibrosis (**Fig.40B**). In some cases, features characteristic for antibody-mediated rejection can be observed. This is mostly manifested as glomerular abnormalities, like thickening of the glomerular basement membrane, dilation of the glomerular capillaries and glomerulitis (**Fig.40C**). In addition, extensive areas of tubular dilation are observed, as a result of ischaemia-reperfusion injury (**Fig.40A**). Interstitial fibrosis and tubular atrophy are also very important features in this model, and they are mostly the result of the sustained cellular and humoral immune responses through a long period of time (**Fig.40A**).

To assess the differences in overall inflammation in the kidney grafts between groups, ED1 staining was performed, and the number of positive cells was counted. Quantification showed that ABCB5-treated animals presented an increased number of ED1+ cells (17421 ± 5019 vs. 11628 ± 6133 cells/ µm², ABCB5-treated vs. control; *p*=0,11). On the other hand, CM-treated animals showed less ED1+ macrophages than cell-treated (14451 ± 3751 vs. 17421 ± 5019 cells/ µm² CM-treated vs. ABCB5-treated; *p*= 0,6), but not less than the control group (14451 ± 3751 vs. 11628 ± 6133 cells/ µm², CM-treated vs. control; *p*=0,62) (**Fig.41**).

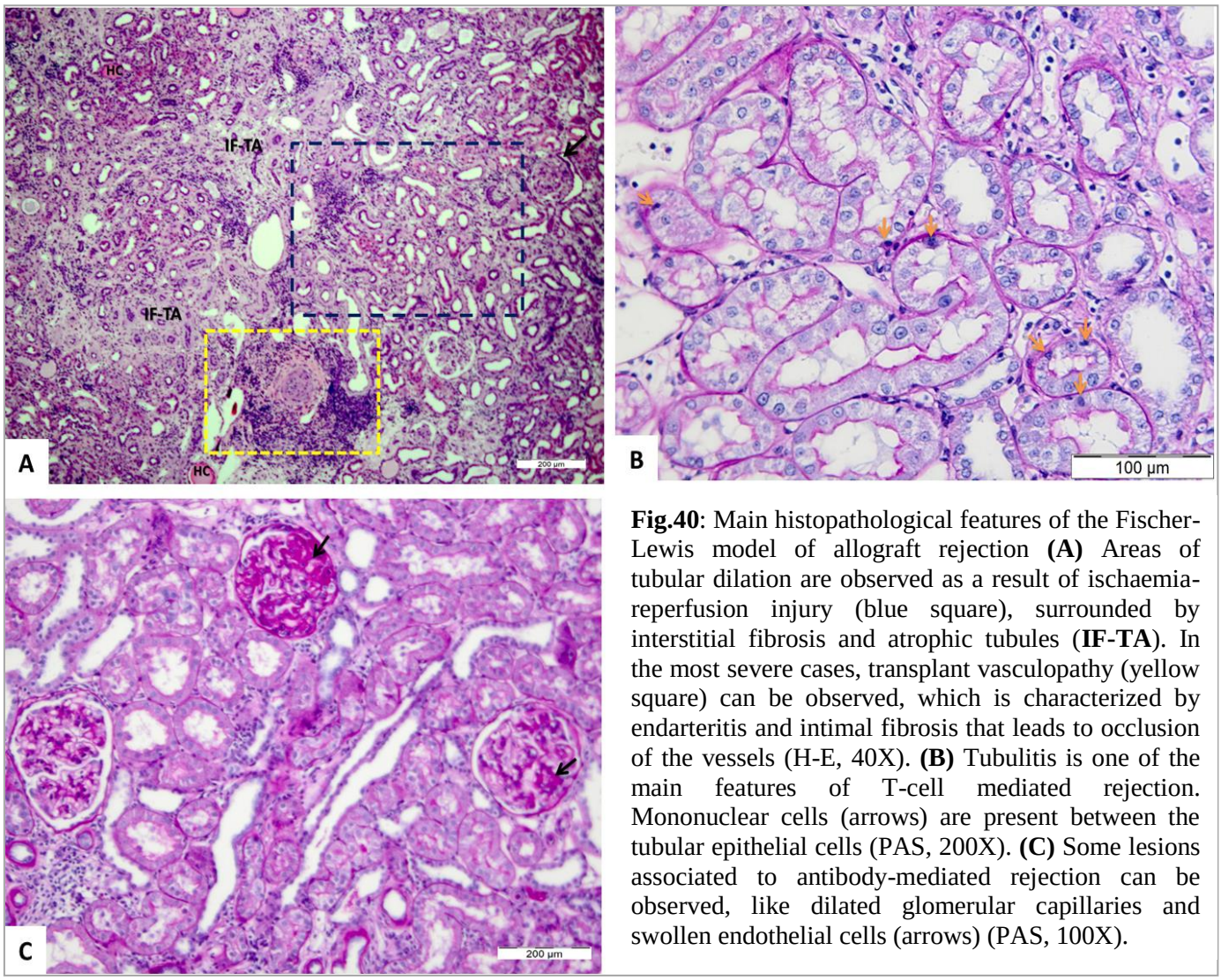

Fig.40: Main histopathological features of the Fischer-Lewis model of allograft rejection **(A)** Areas of tubular dilation are observed as a result of ischaemia-reperfusion injury (blue square), surrounded by interstitial fibrosis and atrophic tubules (**IF-TA**). In the most severe cases, transplant vasculopathy (yellow square) can be observed, which is characterized by endarteritis and intimal fibrosis that leads to occlusion of the vessels (H-E, 40X). **(B)** Tubulitis is one of the main features of T-cell mediated rejection. Mononuclear cells (arrows) are present between the tubular epithelial cells (PAS, 200X). **(C)** Some lesions associated to antibody-mediated rejection can be observed, like dilated glomerular capillaries and swollen endothelial cells (arrows) (PAS, 100X).

Apart from ED1+ macrophages also CD3+ T-cells infiltrate into the renal allograft. The number of CD3+ cells was higher in the ABCB5 cell-treated group as compared to the CM-treated or control group (136,93 ± 50,53 vs. 98,03 ±3 6,62 CD3+ cells; ABCB5-cell treated vs. control; *p*=0,18) In the CM-treated group, the number of CD3+ cells was slightly lower than in the control group (92,44 ± 20,4 vs. 98,03 ± 36,62 CD3+ cells, CM-treated vs. control; *p*=0,96). In none of the comparisons statistical significance was reached (**Fig.42**). No major differences in the distribution or location of the CD3+ cells were found between the three groups

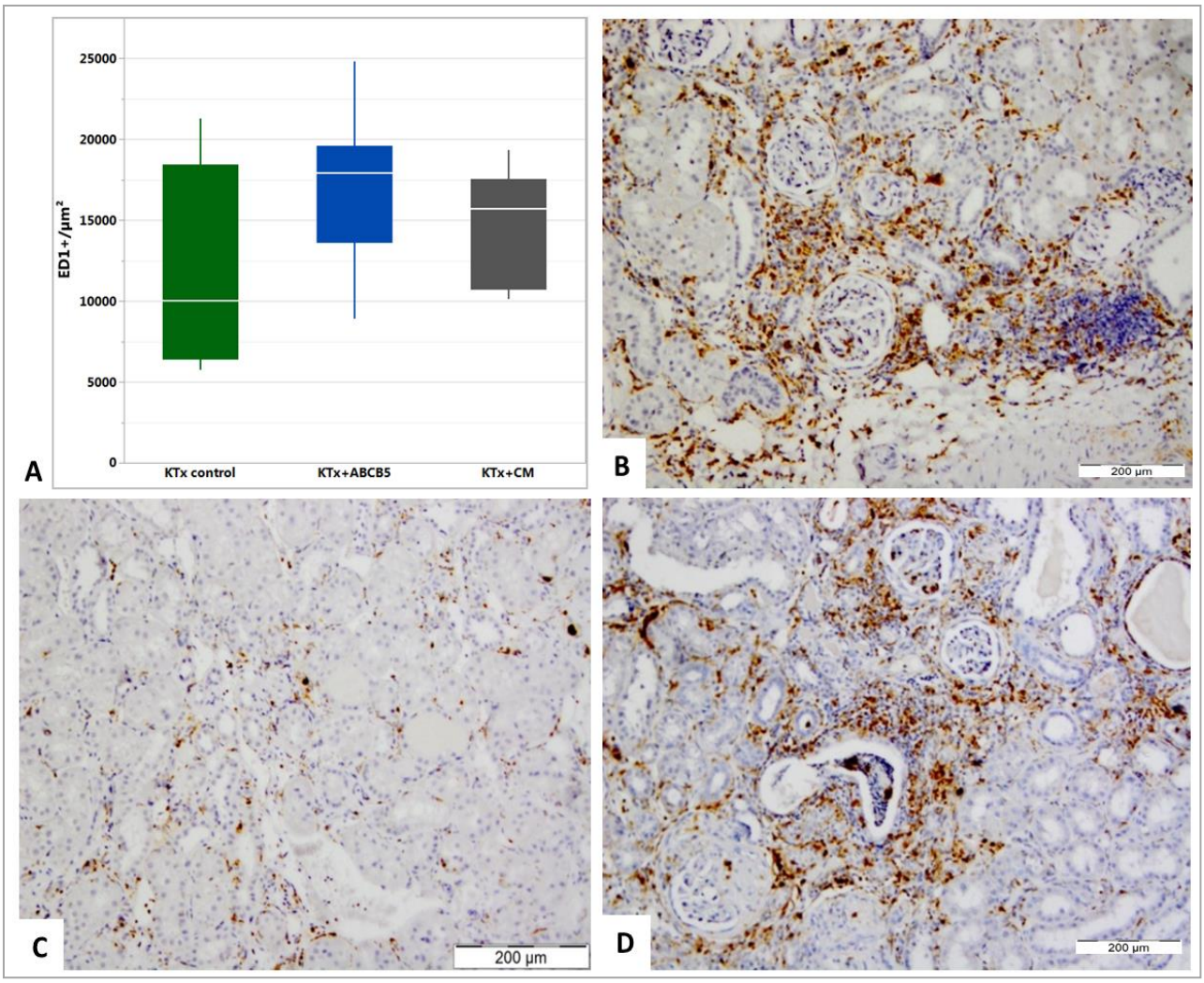

Fig.41: **(A)** Quantification of ED1 cells (positivity/µm²) in kidney allograft sections of control (n=6), ABCB5+ (n=7) and CM-treated (n=5) groups showed that ABCB5+cell treated group presented increased number ED1+ macrophages compared to control and CM-treated animals. Nevertheless, the number of ED1+ cells in CM-treated was not lower than in the control group. ED1 staining shows the presence of ED1+ macrophages in the kidney allografts of control. The results are displayed as boxplots, with the median (middle line), upper and lower quartile (interquartile range, IQR) and whiskers (1,5*IQR). Kidney sections of (**B**), ABCB5 (**C**) CM-treated and (**D**) control animals 98 days after transplantation (ED1, 100X).

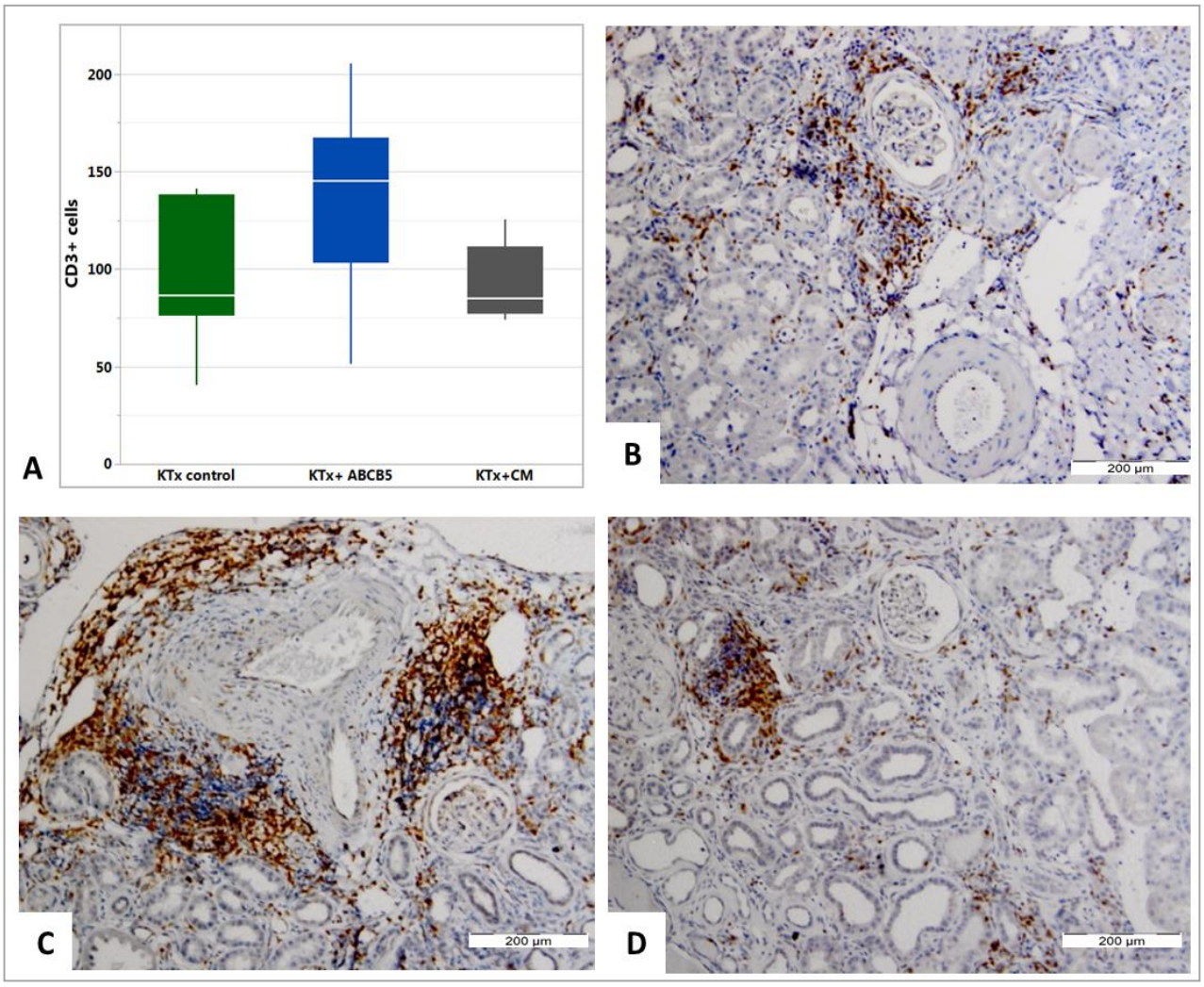

Fig:42: (A) Quantification of CD3+ cells in the kidney allograft sections of control (n=6), ABCB5+ (n=7) and CM-treated (n=5) animals was performed as described in section 2.9, and showed a higher number of CD3+ T cells in ABCB5+ treated animals compared to the other two groups. CM-treated animals showed slightly lower amount of CD3+ T cells compared to control group, but this difference was not statistically significant. The results are displayed as boxplots, with the median (middle line), upper and lower quartile (interquartile range, IQR) and whiskers (1,5*IQR). Kidney sections of **(B)** Control, **(C)** ABCB5 and **(D)** CM-treated animals 98 days after Kidney transplantation (ED1, 100X)

We next assessed the Banff classification scores as described in section 2.11, following the guidelines by Roufosse *et al*.[134]

The first criterion assessed was the degree of *tubulitis (t)*, scored as follows:

t0= No mononuclear cells in tubules or single focus of tubulitis only (**Fig.43a**)
t1= Foci with 1 to 4 mononuclear cells/tubular cross section (**Fig.43b**)
t2= Foci with 5 to 10 mononuclear cells/tubular cross section (**Fig.43c**)
t3= Foci with >10 mononuclear cells/tubular cross section (**Fig.43d**)

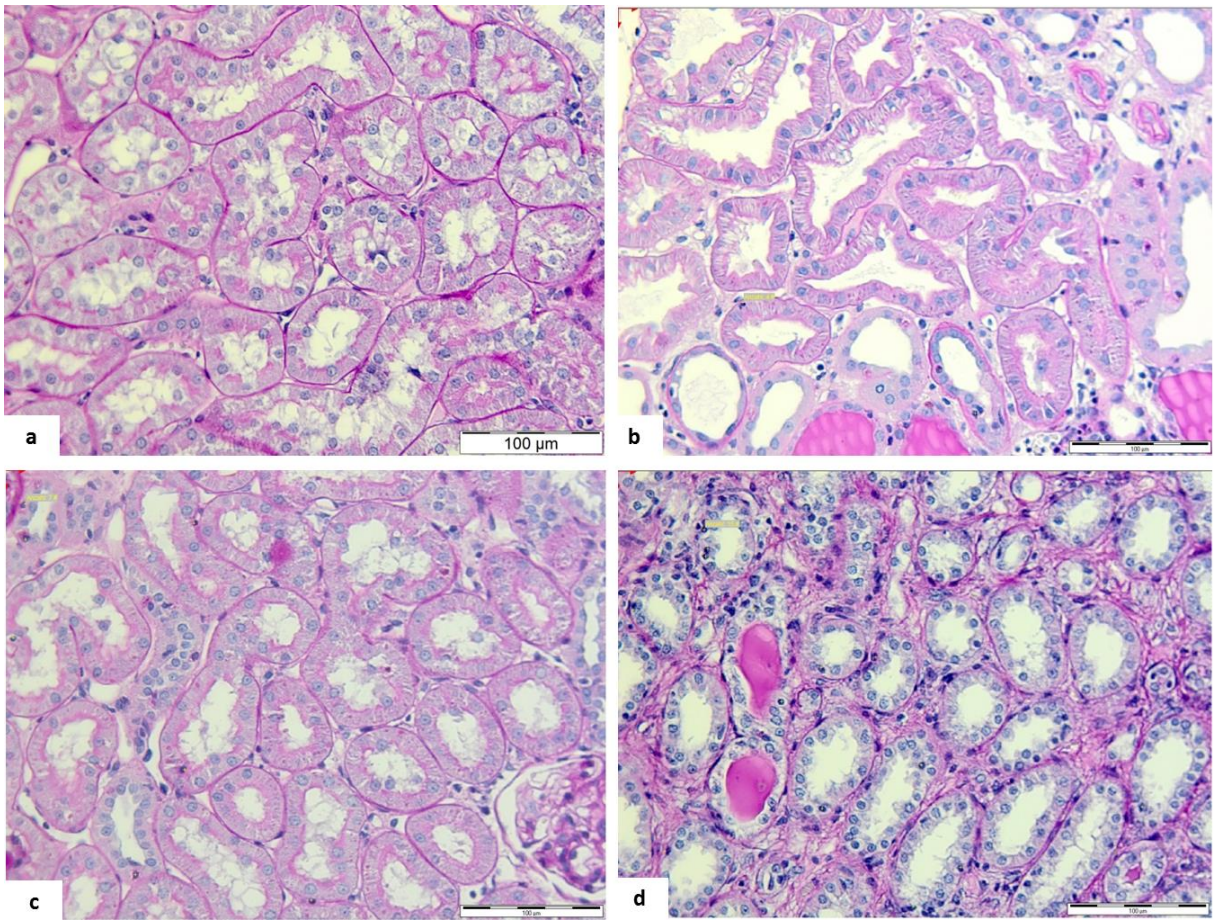

Fig.43: Representative images of the four tubulitis scores (t) in the Banff classification **a**) *t0* No mononuclear cells in tubules or single focus of tubulitis only; **b)** *t1*= Foci with 1 to 4 mononuclear cells/tubular cross section; **c)** *t2*= Foci with 5 to 10 mononuclear cells/tubular cross section; **d)** *t3*= Foci with >10 mononuclear cells/tubular cross section. (PAS, 100X)

Animals treated with hABCB5+ cells showed the highest tubulitis scores, with one animal presenting severe tubulitis. The degree of tubulitis was similar between CM-treated and control animals (**Table 2**).

Table 2: Tubulitis (*t*) scores in the allograft sections of KTx control (n=8), KTx+ABCB5 (n=7) and KTx+CM (n=5) 98 days after transplantation.

Tubulitis (t)	KTx control	KTx+ABCB5	KTx+CM
None (0)	-	-	-
Mild (1)	3 (**37,5%**)	3 (**42,86%**)	2 (**40%**)
Moderate (2)	5 (**62,5%**)	3 (**42,86%**)	3 (**60%**)
Severe (3)	-	1 (**14,29%**)	-

The second Banff criterion assessed was *vasculitis (v)*. To determine the degree of vasculitis, the presence of subendothelial mononuclear cells as well as intimal fibrosis and the degree of vascular occlusion are taken into consideration, as follows:

v0—No vasculitis (**Fig.44a**)
v1—Mild to moderate intimal vasculitis in at least 1 vessel cross section (**Fig.44b**)
v2—Severe intimal vasculitis with at least 25% luminal area lost in at least 1 vessel cross section (**Fig.44c**)
v3—Transmural vasculitis and/or arterial fibrinoid change and medial smooth muscle necrosis with lymphocytic infiltrate in vessel (**Fig.44d**)

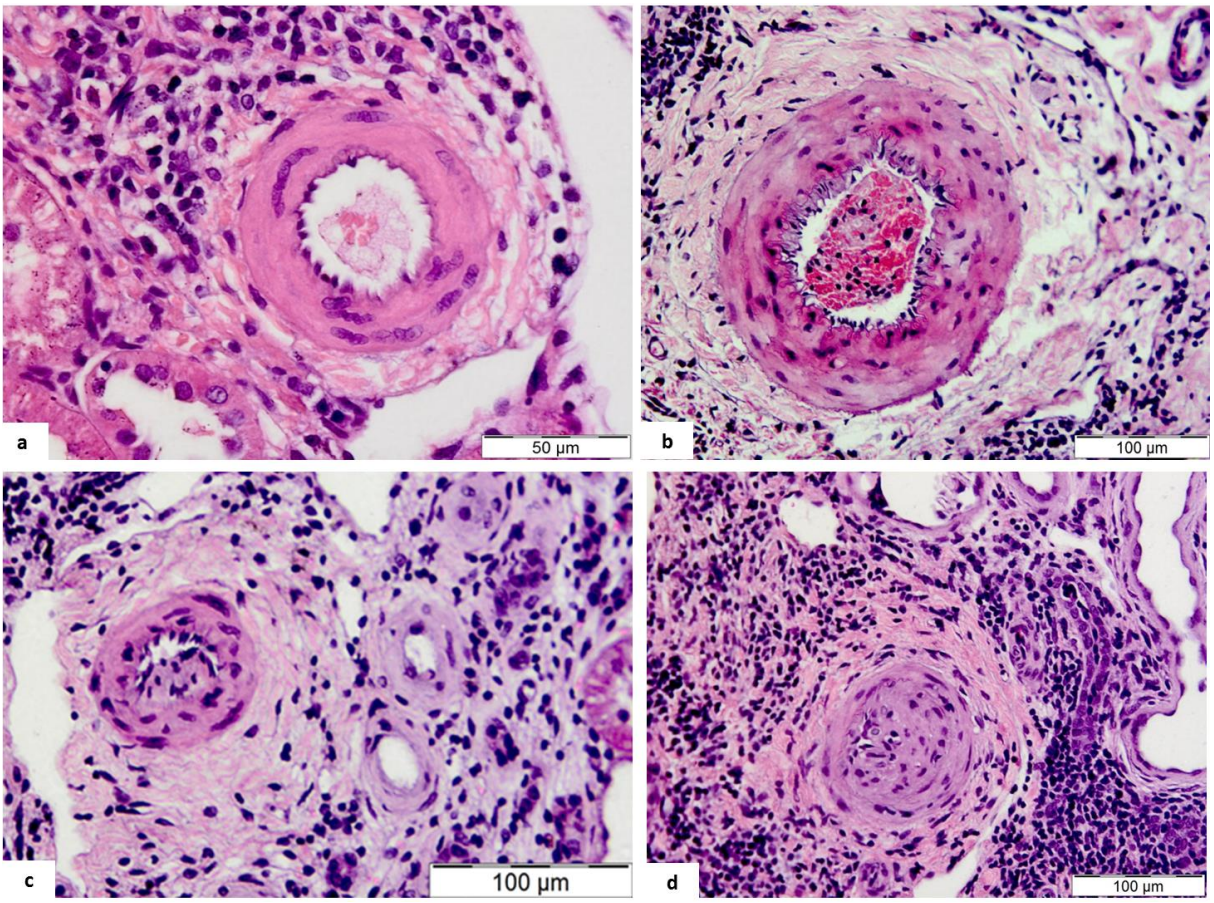

Fig.44: Representative images of the four vasculitis scores (v) in the Banff classification.**a)** *v0*=No vasculitis; **b)** *v1*=Mild to moderate intimal vasculitis in at least 1 vessel cross section; **c)** *v2*=Severe intimal vasculitis with at least 25% luminal area lost; **d)** *v3*=Transmural vasculitis and/or arterial fibrinoid change (H-E, 200X)

In terms of vasculitis, the scores went from no (0) to moderate (2) vasculitis, with no animal showing severe signs of vasculitis in any of the groups. As observed for tubulitis, the ABCB5 cell-treated group showed the worst outcome, with 28,57% of animals presenting moderate vasculitis. The CM-treated and control groups did not reach vasculitis scores above

v1, meaning animals presented mild signs of vasculitis. The CM-treated group was slightly worse than the control group, but slightly better than the ABCB5 cell-treated group (**Table 3**).

Table 3: Vasculitis (*v*) scores in the allograft sections of KTx control (n=8), KTx+ABCB5 (n=7) and KTx+CM (n=5) 98 days after transplantation

Vasculitis (v)	KTx control	KTx+ABCB5	KTx+CM
None (0)	1 (**12,5%**)	1 (**14,29%**)	-
Mild (1)	7 (**87,5%**)	4 (**57,14%**)	5 (**100%**)
Moderate (2)	-	2 (**28,57%**)	-
Severe (3)	-	-	-

The third criterion analysed was *interstitial fibrosis (ci)*, which was assessed with Masson-Goldner trichrome staining, which specifically demonstrates the presence of connective tissue, as follows:

ci0—Interstitial fibrosis in up to 5% of cortical area.
ci1—Interstitial fibrosis in 6 to 25% of cortical area (**Fig.45a**)
ci2—Interstitial fibrosis in 26 to 50% of cortical area (**Fig.45b**)
ci3—Interstitial fibrosis in >50% of cortical area (**Fig.45c**)

As previously mentioned, interstitial fibrosis is very severe in the Fischer-Lewis model, and is the result of chronic cellular and humoral responses against the donor foreign MHC molecules. In accordance with this, renal sections of 75% of the animals in the control group were classified as ci3. Interstitial fibrosis was even worse in the ABCB5 cell treated group where 85,7% of these animals had ci3 scored renal sections. On the other hand, CM treatment ameliorates interstitial fibrosis slightly, with 60% of the animals in this group presenting a ci3 score (**Table 4**).

Table 4: Interstitial fibrosis (*ci*) scores in the allograft sections of KTx control (n=8), KTx+ABCB5 (n=7) and KTx+CM (n=5) 98 days after transplantation

Interstitial fibrosis (ci)	KTx control	KTx+ABCB5	KTx+CM
None (0)	-	-	-
Mild (1)	1 (**12,5%**)	-	1 (**20%**)
Moderate (2)	1 (**12,5%**)	1 (**14%**)	1 (**20%**)
Severe (3)	6 (**75%**)	6 (**85,7%**)	3 (**60%**)

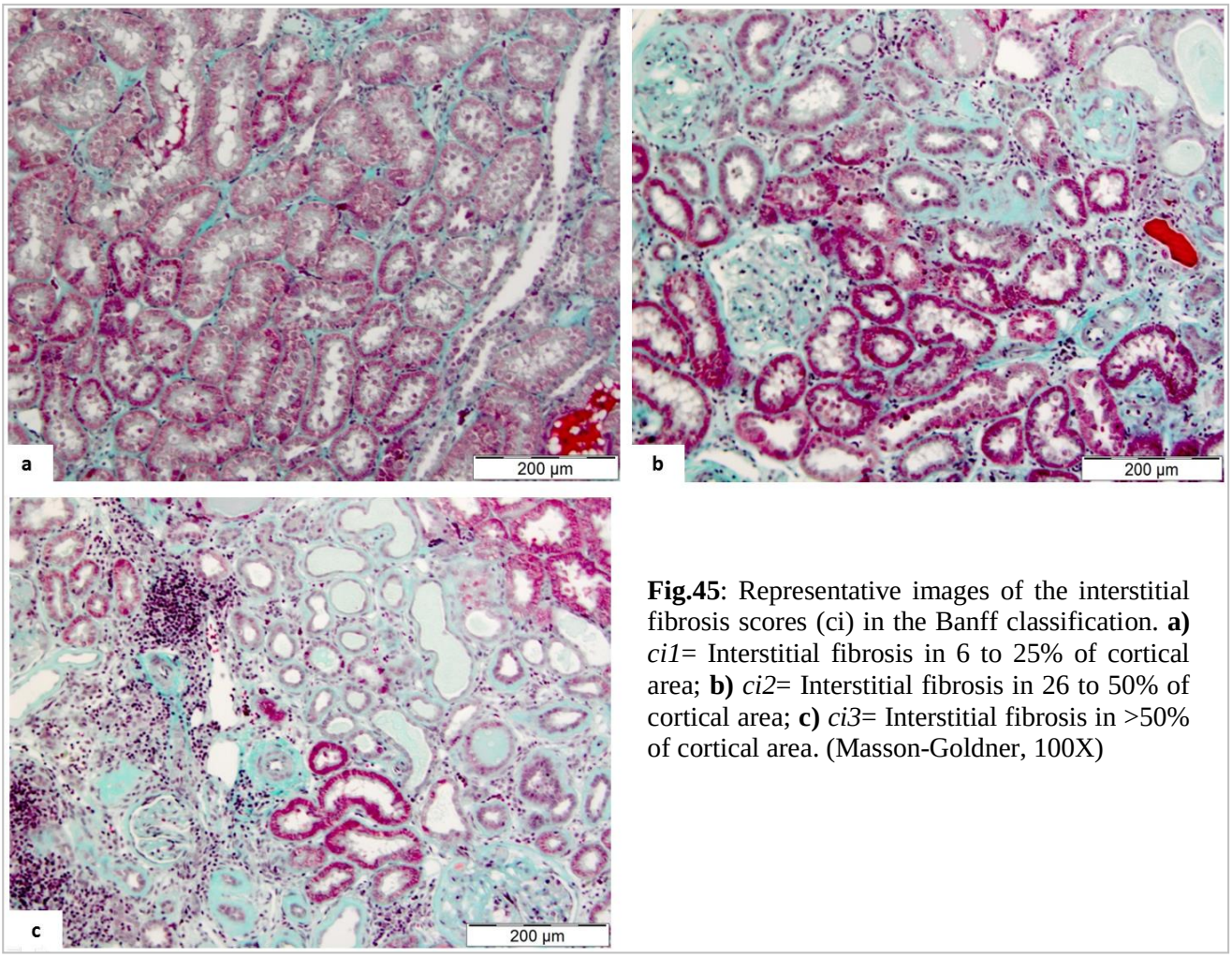

Fig.45: Representative images of the interstitial fibrosis scores (ci) in the Banff classification. **a)** *ci1*= Interstitial fibrosis in 6 to 25% of cortical area; **b)** *ci2*= Interstitial fibrosis in 26 to 50% of cortical area; **c)** *ci3*= Interstitial fibrosis in >50% of cortical area. (Masson-Goldner, 100X)

The degree of interstitial fibrosis is tightly connected to *tubular atrophy (ct)*, which is the next Banff criteria assessed. Tubular atrophy is characterized by a thickening of the tubular epithelial cell basement membrane causing a reduction of the tubular diameter that leads to its malfunction. The assessment was performed as follows:

ct0—No tubular atrophy.
ct1—Tubular atrophy involving up to 25% of the area of cortical tubules (**Fig.46a**).
ct2—Tubular atrophy involving 26 to 50% of the area of cortical tubules (**Fig.46b**).
ct3—Tubular atrophy involving in >50% of the area of cortical tubules (**Fig.46c**).

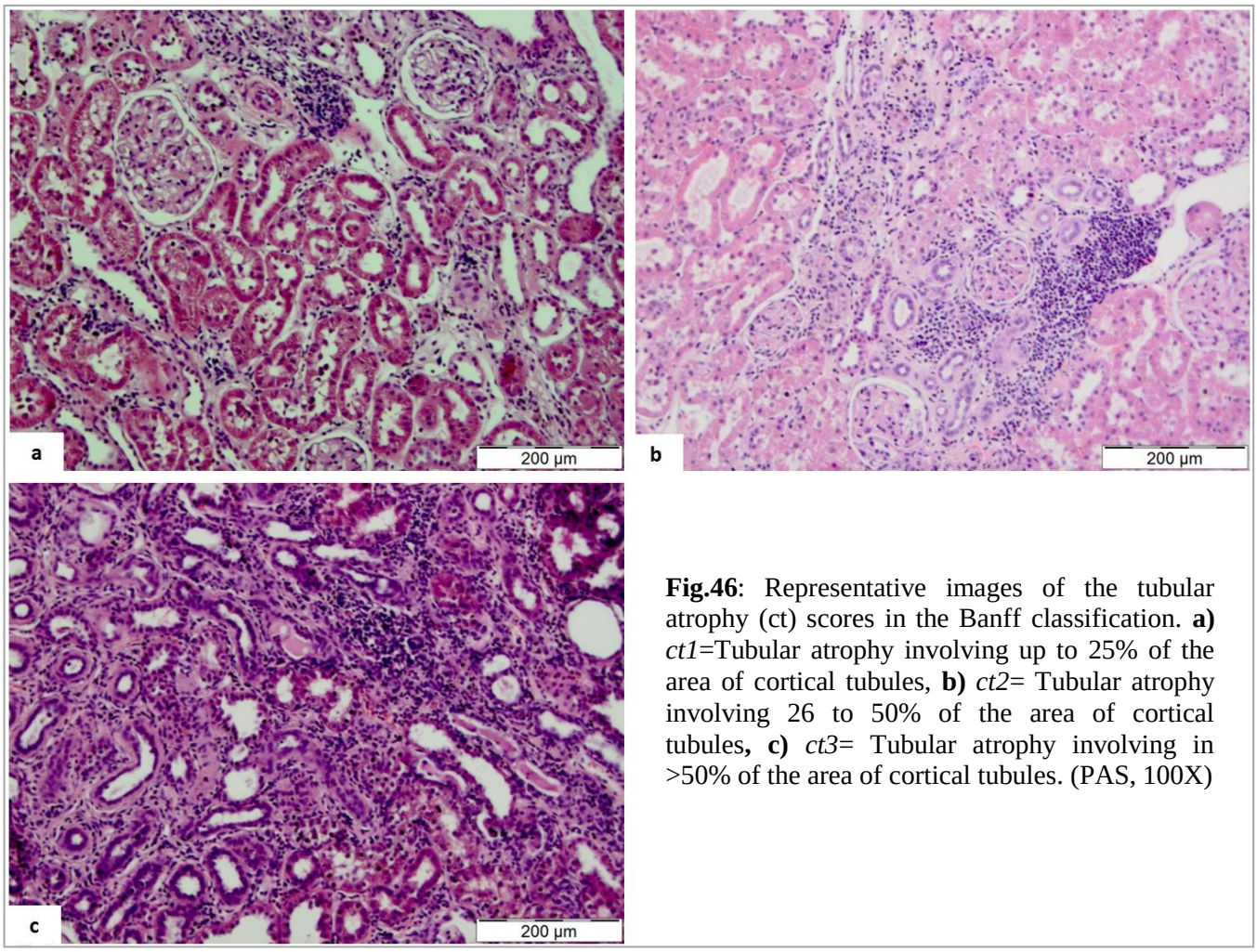

Fig.46: Representative images of the tubular atrophy (ct) scores in the Banff classification. **a)** *ct1*=Tubular atrophy involving up to 25% of the area of cortical tubules, **b)** *ct2*= Tubular atrophy involving 26 to 50% of the area of cortical tubules**, c)** *ct3*= Tubular atrophy involving in >50% of the area of cortical tubules. (PAS, 100X)

The severity of tubular atrophy corresponded to the severity observed for interstitial fibrosis, as no animal in any of the groups showed signs of no tubular atrophy. In the control group, 62,5% of the animals presented severe tubular atrophy, which was worsened with the cell treatment with 71,43% of the animals presenting a *ct3* score. The scores for CM-treated animals were milder, with 40% of the animals showing *ct3* and 40% of the animals presenting mild tubular atrophy (*ct1*) (**Table 5**)

Table 5: Tubular atrophy (*ct*) scores in the allograft sections of KTx control (n=8), KTx+ABCB5 (n=7) and KTx+CM (n=5) 98 days after transplantation

Tubular atrophy (ct)	KTx control	KTx+ABCB5	KTx+CM
None (0)	-	-	-
Mild (1)	2 (**25%**)	1 (**14,29%**)	2 (**40%**)
Moderate (2)	1 (**12,5%**)	1 (**14,29%**)	1 (**20%**)
Severe (3)	5 (**62,5%**)	5 (**71,43%**)	2 (**40%**)

4. Discussion

4.1. Long-term renal outcomes of unilateral kidney ischaemia without contralateral nephrectomy

One of the goals of this project was to assess whether the MSC treatment leads to amelioration of chronic renal damage after warm ischaemic injury. To that end, we first aimed to find the most suitable murine ischaemia-induced AKI model to prompt strong clinical and morphological end-points associated to progressive CKD to subsequently determine therapeutic efficacy of MSC. The vast majority of murine AKI models are based on renal ischaemia. Depending on the duration of renal ischaemia, these models can inflict severe kidney function impairment and hence are valuable tools to study the mechanisms underlying the initial injury[135].However, long-term studies showing progression to chronic kidney disease after an ischaemic insult are scarce and the observation time in most cases is too short to draw reliable conclusions[45].The two models of ischaemia- induced AKI that have been studied mostly in this context are: induction of renal ischaemia followed by nephrectomy of the contralateral kidney and similarly, without removal of the non-ischaemic kidney. The latter model seems more suitable as it allows longer ischaemia times without increased mortality rates.[44] Therefore, for our first approach we decided to implement the model without contralateral nephrectomy after ischaemic injury in order to assess whether indeed signs of progressive CKD were observed in the long-term. However, the main down-side is the difficulty to monitor the function of the post-ischaemic kidney in the acute phase when a fully functional kidney is also present. Renal function of the post-ischaemic kidney is mostly studied at later time-points when the non-ischaemic contralateral kidney is removed.

Additionally, it is important to remark that most long-term studies to assess progression to CKD after ischaemic injury base their conclusions regarding kidney function deterioration solely on the assessment of proteinuria[136,137]. Proteinuria has been classically regarded as a reliable parameter to assess progressive kidney function deterioration. However, a recent epidemiological study suggests that the combination of GFR and proteinuria are the best predictors to assess progression to CKD[138]. Consequently, we implemented both the assessment of proteinuria and GFR in our study. The latter was performed by a minimally invasive technique that measures the clearance of FITC-S transcutaneously. Since FITC-S is exclusively cleared by the kidney, it is an optimal marker for the estimation of GFR[126].

When ischaemia-reperfusion injury was induced in non-uninephrectomized animals, kidney function parameters remained within the non-pathologic range, until the contralateral non-ischaemic kidney was removed. This underscores the difficulties in measuring renal function parameters of the ischaemic kidney in the acute phase. Proteinuria was the only exception, being mildly increased (≥22mg/24h) at day 150 when the non-ischaemic kidney was still present. Hence, even though FITC-S clearance was not impaired, proteinuria was present in these animals. This phenomenon has been reported in epidemiologic studies where 25% of patients with proteinuria also presented normal GFR[138]. As a matter of fact, the presence of proteinuria in absence of impaired GFR may identify a subpopulation of patients that have an increased risk to progress to chronic kidney disease[139].

Interestingly, in this model the right non-ischaemic kidney was significantly increased in size compared to the right kidney of control animals that were not subjected to renal ischaemia. In contrast, the ischaemic kidney was small and showed an irregular and a wrinkly surface possibly due to accumulation of fibrotic tissue. A compensatory growth of the

contralateral non-ischaemic kidney is therefore expected and known to occur after kidney injury. Although the underlying mechanisms are not completely elucidated, it is believed that loss of nephron mass results in the local production of several growth factors, e.g. Insulin-like growth factor (IGF), fibroblast growth factor (FGF), vascular epithelial growth factor (VEGF), epidermal growth factor (EGF), nerve growth factor (NGF) and hepatocyte growth factor (HGF), which act in an autocrine or paracrine manner mostly leading to hyperplasia or hypertrophy. [140 141]

Another compelling finding was the presence of different sized cysts in half of the animals that were subjected to AKI. The presence of solitary cysts located in the renal cortex (cysts stage I) in asymptomatic individuals is considered benign[142]. However, in individuals with kidney function impairment a simple renal cyst is associated with poorer outcome and is considered a feature toward progression to chronic kidney disease[143]. Loss of functional tissue may trigger residual nephrons to undergo epithelial hypertrophy and hyperplasia, leading to increased size of tubular structures and thus cyst formation. Also fibrosis facilitates cyst formation as the normal flow of urine is compromised and thus, fluid accumulates within the hyperplastic renal tubules[144].

Progressive chronic kidney disease is associated with interstitial fibrosis (IF). IF is the result of persistent stimuli that causes sustained production of growth factors, proteolytic enzymes, angiogenic factors and fibrogenic cytokines that promote extracellular matrix (ECM) deposition between tubules and peritubular capillaries, eventually leading to the disruption of the normal tissue architecture[145].The degree of IF was quantified in the post-ischaemic kidneys using a technique in which the positively stained ECM components were identified and quantified as percentage of the whole surface area of a particular renal section. This technique let us put aside the use of IF scores, which have the disadvantage of being less reproducible and objective, as usually the results vary depending on the observer[146]. As to be expected, the percentage of IF presented in the cortex was significantly higher than in the control group. However, the degree of IF observed in the post-ischaemic kidneys was relatively mild, with a maximum value of 0,676% out of total cortex. A recent study has shown that IF is an imperfect predictor of chronic kidney disease in some patients, emphasizing the superiority of reliable kidney function parameters, like eGFR[147]. Thus, the model employed in this approach leads to clinically relevant endpoints, e.g. renal function deterioration, interstitial inflammation and cyst formation, making it a good candidate model for interventional studies.

4.2. Role of the kidney mass at the time of ischaemic injury in the long-term renal outcomes

Our second approach was based on the existing discrepancy in scientific literature regarding the role of the renal mass at the time of ischaemic injury in animal models. Some authors suggest that unilateral kidney ischaemia with contralateral nephrectomy at the time of injury leads to a worse long-term outcome[136,148]; whereas others claim that unilateral ischaemia without contralateral nephrectomy worsens outcome, as the presence of an undamaged contralateral kidney might have a deleterious effect rather than a protective one in the long-term[49,149].Thus, in order to shed light upon this topic we aimed to compare the long-term functional and morphological outcomes between the aforementioned models.

Kidney function was assessed in the early phase of the ischaemic injury (1-3 days after AKI induction) to understand how the initial response to injury might affect the long-term

outcomes. As expected, the initial ischaemic injury led to profound kidney function impairment in the nephrectomised animals 1 day after AKI-induction. Function remained impaired at day 3 after AKI and returned to baseline values after 7 days. On the other hand, non-uninephrectomised animals showed kidney function parameters values within the physiological range at all the early time points, meaning that the non-ischaemic kidney was able to compensate the injury to the contralateral kidney and thus, the overall kidney function was preserved. However, despite this initial impact on kidney function, uninephrectomised animals were able to recover and showed no signs of functional deterioration at day 177 after AKI. In contrast, non-uninephrectomised animals presented signs of renal impairment once the non-ischaemic kidney was removed.

Histopathological findings are in agreement with functional assessment as uninephrectomised animals presented less ED1+ macrophage infiltration and thus, a lesser degree of interstitial fibrosis in the cortex compared to non-uninephrectomised animals when kidney sections were analysed 180 days after the initial ischaemic injury. Interestingly, the lesion pattern found was different among the two groups. In the uninephrectomised animals a higher number of greatly dilated tubules was found, mostly in the inner cortex; whereas in the non-uninephrectomised group tubular dilation to such extent was not observed and fibrotic tissue accompanied by atrophic tubules were found in the very outer cortex. This higher extent of tubular dilation in uninephrectomised animals could be explained by the fact that initial injury lays on a single kidney and tubular dilation is found during acute tubular necrosis, where tubular epithelial cells undergo apoptosis after the ischaemic injury, detach from the basement membrane and obstruct the tubules, leading to their dilation[148150].

In the light of our results, it can be inferred that unilateral ischaemia without contralateral nephrectomy at the time of injury leads to a more severe long-term functional and morphological kidney deterioration. The reasons for this are not fully known, although it has been observed by other authors.[49,151,152]

The question that needs to be discussed is the role of the contralateral kidney in ischaemia induced AKI. In the following I will discuss the studies that provided evidence that the presence of the contralateral kidney is not beneficial for renal function recovery after an ischaemic insult, and therefore unilateral nephrectomy might ameliorate long term renal function decline.

It is believed that presence of a contralateral kidney intensifies early post-ischaemic renal vasoconstriction, thus increasing renal hypoperfusion[149]. Therefore, the potential protective role of uninephrectomy (uNx) is a phenomenon that has been extensively studied. It has been suggested that uNx leads to a reduction of apoptotic cells and DNA fragmentation and enhanced proliferation of tubular cells leading to tissue repair in the remnant kidney[153]. This might be caused by an increased intrarenal expression of several growth factors such as EGF, IGF and HGF in the post-ischaemic kidney, favouring tissue regeneration. Also thromboxane A_2 (TxA_2) synthesis is decreased in the post-ischaemic kidney, which may cause less vasoconstriction, less secondary ischaemia und thus less apoptosis[154]. Not only TxA_2, but also the prominent vasoconstrictor endothelin-1 (ET-1) is decreased in uNx animals compared to non uNx. Compatible with this, it has been shown that administration of ET-1 receptor antagonists can amelioration of GFR decline and tubular injury[155].The protective role of uNx in ischaemic injury has also been demonstrated in dynamic contrast enhanced MRI (DCE-MRI) studies, in which it was found that uNx enhances perfusion to the inner medulla in the remnant kidney[152].Gene expression profiling studies in AKI-induced uninephrectomised animals have shown that uNx mostly downregulates genes involved in

would healing, ECM and myofibroblast differentiation[152,156].These gene expression results correlate with our histopathology findings, as a much milder degree of interstitial fibrosis was found in the post-ischaemic kidneys of uninephrectomised animals.

Another interesting hypothesis is that the ischaemic insult to one kidney leads to injury to the non-ischaemic kidney because of kidney cross-talk. This is reflected by a change in macrophage population (M1)[151,157], increased pro-inflammatory cytokines such as TNF-α which was much more prevalent in tubular cells of ischaemic kidneys, in contrast to the non-ischaemic kidneys, where higher TNF-α expression is observed in glomerular cells, suggesting that circulating factors might be involved in this remote cellular injury[158].

In the present study, the non-ischaemic kidneys and the ischaemic kidneys were collected for histopathology assessment 170 or 180 days after ischaemic induction, respectively. At these time points, ED1+ macrophages were not increased in the non-ischaemic kidneys, and no signs of morphological alterations or tissue fibrosis were observed. However, even though no histopathological changes were observed in the non-ischaemic kidneys, the finding that the long-term injury is more severe when a functional kidney is present, warrants further studies to address if this is attributable to kidney cross-talk.

4.3. Role of human adipose-derived MSC (hASC) in the amelioration of chronic renal damage caused by warm ischaemia

In recent years, adipose-derived MSC (ASC) have gained relevance over bone marrow-derived MSC (BM-MSC) in preclinical studies because they are easier to obtain and in larger quantities using less invasive techniques. For instance, it has been reported that from lipoaspirates 2% of nucleated cells can be recovered as MSC in comparison to the 0,002% obtained from bone marrow[159]. Furthermore, several *in vitro* studies have shown that ASC present higher immunomodulatory capacities compared to BM-MSC[160,161]. In the light of the results of the previous experiments in the AKI models, hASC, treatment was implemented in the model leading to more long-term kidney function deterioration.

When our experiments were being planned, one of the main setbacks was the lack of consensus in literature concerning the most suitable administration route and cell dose to achieve the most favourable outcome, as it would depend on several factors like species or target organ(s). In our study, hASC were injected intravenously, representing the most commonly used administration route in clinical practise. Although in one study intra-arterial administration in the aorta has been reported to be more efficient than intravenous injection, as it ensures that the cells reach the kidney[162]; intra-aortic injection was not considered in our study because of the need to subject the animals to a second surgical procedure within a short period of time. Even though intravenous injection may lead to hASC entrapment into the lung capillary system[163], a large body of evidence suggests that the therapeutic efficacy of MSC is independent of cell engraftment into the target organ. In fact, secretion of paracrine factors is recognized as the primary mechanism used by MSC to promote regeneration of the injured tissue[111,164]. Similar to the administration route, also the amount of stem cells that should be injected is ambiguously discussed, albeit that most rodent-based preclinical models use a cell concentration that ranges from $5x10^5$ to $1x10^6$ cells[165]. The assessment of therapeutic efficacy of MSC in AKI murine models has been widely addressed in preclinical studies that focus mostly in the acute phase of the injury and use autologous or allogeneic cells as a source for treatment[166]. In this study, however, human ASC were incorporated in a rat model

of ischaemia-induced AKI to assess the long-term outcomes. Human MSC have been reported to be hypoimmunogenic or 'immune privileged', as they display intermediate levels of HLA class I, no basal expression of HLA class II and no expression of the costimulatory molecules CD80, CD86 and CD40. However, in recent studies the hypoimmunogenic status of MSC is being questioned[167], as it was shown that MHC mismatched MSC are able to induce both cell-mediated and humoral immune responses *in vivo*[168,169] . In our study, after cell injection all animals were under observation for at least 2 hours, as it has been reported that intravenous cell injection might present side effects ranging from death by lung emboli formation to fever or nausea[170]. No incidences were reported after IV injection, it was well-tolerated and animals showed no signs of respiratory distress or lethargy caused by fever. Nevertheless, this lack of clinical signs does not necessarily correlate with immune responses or rejection of MSC, so in future studies it would be interesting to assess T cell-mediated and humoral responses through *ex-vivo* assays and see whether there is a correlation with the outcome of the treatment.

It has been shown that neither human nor murine MSC are able to induce any immunoregulatory action *per se* unless they have been previously stimulated by IFN-γ. In the presence of an inflammatory environment (high levels of IFN-γ and TNF-α) MSC are activated and adopt an immunosuppressive phenotype (MSC2), secreting soluble inhibitory factors. It seems that IFN-γ induces the expression of IDO-1[171], the first and rate-limiting enzyme of tryptophan degradation through the kynurenine pathway. Suppression is mostly explained by deprivation of tryptophan for T lymphocyte proliferation[172] but can also be explained by the cytotoxic action of kynurenines on T lymphocytes and NK cells[173]. Similarly, induction of iNOS in murine MSC by IFN-γ and TNF-α is a prerequisite for their immune suppressive properties. Other immune-inhibitory molecules such as PGE_2 are produced by both human and rodent MSC[174].Even though human MSC cannot be activated by murine IFN-γ, human MSC have shown cross-species reactivity with murine TNF-α [175],which may explain the success of human MSC in a number of murine models.[85] In the absence of an inflammatory milieu (low levels of IFN-γ and TNF-α) MSC adopt a pro-inflammatory phenotype (MSC1)[176].In this study, cell treatment was implemented at day 14 after AKI induction. Based on gene expression profiling studies it is likely that at his time point sufficient pro-inflammatory cytokines (e.g.TNF-α) are present in the renal environment that would allow hASC to display a MSC2 immunosuppressive behaviour[177]. Indeed, one of the main findings regarding hASC treatment in this ischaemia-induced AKI model was the highly significant decrease in ED1+ macrophages in the post-ischaemic kidneys. Macrophages constitute the first wave of inflammatory cells that migrate to the kidney during ischaemia-reperfusion injury, and thus, they play an important role in activation and continuation of the inflammatory response. They are also involved in tissue fibrosis, as once macrophages are activated by IFN-γ and TNF-α, they subsequently produce TGF-β1, which acts as a feedback mechanism in inflammation resolution, but also triggers fibroblast activation and differentiation into myofibroblasts, which are the main producers of ECM component[178].

The mechanism by which hASC might have been able to reduce ED1+ macrophages in the post-ischaemic kidneys is in agreement with what has been previously stated. hASC injection in a pro-inflammatory environment where TNF-α is present, adopt an immunosuppressive phenotype. This might lead to PGE_2 production by hASC, which can polarize monocytes to M2 macrophages, a subtype of macrophages which produces anti-inflammatory cytokines and shows higher phagocytic activity. This mechanism of action is supported by an *in vitro* study by Manferdini *et al.,*[86]where it was found that when M1 macrophages from synovium of osteoarthritis patients were co-cultured with hASC, M1 markers like IL-1β, IL-6, MIP1α/CCL3 were decreased in indirect and direct co-culture

conditions. Furthermore, M2 markers IL-10, CD163 and CD206, were enhanced, meaning that hASC were able to cause polarization to M2 macrophages. In addition, it was also found that PGE2 was upregulated in the co-cultures and that blocking PGE2 with an antagonist led to no decrease in TNF-α, IL-6 and no increase in IL-10, CD163 and CD206, suggesting that PGE2 presents a specific role in this mechanism. This polarization to M2 macrophages mediated by PGE2 is produced by cell-to-cell contact or when PGE2 binds to the EP2 and EP4 receptors (prostaglandin E2 receptor subtype 2 and 4) in the macrophages[179].

It must be noted that ED1 is a monoclonal antibody directed against the rat protein CD68, which is a pan marker of macrophages, meaning that it is not able to distinguish between M1 and M2 macrophages[180]. Nevertheless, the fact that hASC treatment was able to reduce the degree of kidney fibrosis in the post-ischaemic kidneys supports the idea that cell treatment was able to switch macrophage activity to an anti-inflammatory state.

On the other hand, one of the pitfalls of this study is the administration time chosen. Even though it has been shown that 14 days after AKI induction there is still ongoing inflammation, it is a rather late time point to implement a treatment and a quite improbable scenario in clinical practise. This time point was initially chosen because hASC treatment was conceived to boost repair, which takes place later in time, toward adaptive mechanisms, and thus help halt the progression to CKD[38]. Nevertheless, as it has been stated, a highly pro-inflammatory environment confers MSC the immunomodulatory phenotype, and therefore, in future studies, treatment should be implemented in the early phases of AKI induction.

4.4. Role of human ABCB5+ cells and its derived CM on the amelioration of chronic renal damage after cold ischaemia and minor MHC disparity

In contrast to what occurs in humans[181], our murine warm ischaemia approaches led to a rather mild degree of kidney function impairment and overall kidney fibrosis in the long-run, even when the initial ischaemic insult was severe. Therefore, we aimed to find a chronicity model resulting in strong clinical and morphological end-points and wondered whether this could be achieved by implementing cold ischaemia and minor MHC disparity. Thus, in this approach a Fischer-Lewis allograft rejection model, with 8 hours of cold ischaemia was employed. To investigate whether cell therapy could mitigate the functional and histopathological features found in this model, human stromal cells expressing the ATP-binding cassette B member 5 P-glycoprotein (ABCB5+ cells) were implemented as intervention strategy. P-glycoproteins and members of the ABC superfamily are cell membrane proteins that use an ATP-dependent pump to efflux different types of xenobiotics out of the cell and mediate drug resistance in mammalian cancers, as well as physiologic transport, differentiation and survival in non-cancerous cells. ABCB5 was first described by Frank *et al*. on the CD133-positive progenitor cell subpopulation in human epidermal melanocytes in 2003[182], and it has also been found in human placenta[183] as well as in corneal limbal stem cells thereafter[184]. Interestingly, ABCB5 has been shown to identify a phenotypically distinct subpopulation of dermal cells that can exert immunomodulatory actions[185], and since more than 90% of ABCB5+ cells fulfil the criteria for MSC (no expression of CD34, CD31 and CD45 and positive expression of CD29, CD44, CD49e, CD73, CD105 and CD166)[84], they are considered a subtype of MSC with similar therapeutic potential as the adipose-derived or bone marrow-derived counterparts. Furthermore, ABCB5+ cells have been used with promising results in a murine heart allograft rejection model[185] and are being tested in a number of clinical trials (ie: acute on chronic liver failure, epidermolysis bullosa, chronic venous ulcers[186-188]).

Additionally, we also aimed to assess whether cell-free therapy in the form of ABCB5-derived conditioned media showed better outcomes compared to the cell counterpart. MSC-CM content has been reported to differ greatly depending on the cell type used as a source and the culture conditions[189], but several proteomic analyses have revealed that angiogenic factors (angiogenin, angiopoietin, VEGF), chemokines (CX3CL1, CCL1, CCL2, CCL5…), cytokines (IL-1α, IL-1β, IL-10, TNF- α, IFN-γ, M-CSF, TSG-6…), growth factors (HGF, EGF, PIGF, PDGF, BMP-7…) and other proteins (leptin, adiponectin…) are general components of MSC-CM[190]. In addition, MSC-CM is reported to contain extracellular vesicles which carry mRNAs involved in transcription, immune regulation, cell cycle regulation, angiogenesis, actin cytoskeleton regulation and extracellular matrix remodelling [191,192]. Furthermore, several clinical trials using MSC-CM are being conducted for a number of conditions (ie: retinitis pigmentosa, osteoarthritis, chronic ulcer wounds[193-195]).

Before assessing the therapeutic efficacy of the treatments in a transplantation model it is important to elucidate how much of the functional and morphological changes observed are due non-allogeneic factors like ischaemia-reperfusion injury and cold preservation and how these changes vary when allogeneic factors are also involved. For that reason, syngeneic transplantation data is important to assess the changes caused solely by IRI and cold preservation. In a study by Gottmann *et al*., syngeneic transplantation in Lewis rats (Lew-Lew) was performed after 24 hours of cold preservation, and the outcome of the procedure was assessed for 24 weeks[196]. Throughout the experimental time it was observed that p-crea values remained stable and within the physiologic range, and that a slight proteinuria was developed in the beginning, but did not progress over time. As for the Banff classification, the totality of the animals showed no signs of interstitial infiltration (ci0), tubular atrophy (ct0), glomerulosclerosis (cg0) or vasculopathy (v0). We therefore used in our study an allogeneic transplantation model with minor MHC differences, and implemented a cold ischaemia time of 8 hours. This resulted in severe renal function impairment at all time points after transplantation accompanied by moderate tubulitis, mild vasculitis, severe interstitial fibrosis and severe tubular atrophy. Hence, syngeneic transplantation after 24 h of ischaemia leads to a milder outcome compared to an allogeneic transplantation model with shorter cold ischaemia time (8h). This underscores the role of the ongoing allogeneic response on top of the IRI. The functional and morphological findings in the Fischer-Lewis model used in our study correlate with what has been described in literature[197].

Like for the AKI experiments, transcutaneous assessment of kidney function was implemented in this model by measuring FITC-S clearance. It is worth to mention that this technique was quite troublesome in animals with severe kidney function deterioration, as the optimal FITC-S dosage had to be adjusted various times in order to maintain in a fluorescence intensity range that allows capturing of the maximum fluorescence intensity during the flooding phase. Yet the peak needs to be sufficiently high for obtaining a valid elimination curve. Additionally, it must be noted that in this section of the study we faced great peri-operative mortality due to the severity of the surgical procedure. As a consequence, group sizes were dramatically reduced, hence the lack of statistical significance observed for the clinical and histopathological parameters among the three experimental groups.

Similar as reported for the AKI experiments, the time of ABCB5 cell administration plays a crucial role in transplantation outcome. It has been reported that MSC administration before renal transplantation leads to MSC engraftment into secondary lymphoid organs, favouring graft survival[198]. In contrast, a single post-transplant injection has been shown to induce MSC migration directly into the graft, resulting in neutrophil infiltration, complement deposition and acute kidney injury, both in animal and human studies[199]. The first study with

the use of ABCB5+ cells *in vivo*[185]was a heterotopic allogeneic heart transplantation model in C57BL/6 mice. It was found that when recipient-derived ABCB5+ cells were injected 7 days before transplantation, no significant graft survival was observed. Similarly, donor- BALB/c derived ABCB5+ injection at the same time point led to modest prolongation of graft survival. However, when a third-party C3H/HeJ heart was transplanted into a C57BL/6 mouse and BALB/c-derived ABCB5+ cells were injected, survival of the graft was greatly increased, suggesting that the enhancement of survival mediated by ABCB5+ cells required previous allogeneic stimulation. Taking this into account, we considered one day before kidney transplantation as the optimal time point for cell administration in our study. Because it also was reported that survival of exogenously administered MSC decays after 24 hours[200]we performed a second cell injection 17 days after kidney transplantation. This time point was chosen because the animals underwent contralateral nephrectomy 10 days after kidney transplantation, allowing them to recover from the surgical procedure before cell injection.

As it has been previously mentioned, the Fischer-Lewis model of chronic allograft rejection leads mostly to histopathology lesions associated with T-cell mediated rejection. Therefore, hABCB5+ treatment was aimed to decrease the main histopathologic features associated with T-cell mediated rejection, namely tubulitis, interstitial fibrosis and endarteritis. ABCB5+ cells have been shown to exert immunosuppressive effects on effector T cells and to induce the production of CD4+CD25+Foxp3+ Tregs via PD-1/PD-L1 signaling interactions *in vivo* and *in vitro*[185]. PD-1 is a negative regulator of T cell activity and when it binds to either of its two ligands (PD-L1 and PD-L2) it inhibits kinase signalling pathways that lead to CD4+T cell activation[201]. Our findings, however, suggest that hABCB5+ were not only unable to suppress T mediated rejection, but rather show exacerbation in histological findings for T-cell mediated rejection, albeit that this was not significant. The reasons for this are still elusive. Notwithstanding that in some preclinical transplantation studies cell pre-treatment was associated with better outcome[198], in a safety assessment study using hACB5+ in mice it was found that after IV injection cells were mostly detectable in the lungs[122], and not in the lymphoid tissue. Moreover, as discussed earlier, the injection of MSC in the absence of a pro-inflammatory environment might lead to a MSC switch toward a pro-inflammatory phenotype (MSC1) and as a consequence, to enhancement of T cell responses[176]. Most importantly, MSC have been shown to express and secrete PD-L1 and PD-L2 only when exposed to IFN-γ and TNF-α[202]. Hence pre-treatment bears the risk of MSC switching if at the time of injection no inflammation is present.

On the other hand, ABCB5+ cells role on macrophage activity is associated to their ability to trigger the switch from M1 to M2 macrophages trough the secretion of IL-1 receptor antagonist (IL1-RA)[128].As observed for T cells, kidney allograft sections of hABCB5+ treated animals presented a trend toward increased infiltration of ED1+ macrophages compared to CM-treated or the control group. Macrophages upregulate mediators involved in microvascular damage, leucocyte recruitment and induction of donor-specific cytotoxic responses[203], and it has been reported that 38-60% of infiltrating leukocytes in the rejecting organs are macrophages, being their presence is associated with poorer outcome[204]. In the presence of a pro-inflammatory environment, MSC have been shown to increase their expression of IL-1RA[87], which in our study, could mean that after the second injection, 17 days after KTx, the conditions were favourable to induce macrophage polarization to M2 phenotype. However, prolonged activation of M2 macrophages may also lead to activation of resident fibroblasts through continuous activation of TGFβ and growth factors, thus promoting fibrosis[203]. As a matter of fact, in studies using biopsies from patients undergoing chronic allograft rejection, M2 macrophages have been found to be the predominant macrophage population[205], and this finding has been linked to the development of a higher

extent of interstitial fibrosis and tubular atrophy[206]. Therefore, even though in our study ED1staining is not able to differentiate between M1 and M2 macrophages, the higher interstitial fibrosis and tubular atrophy scores in the cell-treated group could be explained by a macrophage shift toward M2 phenotype by ABCB5+ cells, that promoted fibrosis in the long-term. This needs to be addressed in future studies.

Although not statistically significant, treatment with conditioned media showed a trend towards milder vasculitis, interstitial fibrosis and tubular atrophy Banff scores compared to control and cell-treated group. Likewise there was a trend for a better FITC-S clearance at day 98 after transplantation in the CM treated group. In this context, ABCB5+-derived CM might have helped reduce vasculitis through enhancement of pro-angiogenic mechanisms, as one of the main properties attributed to MSC-CM is their angiogenesis potential. In a study by Estrada *et al.*[207] it was found that MSC-CM can induce angiogenesis via cysteine-rich protein 61 (Cyr61), which was found to induce neovascularization in vivo. This angiogenic effect has also been reported to take place through the release of exosomes by MSC, which are able to deliver miRNA to endothelial cells, subsequently upregulating angiogenic factors[208]. As previously mentioned, the treatment with ABCB5+ derived CM lead to a milder interstitial fibrosis and tubular atrophy score, which can be attributed to the reported anti-fibrotic potential of CM. MSC-CM has been shown to attenuate fibrosis in unilateral ureteral obstruction (UUO) models by reducing TGF-β1, α-SMA, TNF-α and collagen I expression[209]. Furthermore, MSC-CM treatment helped reduce ECM deposition, inflammatory cell infiltration and inhibited the TLR4/NF-κB signalling pathway[210], whose is activation is reported to enhance interstitial fibrosis[211]. Nevertheless, functional and morphological differences between CM-treated and control group were very subtle. This could be partially explained by the fact that CM was obtained from unstimulated cells. As a matter of fact, it has been reported that hypoxic preconditioning of MSC enhances their angiogenic and cytoprotective potential[212]. Hypoxia induces MSC to express higher levels of HIF-1α, and the growth factors GDNF (glial cell line-derived neurotrophic factor), BDNF (brain-derived neurotrophic factor), VEGF, Ang-1, SDF-1 (stromal cell-derived factor 1) and its receptor CXCR4, as well as increased expression of EPO (erythropoietin) and its receptor EPOR[213]. This pro-angiogenic enhancement was further assayed in vivo in an acute myocardial infarction model, where an improvement was observed due to increased vascularization[214]. Thus, for future studies it might be interesting to address the outcomes after implementing the treatment with CM obtained from MSC cultured in hypoxic conditions in a transplantation setting.

4.5. Conclusions

To sum up our study suggests that:

1. Murine models that implement 60 minutes of warm kidney ischaemia without contralateral nephrectomy at the time of injury are better candidates for interventional studies on progression of CKD compared to kidney ischemia models with contralateral nephrectomy. However, in long term neither of these models shows severe renal function impairment.
2. In contrast, long-term observations in the Fischer-Lewis model of kidney allograft rejection with 8 hours of cold ischaemia are indicating that this model is more superior for interventional studies as it leads to severe renal function impairment with typical histopathological features of chronic rejection.

3. hASC treatment in the AKI model without contralateral nephrectomy leads to a significant decrease in ED1+ macrophages in sections of post-ischaemic kidneys. Furthermore, a decrease in p-crea is observed once the contralateral kidney is removed, compared to the AKI-induced vehicle treated group.
4. CM treatment might be a better candidate compared to MSC treatment in models of allograft rejection, although this needs to be further elucidated.

5. Summary

Several epidemiological studies have shown that AKI is a risk factor for progression to CKD. IRI is one of the main causes of AKI, and for that reason, murine models of AKI are mostly based on renal ischaemia, although in most cases the observation time of these studies is too short to draw reliable conclusions regarding the long-term outcomes. This study provides a description of the long-term renal outcomes of murine models of warm ischaemia and addresses the current discrepancies in scientific literature concerning the role of the renal mass at the time of ischaemic injury. Furthermore, the transcutaneous evaluation of kidney function was implemented measuring FITC-S clearance, which was a very useful, non-invasive and sensible technique, particularly in animals with mild to moderate kidney function impairment, but proved troublesome in animals with severe kidney function deterioration.

In the context of warm ischaemia models, unilateral ischaemia without contralateral nephrectomy at the time of injury led to long-term kidney function deterioration, once the non-ischaemic kidney was removed. Additionally, histopathological analysis revealed cyst formation, increased number of ED1+ macrophages and a higher extent of interstitial fibrosis compared to the animals nephrectomised right after ischaemic injury. Thus, this model makes a good candidate for interventional studies.

Since AKI patients have to rely in supportive care and renal replacement therapy, new therapeutic modalities are greatly needed. Thus, MSC as well as MSC conditioned media therapies have become an interesting choice because of their many attributed properties. Therefore, in this study the treatment with hASC was implemented in the aforementioned warm ischaemia model, with a single injection 14 days after injury. The main finding was a strong reduction of ED1+ macrophages in the post-ischaemic kidneys of the cell treated animals vs. vehicle-treated. This might be explained by the notion that in a pro-inflammatory milieu, hASC adopt an immunosuppressive phenotype that might lead to PGE2 production by hASC, causing monocyte polarization to M2 macrophages.

Cold ischaemia and minor MHC disparity were implemented in order to increase the severity of the model and achieve strong clinical and morphological end-points. This was indeed attained using a Fischer-Lewis kidney transplantation model with 8 hours of cold ischaemia. Thereafter, the treatment with ABCB5+ cells and its derived CM was implemented, one day before and seventeen days after KTx. Neither of the treatments was able to significantly ameliorate any kidney function parameter, although a trend toward worsened kidney function was observed in the cell-treated group. Likewise, the number of ED1+ macrophages and CD3+ T cells in the kidney grafts was not significantly reduced by either treatment. This lack of inhibition might be explained by the cell pre-treatment, as it has been reported that when no inflammation is present MSC can switch to a pro-inflammatory phenotype. As for the Banff classification scores, this model leads to lesions mostly associated mostly to T-cell mediated rejection, namely tubulitis, vasculitis, tubular atrophy and interstitial fibrosis. In this context, cell-treated animals presented the worst scores in all four criteria and no great difference between the control group and CM-treated group were observed, besides a trend toward improved vasculitis and interstitial fibrosis in the CM-treated group. This might be attributed to the angiogenic and anti-fibrotic potential of MSC secretome components.

6. References

1. Togel F, Westenfelder C. Recent advances in the understanding of acute kidney injury. *F1000prime reports.* 2014;6:83.
2. Zuk A, Bonventre JV. Acute Kidney Injury. *Annual review of medicine.* 2016;67:293-307.
3. Kane-Gill SL, Sileanu FE, Murugan R, Trietley GS, Handler SM, Kellum JA. Risk factors for acute kidney injury in older adults with critical illness: a retrospective cohort study. *American journal of kidney diseases : the official journal of the National Kidney Foundation.* 2015;65(6):860-869.
4. Hoste EA, Kellum JA, Katz NM, Rosner MH, Haase M, Ronco C. Epidemiology of acute kidney injury. *Contributions to nephrology.* 2010;165:1-8.
5. Rewa O, Bagshaw SM. Acute kidney injury-epidemiology, outcomes and economics. *Nature reviews Nephrology.* 2014;10(4):193-207.
6. Uchino S, Kellum JA, Bellomo R, et al. Acute renal failure in critically ill patients: a multinational, multicenter study. *Jama.* 2005;294(7):813-818.
7. Chertow GM, Burdick E, Honour M, Bonventre JV, Bates DW. Acute kidney injury, mortality, length of stay, and costs in hospitalized patients. *Journal of the American Society of Nephrology : JASN.* 2005;16(11):3365-3370.
8. National Clinical Guideline C. National Institute for Health and Clinical Excellence: Guidance. In: *Acute Kidney Injury: Prevention, Detection and Management Up to the Point of Renal Replacement Therapy.* London: Royal College of Physicians (UK) National Clinical Guideline Centre.; 2013.
9. Kerr M, Bedford M, Matthews B, O'Donoghue D. The economic impact of acute kidney injury in England. *Nephrology, dialysis, transplantation : official publication of the European Dialysis and Transplant Association - European Renal Association.* 2014;29(7):1362-1368.
10. Sharfuddin AA, Molitoris BA. Pathophysiology of ischaemic acute kidney injury. *Nature reviews Nephrology.* 2011;7(4):189-200.
11. Eltzschig HK, Eckle T. Ischaemia and reperfusion--from mechanism to translation. *Nature medicine.* 2011;17(11):1391-1401.
12. Brezis M, Rosen S. Hypoxia of the renal medulla--its implications for disease. *The New England journal of medicine.* 1995;332(10):647-655.
13. Basile DP, Yoder MC. Renal endothelial dysfunction in acute kidney ischaemia reperfusion injury. *Cardiovascular & hematological disorders drug targets.* 2014;14(1):3-14.
14. Bonventre JV, Yang L. Cellular pathophysiology of ischaemic acute kidney injury. *The Journal of clinical investigation.* 2011;121(11):4210-4221.
15. Satpute SR, Park JM, Jang HR, et al. The role for T cell repertoire/antigen-specific interactions in experimental kidney ischaemia reperfusion injury. *Journal of immunology (Baltimore, Md : 1950).* 2009;183(2):984-992.
16. Li L, Huang L, Sung SS, et al. The chemokine receptors CCR2 and CX3CR1 mediate monocyte/macrophage trafficking in kidney ischaemia-reperfusion injury. *Kidney international.* 2008;74(12):1526-1537.
17. Jang HR, Ko GJ, Wasowska BA, Rabb H. The interaction between ischaemia-reperfusion and immune responses in the kidney. *Journal of molecular medicine (Berlin, Germany).* 2009;87(9):859-864.
18. de Vries B, Kohl J, Leclercq WK, et al. Complement factor C5a mediates renal ischaemia-reperfusion injury independent from neutrophils. *Journal of immunology (Baltimore, Md : 1950).* 2003;170(7):3883-3889.

19. Danobeitia JS, Djamali A, Fernandez LA. The role of complement in the pathogenesis of renal ischaemia-reperfusion injury and fibrosis. *Fibrogenesis & tissue repair.* 2014;7:16.
20. Kanagasundaram NS. Pathophysiology of ischaemic acute kidney injury. *Annals of clinical biochemistry.* 2015;52(Pt 2):193-205.
21. Aderem A, Ulevitch RJ. Toll-like receptors in the induction of the innate immune response. *Nature.* 2000;406(6797):782-787.
22. Rao J, Lu L, Zhai Y. T cells in organ ischaemia reperfusion injury. *Current opinion in organ transplantation.* 2014;19(2):115-120.
23. Ascon DB, Lopez-Briones S, Liu M, et al. Phenotypic and functional characterization of kidney-infiltrating lymphocytes in renal ischaemia reperfusion injury. *Journal of immunology (Baltimore, Md : 1950).* 2006;177(5):3380-3387.
24. Basile DP, Anderson MD, Sutton TA. Pathophysiology of acute kidney injury. *Comprehensive Physiology.* 2012;2(2):1303-1353.
25. Bonventre JV, Weinberg JM. Recent advances in the pathophysiology of ischaemic acute renal failure. *Journal of the American Society of Nephrology : JASN.* 2003;14(8):2199-2210.
26. Haugen E, Nath KA. The involvement of oxidative stress in the progression of renal injury. *Blood purification.* 1999;17(2-3):58-65.
27. Plotnikov EY, Kazachenko AV, Vyssokikh MY, et al. The role of mitochondria in oxidative and nitrosative stress during ischaemia/reperfusion in the rat kidney. *Kidney international.* 2007;72(12):1493-1502.
28. Choi EK, Jung H, Kwak KH, et al. Inhibition of Oxidative Stress in Renal Ischaemia-Reperfusion Injury. *Anesthesia and analgesia.* 2017;124(1):204-213.
29. Nath KA, Norby SM. Reactive oxygen species and acute renal failure. *The American journal of medicine.* 2000;109(8):665-678.
30. Leung KC, Tonelli M, James MT. Chronic kidney disease following acute kidney injury-risk and outcomes. *Nature reviews Nephrology.* 2013;9(2):77-85.
31. Heung M, Chawla LS. Predicting progression to chronic kidney disease after recovery from acute kidney injury. *Current opinion in nephrology and hypertension.* 2012;21(6):628-634.
32. Ponte B, Felipe C, Muriel A, Tenorio MT, Liano F. Long-term functional evolution after an acute kidney injury: a 10-year study. *Nephrology, dialysis, transplantation : official publication of the European Dialysis and Transplant Association - European Renal Association.* 2008;23(12):3859-3866.
33. Ali T, Khan I, Simpson W, et al. Incidence and outcomes in acute kidney injury: a comprehensive population-based study. *Journal of the American Society of Nephrology : JASN.* 2007;18(4):1292-1298.
34. Horne KL, Packington R, Monaghan J, Reilly T, Selby NM. Three-year outcomes after acute kidney injury: results of a prospective parallel group cohort study. *BMJ open.* 2017;7(3):e015316.
35. Mammen C, Al Abbas A, Skippen P, et al. Long-term risk of CKD in children surviving episodes of acute kidney injury in the intensive care unit: a prospective cohort study. *American journal of kidney diseases : the official journal of the National Kidney Foundation.* 2012;59(4):523-530.
36. Wick G, Grundtman C, Mayerl C, et al. The immunology of fibrosis. *Annual review of immunology.* 2013;31:107-135.
37. He L, Wei Q, Liu J, et al. AKI on CKD: heightened injury, suppressed repair, and the underlying mechanisms. *Kidney international.* 2017;92(5):1071-1083.

38. Canaud G, Bonventre JV. Cell cycle arrest and the evolution of chronic kidney disease from acute kidney injury. *Nephrology, dialysis, transplantation : official publication of the European Dialysis and Transplant Association - European Renal Association.* 2015;30(4):575-583.
39. Tchkonia T, Zhu Y, van Deursen J, Campisi J, Kirkland JL. Cellular senescence and the senescent secretory phenotype: therapeutic opportunities. *The Journal of clinical investigation.* 2013;123(3):966-972.
40. Kaissling B, Lehir M, Kriz W. Renal epithelial injury and fibrosis. *Biochimica et biophysica acta.* 2013;1832(7):931-939.
41. Humphreys BD, Lin SL, Kobayashi A, et al. Fate tracing reveals the pericyte and not epithelial origin of myofibroblasts in kidney fibrosis. *The American journal of pathology.* 2010;176(1):85-97.
42. Yang L, Besschetnova TY, Brooks CR, Shah JV, Bonventre JV. Epithelial cell cycle arrest in G2/M mediates kidney fibrosis after injury. *Nature medicine.* 2010;16(5):535-543, 531p following 143.
43. Bechtel W, McGoohan S, Zeisberg EM, et al. Methylation determines fibroblast activation and fibrogenesis in the kidney. *Nature medicine.* 2010;16(5):544-550.
44. Heyman SN, Rosen S, Rosenberger C. Animal models of renal dysfunction: acute kidney injury. *Expert opinion on drug discovery.* 2009;4(6):629-641.
45. Fu Y, Tang C, Cai J, Chen G, Zhang D, Dong Z. Rodent models of AKI-CKD transition. *Am J Physiol Renal Physiol.* 2018;315(4):F1098-f1106.
46. Rosen S, Heyman SN. Difficulties in understanding human "acute tubular necrosis": limited data and flawed animal models. *Kidney international.* 2001;60(4):1220-1224.
47. Heyman SN, Rosenberger C, Rosen S. Experimental ischaemia-reperfusion: biases and myths-the proximal vs. distal hypoxic tubular injury debate revisited. *Kidney international.* 2010;77(1):9-16.
48. Whalen H, Shiels P, Littlejohn M, Clancy M. A novel rodent model of severe renal ischaemia reperfusion injury. *Renal failure.* 2016;38(10):1694-1701.
49. Le Clef N, Verhulst A, D'Haese PC, Vervaet BA. Unilateral Renal Ischaemia-Reperfusion as a Robust Model for Acute to Chronic Kidney Injury in Mice. *PLoS One.* 2016;11(3):e0152153.
50. Barker CF, Markmann JF. Historical overview of transplantation. *Cold Spring Harbor perspectives in medicine.* 2013;3(4):a014977.
51. Shrestha B, Haylor J, Raftery A. Historical perspectives in kidney transplantation: an updated review. *Progress in transplantation (Aliso Viejo, Calif).* 2015;25(1):64-69, 76.
52. Kostro JZ, Hellmann A, Kobiela J, et al. Quality of Life After Kidney Transplantation: A Prospective Study. *Transplantation proceedings.* 2016;48(1):50-54.
53. Garcia GG, Harden P, Chapman J. The global role of kidney transplantation. *American journal of nephrology.* 2012;35(3):259-264.
54. Abouna GM. Organ shortage crisis: problems and possible solutions. *Transplantation proceedings.* 2008;40(1):34-38.
55. Clark R, Hailstone JD, Slade PD. Psychological aspects of dialysis: a semantic differential study. *Psychological medicine.* 1979;9(1):55-62.
56. Stephan A. Organ Shortage: Can We Decrease the Demand? *Experimental and clinical transplantation : official journal of the Middle East Society for Organ Transplantation.* 2017;15(Suppl 1):6-9.
57. Nankivell BJ, Alexander SI. Rejection of the kidney allograft. *The New England journal of medicine.* 2010;363(15):1451-1462.

58. Terasaki PI. Humoral theory of transplantation. *American journal of transplantation : official journal of the American Society of Transplantation and the American Society of Transplant Surgeons.* 2003;3(6):665-673.
59. Becker LE, Morath C, Suesal C. Immune mechanisms of acute and chronic rejection. *Clinical biochemistry.* 2016;49(4-5):320-323.
60. Colvin RB, Smith RN. Antibody-mediated organ-allograft rejection. *Nature reviews Immunology.* 2005;5(10):807-817.
61. Lusco MA, Fogo AB, Najafian B, Alpers CE. AJKD Atlas of Renal Pathology: Acute T-Cell-Mediated Rejection. *American journal of kidney diseases : the official journal of the National Kidney Foundation.* 2016;67(5):e29-30.
62. Kloc M, Ghobrial RM. Chronic allograft rejection: A significant hurdle to transplant success. *Burns & trauma.* 2014;2(1):3-10.
63. Wedel J, Bruneau S, Kochupurakkal N, Boneschansker L, Briscoe DM. Chronic allograft rejection: a fresh look. *Current opinion in organ transplantation.* 2015;20(1):13-20.
64. Alelign T, Ahmed MM, Bobosha K, Tadesse Y, Howe R, Petros B. Kidney Transplantation: The Challenge of Human Leukocyte Antigen and Its Therapeutic Strategies. *Journal of immunology research.* 2018;2018:5986740.
65. Gordon EJ, Ladner DP, Caicedo JC, Franklin J. Disparities in kidney transplant outcomes: a review. *Seminars in nephrology.* 2010;30(1):81-89.
66. Reese PP, Boudville N, Garg AX. Living kidney donation: outcomes, ethics, and uncertainty. *Lancet (London, England).* 2015;385(9981):2003-2013.
67. Horvat LD, Shariff SZ, Garg AX. Global trends in the rates of living kidney donation. *Kidney international.* 2009;75(10):1088-1098.
68. Ponticelli CE. The impact of cold ischaemia time on renal transplant outcome. *Kidney international.* 2015;87(2):272-275.
69. de Vries DK, Lindeman JH, Ringers J, Reinders ME, Rabelink TJ, Schaapherder AF. Donor brain death predisposes human kidney grafts to a proinflammatory reaction after transplantation. *American journal of transplantation : official journal of the American Society of Transplantation and the American Society of Transplant Surgeons.* 2011;11(5):1064-1070.
70. Floerchinger B, Oberhuber R, Tullius SG. Effects of brain death on organ quality and transplant outcome. *Transplantation reviews (Orlando, Fla).* 2012;26(2):54-59.
71. Westendorp WH, Leuvenink HG, Ploeg RJ. Brain death induced renal injury. *Current opinion in organ transplantation.* 2011;16(2):151-156.
72. Chen G, Wang C, Ko DS, et al. Comparison of outcomes of kidney transplantation from donation after brain death, donation after circulatory death, and donation after brain death followed by circulatory death donors. *Clinical transplantation.* 2017;31(11).
73. Wadei HM, Heckman MG, Rawal B, et al. Comparison of kidney function between donation after cardiac death and donation after brain death kidney transplantation. *Transplantation.* 2013;96(3):274-281.
74. Doria C, Margetich L. Recipient Kidney Transplantation Surgery. In: Ramirez CGB, McCauley J, eds. *Contemporary Kidney Transplantation.* Cham: Springer International Publishing; 2018:91-100.
75. Anaise D, Ramsammy L, Lane B, Waltzer WC, Rapaport FT. The pathophysiology of the no-reflow phenomenon in cold-stored kidneys. *Transplantation proceedings.* 1987;19(1 Pt 2):1348-1352.
76. Perico N, Cattaneo D, Sayegh MH, Remuzzi G. Delayed graft function in kidney transplantation. *Lancet (London, England).* 2004;364(9447):1814-1827.

77. Klotz S, Pallavi P, Tsagogiorgas C, et al. N-octanoyl dopamine treatment exerts renoprotective properties in acute kidney injury but not in renal allograft recipients. *Nephrology, dialysis, transplantation : official publication of the European Dialysis and Transplant Association - European Renal Association.* 2016;31(4):564-573.
78. Hoeger S, Fontana J, Jarczyk J, et al. Vagal stimulation in brain dead donor rats decreases chronic allograft nephropathy in recipients. *Nephrology, dialysis, transplantation : official publication of the European Dialysis and Transplant Association - European Renal Association.* 2014;29(3):544-549.
79. Hancock WH, Whitley WD, Tullius SG, et al. Cytokines, adhesion molecules, and the pathogenesis of chronic rejection of rat renal allografts. *Transplantation.* 1993;56(3):643-650.
80. Marco ML. The Fischer-Lewis model of chronic allograft rejection--a summary. *Nephrology, dialysis, transplantation : official publication of the European Dialysis and Transplant Association - European Renal Association.* 2006;21(11):3082-3086.
81. Friedenstein AJ, Chailakhjan RK, Lalykina KS. The development of fibroblast colonies in monolayer cultures of guinea-pig bone marrow and spleen cells. *Cell and tissue kinetics.* 1970;3(4):393-403.
82. Bieback K, Wuchter P, Besser D, et al. Mesenchymal stromal cells (MSCs): science and f(r)iction. *Journal of molecular medicine (Berlin, Germany).* 2012;90(7):773-782.
83. Mendez-Ferrer S, Michurina TV, Ferraro F, et al. Mesenchymal and haematopoietic stem cells form a unique bone marrow niche. *Nature.* 2010;466(7308):829-834.
84. Dominici M, Le Blanc K, Mueller I, et al. Minimal criteria for defining multipotent mesenchymal stromal cells. The International Society for Cellular Therapy position statement. *Cytotherapy.* 2006;8(4):315-317.
85. Torres Crigna A, Daniele C, Gamez C, et al. Stem/Stromal Cells for Treatment of Kidney Injuries With Focus on Preclinical Models. *Frontiers in medicine.* 2018;5:179.
86. Manferdini C, Paolella F, Gabusi E, et al. Adipose stromal cells mediated switching of the pro-inflammatory profile of M1-like macrophages is facilitated by PGE2: in vitro evaluation. *Osteoarthritis and cartilage.* 2017;25(7):1161-1171.
87. Luz-Crawford P, Djouad F, Toupet K, et al. Mesenchymal Stem Cell-Derived Interleukin 1 Receptor Antagonist Promotes Macrophage Polarization and Inhibits B Cell Differentiation. *Stem cells (Dayton, Ohio).* 2016;34(2):483-492.
88. Braza F, Dirou S, Forest V, et al. Mesenchymal Stem Cells Induce Suppressive Macrophages Through Phagocytosis in a Mouse Model of Asthma. *Stem cells (Dayton, Ohio).* 2016;34(7):1836-1845.
89. Djouad F, Charbonnier LM, Bouffi C, et al. Mesenchymal stem cells inhibit the differentiation of dendritic cells through an interleukin-6-dependent mechanism. *Stem cells (Dayton, Ohio).* 2007;25(8):2025-2032.
90. English K, Barry FP, Mahon BP. Murine mesenchymal stem cells suppress dendritic cell migration, maturation and antigen presentation. *Immunology letters.* 2008;115(1):50-58.
91. Selleri S, Dieng MM, Nicoletti S, et al. Cord-blood-derived mesenchymal stromal cells downmodulate CD4+ T-cell activation by inducing IL-10-producing Th1 cells. *Stem cells and development.* 2013;22(7):1063-1075.
92. Mattar P, Bieback K. Comparing the Immunomodulatory Properties of Bone Marrow, Adipose Tissue, and Birth-Associated Tissue Mesenchymal Stromal Cells. *Frontiers in immunology.* 2015;6:560.
93. Weiss ARR, Dahlke MH. Immunomodulation by Mesenchymal Stem Cells (MSCs): Mechanisms of Action of Living, Apoptotic, and Dead MSCs. *Frontiers in immunology.*2019;10:1191.

94. Melief SM, Schrama E, Brugman MH, et al. Multipotent stromal cells induce human regulatory T cells through a novel pathway involving skewing of monocytes toward anti-inflammatory macrophages. *Stem cells (Dayton, Ohio).* 2013;31(9):1980-1991.
95. Luk F, Carreras-Planella L, Korevaar SS, et al. Inflammatory Conditions Dictate the Effect of Mesenchymal Stem or Stromal Cells on B Cell Function. *Frontiers in immunology.* 2017;8:1042.
96. Franquesa M, Mensah FK, Huizinga R, et al. Human adipose tissue-derived mesenchymal stem cells abrogate plasmablast formation and induce regulatory B cells independently of T helper cells. *Stem cells (Dayton, Ohio).* 2015;33(3):880-891.
97. Spaggiari GM, Capobianco A, Abdelrazik H, Becchetti F, Mingari MC, Moretta L. Mesenchymal stem cells inhibit natural killer-cell proliferation, cytotoxicity, and cytokine production: role of indoleamine 2,3-dioxygenase and prostaglandin E2. *Blood.* 2008;111(3):1327-1333.
98. Sato K, Ozaki K, Oh I, et al. Nitric oxide plays a critical role in suppression of T-cell proliferation by mesenchymal stem cells. *Blood.* 2007;109(1):228-234.
99. Semedo P, Correa-Costa M, Antonio Cenedeze M, et al. Mesenchymal stem cells attenuate renal fibrosis through immune modulation and remodeling properties in a rat remnant kidney model. *Stem cells (Dayton, Ohio).* 2009;27(12):3063-3073.
100. Usunier B, Benderitter M, Tamarat R, Chapel A. Management of fibrosis: the mesenchymal stromal cells breakthrough. *Stem cells international.* 2014;2014:340257.
101. Qi Y, Jiang D, Sindrilaru A, et al. TSG-6 released from intradermally injected mesenchymal stem cells accelerates wound healing and reduces tissue fibrosis in murine full-thickness skin wounds. *The Journal of investigative dermatology.* 2014;134(2):526-537.
102. Zhou Y, Xu H, Xu W, et al. Exosomes released by human umbilical cord mesenchymal stem cells protect against cisplatin-induced renal oxidative stress and apoptosis in vivo and in vitro. *Stem cell research & therapy.* 2013;4(2):34.
103. Yan B, Singla DK. Transplanted induced pluripotent stem cells mitigate oxidative stress and improve cardiac function through the Akt cell survival pathway in diabetic cardiomyopathy. *Molecular pharmaceutics.* 2013;10(9):3425-3432.
104. Zhang W, Liu L, Huo Y, Yang Y, Wang Y. Hypoxia-pretreated human MSCs attenuate acute kidney injury through enhanced angiogenic and antioxidative capacities. *BioMed research international.* 2014;2014:462472.
105. Kholia S, Ranghino A, Garnieri P, et al. Extracellular vesicles as new players in angiogenesis. *Vascular pharmacology.* 2016;86:64-70.
106. Casiraghi F, Perico N, Cortinovis M, Remuzzi G. Mesenchymal stromal cells in renal transplantation: opportunities and challenges. *Nature reviews Nephrology.* 2016;12(4):241-253.
107. Fischer UM, Harting MT, Jimenez F, et al. Pulmonary passage is a major obstacle for intravenous stem cell delivery: the pulmonary first-pass effect. *Stem cells and development.* 2009;18(5):683-692.
108. Burst V, Putsch F, Kubacki T, et al. Survival and distribution of injected haematopoietic stem cells in acute kidney injury. *Nephrology, dialysis, transplantation : official publication of the European Dialysis and Transplant Association - European Renal Association.* 2013;28(5):1131-1139.
109. Imasawa T, Utsunomiya Y, Kawamura T, et al. The potential of bone marrow-derived cells to differentiate to glomerular mesangial cells. *Journal of the American Society of Nephrology : JASN.* 2001;12(7):1401-1409.

110. Li K, Han Q, Yan X, Liao L, Zhao RC. Not a process of simple vicariousness, the differentiation of human adipose-derived mesenchymal stem cells to renal tubular epithelial cells plays an important role in acute kidney injury repairing. *Stem cells and development.* 2010;19(8):1267-1275.
111. Togel F, Hu Z, Weiss K, Isaac J, Lange C, Westenfelder C. Administered mesenchymal stem cells protect against ischaemic acute renal failure through differentiation-independent mechanisms. *Am J Physiol Renal Physiol.* 2005;289(1):F31-42.
112. Maguire G. Stem cell therapy without the cells. *Communicative & integrative biology.* 2013;6(6):e26631.
113. Gunawardena TNA, Rahman MT, Abdullah BJJ, Abu Kasim NH. Conditioned media derived from mesenchymal stem cell cultures: The next generation for regenerative medicine. *Journal of tissue engineering and regenerative medicine.* 2019;13(4):569-586.
114. Timmers L, Lim SK, Arslan F, et al. Reduction of myocardial infarct size by human mesenchymal stem cell conditioned medium. *Stem cell research.* 2007;1(2):129-137.
115. Kay AG, Long G, Tyler G, et al. Mesenchymal Stem Cell-Conditioned Medium Reduces Disease Severity and Immune Responses in Inflammatory Arthritis. *Scientific reports.* 2017;7(1):18019.
116. Egashira Y, Sugitani S, Suzuki Y, et al. The conditioned medium of murine and human adipose-derived stem cells exerts neuroprotective effects against experimental stroke model. *Brain research.* 2012;1461:87-95.
117. Konala VB, Mamidi MK, Bhonde R, Das AK, Pochampally R, Pal R. The current landscape of the mesenchymal stromal cell secretome: A new paradigm for cell-free regeneration. *Cytotherapy.* 2016;18(1):13-24.
118. Koch M, Lemke A, Lange C. Extracellular Vesicles from MSC Modulate the Immune Response to Renal Allografts in a MHC Disparate Rat Model. *Stem cells international.* 2015;2015:486141.
119. Cantaluppi V, Gatti S, Medica D, et al. Microvesicles derived from endothelial progenitor cells protect the kidney from ischaemia-reperfusion injury by microRNA-dependent reprogramming of resident renal cells. *Kidney international.* 2012;82(4):412-427.
120. Han SJ, Lee HT. Mechanisms and therapeutic targets of ischaemic acute kidney injury. *Kidney research and clinical practice.* 2019.
121. Squillaro T, Peluso G, Galderisi U. Clinical Trials With Mesenchymal Stem Cells: An Update. *Cell transplantation.* 2016;25(5):829-848.
122. Tappenbeck N, Schroder HM, Niebergall-Roth E, et al. In vivo safety profile and biodistribution of GMP-manufactured human skin-derived ABCB5-positive mesenchymal stromal cells for use in clinical trials. *Cytotherapy.* 2019;21(5):546-560.
123. Klotz S. *Experimentelle Untersuchungen des nephroprotektiven Potenzials von N–Oktanoyl–Dopamin in vivo bei akutem ischämischen Nierenversagen und nach Nierentransplantation*. Berlin, Mensch und Buch Verl.; 2014.
124. Pill J, Kraenzlin B, Jander J, et al. Fluorescein-labeled sinistrin as marker of glomerular filtration rate. *European journal of medicinal chemistry.* 2005;40(10):1056-1061.
125. Schreiber A, Shulhevich Y, Geraci S, et al. Transcutaneous measurement of renal function in conscious mice. *Am J Physiol Renal Physiol.* 2012;303(5):F783-788.
126. Schock-Kusch D, Sadick M, Henninger N, et al. Transcutaneous measurement of glomerular filtration rate using FITC-sinistrin in rats. *Nephrology, dialysis,*

transplantation : official publication of the European Dialysis and Transplant Association - European Renal Association. 2009;24(10):2997-3001.
127. Herrera Perez Z, Weinfurter S, Gretz N. Transcutaneous Assessment of Renal Function in Conscious Rodents. *Journal of visualized experiments : JoVE.* 2016(109):e53767.
128. Vander Beken S, de Vries JC, Meier-Schiesser B, et al. Newly Defined ATP-binding cassette subfamily B member 5 Positive Dermal Mesenchymal Stem Cells Promote Healing of Chronic Iron-Overload Wounds via Secretion of Interleukin-1 Receptor Antagonist. *Stem cells (Dayton, Ohio).* 2019.
129. Damoiseaux JG, Dopp EA, Calame W, Chao D, MacPherson GG, Dijkstra CD. Rat macrophage lysosomal membrane antigen recognized by monoclonal antibody ED1. *Immunology.* 1994;83(1):140-147.
130. Dijkstra CD, Dopp EA, Joling P, Kraal G. The heterogeneity of mononuclear phagocytes in lymphoid organs: distinct macrophage subpopulations in rat recognized by monoclonal antibodies ED1, ED2 and ED3. *Advances in experimental medicine and biology.* 1985;186:409-419.
131. Chetty R, Gatter K. CD3: structure, function, and role of immunostaining in clinical practice. *The Journal of pathology.* 1994;173(4):303-307.
132. Tanaka T, Masuko T, Yagita H, Tamura T, Hashimoto Y. Characterization of a CD3-like rat T cell surface antigen recognized by a monoclonal antibody. *Journal of immunology (Baltimore, Md : 1950).* 1989;142(8):2791-2795.
133. Solez K, Axelsen RA, Benediktsson H, et al. International standardization of criteria for the histologic diagnosis of renal allograft rejection: the Banff working classification of kidney transplant pathology. *Kidney international.* 1993;44(2):411-422.
134. Roufosse C, Simmonds N, Clahsen-van Groningen M, et al. A 2018 Reference Guide to the Banff Classification of Renal Allograft Pathology. *Transplantation.* 2018;102(11):1795-1814.
135. Heyman SN, Rosenberger C, Rosen S. Acute kidney injury: lessons from experimental models. *Contributions to nephrology.* 2011;169:286-296.
136. Cruzado JM, Torras J, Riera M, et al. Influence of nephron mass in development of chronic renal failure after prolonged warm renal ischaemia. *Am J Physiol Renal Physiol.* 2000;279(2):F259-269.
137. Azuma H, Nadeau K, Takada M, Mackenzie HS, Tilney NL. Cellular and molecular predictors of chronic renal dysfunction after initial ischaemia/reperfusion injury of a single kidney. *Transplantation.* 1997;64(2):190-197.
138. Turin TC, James M, Ravani P, et al. Proteinuria and rate of change in kidney function in a community-based population. *Journal of the American Society of Nephrology : JASN.* 2013;24(10):1661-1667.
139. Lamb EJ, MacKenzie F, Stevens PE. How should proteinuria be detected and measured? *Annals of clinical biochemistry.* 2009;46(Pt 3):205-217.
140. Fattah H, Layton A, Vallon V. How Do Kidneys Adapt to a Deficit or Loss in Nephron Number? *Physiology (Bethesda, Md).* 2019;34(3):189-197.
141. Schena FP, Strippoli GF, Wankelmuth P. Renal growth factors: past, present and future. *American journal of nephrology.* 1999;19(2):308-312.
142. Simms RJ, Ong AC. How simple are 'simple renal cysts'? *Nephrology, dialysis, transplantation : official publication of the European Dialysis and Transplant Association - European Renal Association.* 2014;29 Suppl 4:iv106-112.
143. Tatar E, Ozay E, Atakaya M, et al. Simple renal cysts in the solitary kidney: Are they innocent in adult patients? *Nephrology (Carlton, Vic).* 2017;22(5):361-365.

144. Nahm AM, Ritz E. Acquired renal cysts. *Nephrology, dialysis, transplantation : official publication of the European Dialysis and Transplant Association - European Renal Association.* 2001;16(7):1506-1508.
145. Djudjaj S, Boor P. Cellular and molecular mechanisms of kidney fibrosis. *Molecular aspects of medicine.* 2019;65:16-36.
146. Farris AB, Alpers CE. What is the best way to measure renal fibrosis?: A pathologist's perspective. *Kidney international supplements.* 2014;4(1):9-15.
147. Menn-Josephy H, Lee CS, Nolin A, et al. Renal Interstitial Fibrosis: An Imperfect Predictor of Kidney Disease Progression in Some Patient Cohorts. *American journal of nephrology.* 2016;44(4):289-299.
148. Azuma H, Nadeau K, Takada M, Tilney NL. Initial ischaemia/reperfusion injury influences late functional and structural changes in the kidney. *Transplantation proceedings.* 1997;29(1-2):1528-1529.
149. Zager RA, Johnson AC, Becker K. Acute unilateral ischaemic renal injury induces progressive renal inflammation, lipid accumulation, histone modification, and "end-stage" kidney disease. *Am J Physiol Renal Physiol.* 2011;301(6):F1334-1345.
150. Shimizu A, Masuda Y, Ishizaki M, Sugisaki Y, Yamanaka N. Tubular dilatation in the repair process of ischaemic tubular necrosis. *Virchows Archiv : an international journal of pathology.* 1994;425(3):281-290.
151. Kato J, Nakayama M, Zhu WJ, Yokoo T, Ito S. Ischaemia/reperfusion of unilateral kidney exaggerates aging-induced damage to the heart and contralateral kidney. *Nephron Experimental nephrology.* 2014;126(4):183-190.
152. Kierulf-Lassen C, Nielsen PM, Qi H, et al. Unilateral nephrectomy diminishes ischaemic acute kidney injury through enhanced perfusion and reduced pro-inflammatory and pro-fibrotic responses. *PLoS One.* 2017;12(12):e0190009.
153. Nakajima T, Miyaji T, Kato A, Ikegaya N, Yamamoto T, Hishida A. Uninephrectomy reduces apoptotic cell death and enhances renal tubular cell regeneration in ischaemic ARF in rats. *The American journal of physiology.* 1996;271(4 Pt 2):F846-853.
154. Kato A, Hishida A, Nakajima T. Role of thromboxane A2 and prostacyclin in uninephrectomy-induced attenuation of ischaemic renal injury. *Kidney international.* 1995;48(5):1577-1583.
155. Kato A, Hishida A. Amelioration of post-ischaemic renal injury by contralateral uninephrectomy: a role of endothelin-1. *Nephrology, dialysis, transplantation : official publication of the European Dialysis and Transplant Association - European Renal Association.* 2001;16(8):1570-1576.
156. Hauser P, Kainz A, Perco P, et al. Transcriptional response in the unaffected kidney after contralateral hydronephrosis or nephrectomy. *Kidney international.* 2005;68(6):2497-2507.
157. Tokuyama H, Kelly DJ, Zhang Y, Gow RM, Gilbert RE. Macrophage infiltration and cellular proliferation in the non-ischaemic kidney and heart following prolonged unilateral renal ischaemia. *Nephron Physiology.* 2007;106(3):p54-62.
158. Meldrum KK, Meldrum DR, Meng X, Ao L, Harken AH. TNF-alpha-dependent bilateral renal injury is induced by unilateral renal ischaemia-reperfusion. *American journal of physiology Heart and circulatory physiology.* 2002;282(2):H540-546.
159. McIntosh K, Zvonic S, Garrett S, et al. The immunogenicity of human adipose-derived cells: temporal changes in vitro. *Stem cells (Dayton, Ohio).* 2006;24(5):1246-1253.
160. Ivanova-Todorova E, Bochev I, Mourdjeva M, et al. Adipose tissue-derived mesenchymal stem cells are more potent suppressors of dendritic cells differentiation

compared to bone marrow-derived mesenchymal stem cells. *Immunology letters.* 2009;126(1-2):37-42.
161. Li X, Bai J, Ji X, Li R, Xuan Y, Wang Y. Comprehensive characterization of four different populations of human mesenchymal stem cells as regards their immune properties, proliferation and differentiation. *International journal of molecular medicine.* 2014;34(3):695-704.
162. Zonta S, De Martino M, Bedino G, et al. Which is the most suitable and effective route of administration for mesenchymal stem cell-based immunomodulation therapy in experimental kidney transplantation: endovenous or arterial? *Transplantation proceedings.* 2010;42(4):1336-1340.
163. Schrepfer S, Deuse T, Reichenspurner H, Fischbein MP, Robbins RC, Pelletier MP. Stem cell transplantation: the lung barrier. *Transplantation proceedings.* 2007;39(2):573-576.
164. Lee RH, Pulin AA, Seo MJ, et al. Intravenous hMSCs improve myocardial infarction in mice because cells embolized in lung are activated to secrete the anti-inflammatory protein TSG-6. *Cell stem cell.* 2009;5(1):54-63.
165. Galipeau J, Sensebe L. Mesenchymal Stromal Cells: Clinical Challenges and Therapeutic Opportunities. *Cell stem cell.* 2018;22(6):824-833.
166. Little MH, Rae FK. Review article: Potential cellular therapies for renal disease: can we translate results from animal studies to the human condition? *Nephrology (Carlton, Vic).* 2009;14(6):544-553.
167. Berglund AK, Fortier LA, Antczak DF, Schnabel LV. Immunoprivileged no more: measuring the immunogenicity of allogeneic adult mesenchymal stem cells. *Stem cell research & therapy.* 2017;8(1):288.
168. Poncelet AJ, Vercruysse J, Saliez A, Gianello P. Although pig allogeneic mesenchymal stem cells are not immunogenic in vitro, intracardiac injection elicits an immune response in vivo. *Transplantation.* 2007;83(6):783-790.
169. Owens SD, Kol A, Walker NJ, Borjesson DL. Allogeneic Mesenchymal Stem Cell Treatment Induces Specific Alloantibodies in Horses. *Stem cells international.* 2016;2016:5830103.
170. Lalu MM, McIntyre L, Pugliese C, et al. Safety of cell therapy with mesenchymal stromal cells (SafeCell): a systematic review and meta-analysis of clinical trials. *PLoS One.* 2012;7(10):e47559.
171. Francois M, Romieu-Mourez R, Li M, Galipeau J. Human MSC suppression correlates with cytokine induction of indoleamine 2,3-dioxygenase and bystander M2 macrophage differentiation. *Molecular therapy : the journal of the American Society of Gene Therapy.* 2012;20(1):187-195.
172. Lee GK, Park HJ, Macleod M, Chandler P, Munn DH, Mellor AL. Tryptophan deprivation sensitizes activated T cells to apoptosis prior to cell division. *Immunology.* 2002;107(4):452-460.
173. Frumento G, Rotondo R, Tonetti M, Damonte G, Benatti U, Ferrara GB. Tryptophan-derived catabolites are responsible for inhibition of T and natural killer cell proliferation induced by indoleamine 2,3-dioxygenase. *The Journal of experimental medicine.* 2002;196(4):459-468.
174. Kalinski P. Regulation of immune responses by prostaglandin E2. *Journal of immunology (Baltimore, Md : 1950).* 2012;188(1):21-28.
175. Bernardo ME, Fibbe WE. Mesenchymal stromal cells: sensors and switchers of inflammation. *Cell stem cell.* 2013;13(4):392-402.
176. Waterman RS, Tomchuck SL, Henkle SL, Betancourt AM. A new mesenchymal stem cell (MSC) paradigm: polarization into a pro-inflammatory MSC1 or an Immunosuppressive MSC2 phenotype. *PLoS One.* 2010;5(4):e10088.

177. Ko GJ, Linfert D, Jang HR, et al. Transcriptional analysis of infiltrating T cells in kidney ischaemia-reperfusion injury reveals a pathophysiological role for CCR5. *Am J Physiol Renal Physiol.* 2012;302(6):F762-773.
178. Wynn TA, Vannella KM. Macrophages in Tissue Repair, Regeneration, and Fibrosis. *Immunity*. 2016;44(3):450-462.
179. Kim J, Hematti P. Mesenchymal stem cell-educated macrophages: a novel type of alternatively activated macrophages. *Exp Hematol.* 2009;37(12):1445-1453.
180. Barros MH, Hauck F, Dreyer JH, Kempkes B, Niedobitek G. Macrophage polarisation: an immunohistochemical approach for identifying M1 and M2 macrophages. *PLoS One.* 2013;8(11):e80908.
181. Chawla LS, Amdur RL, Amodeo S, Kimmel PL, Palant CE. The severity of acute kidney injury predicts progression to chronic kidney disease. *Kidney international.* 2011;79(12):1361-1369.
182. Frank NY, Pendse SS, Lapchak PH, et al. Regulation of progenitor cell fusion by ABCB5 P-glycoprotein, a novel human ATP-binding cassette transporter. *The Journal of biological chemistry.* 2003;278(47):47156-47165.
183. Volpicelli ER, Lezcano C, Zhan Q, et al. The multidrug-resistance transporter ABCB5 is expressed in human placenta. *International journal of gynecological pathology : official journal of the International Society of Gynecological Pathologists.* 2014;33(1):45-51.
184. Ksander BR, Kolovou PE, Wilson BJ, et al. ABCB5 is a limbal stem cell gene required for corneal development and repair. *Nature.* 2014;511(7509):353-357.
185. Schatton T, Yang J, Kleffel S, et al. ABCB5 Identifies Immunoregulatory Dermal Cells. *Cell reports.* 2015;12(10):1564-1574.
186. Allogeneic ABCB5-positive Stem Cells for Treatment of Acute-on-Chronic Liver Failure. In: https://ClinicalTrials.gov/show/NCT03860155.
187. Allogeneic ABCB5-positive Stem Cells for Treatment of Epidermolysis Bullosa. In: https://ClinicalTrials.gov/show/NCT03529877.
188. Allogeneic ABCB5-positive Stem Cells for Treatment of CVU. In: https://ClinicalTrials.gov/show/NCT03257098.
189. Tsuji K, Kitamura S, Wada J. Secretomes from Mesenchymal Stem Cells against Acute Kidney Injury: Possible Heterogeneity. *Stem cells international.* 2018;2018:8693137.
190. Sze SK, de Kleijn DP, Lai RC, et al. Elucidating the secretion proteome of human embryonic stem cell-derived mesenchymal stem cells. *Molecular & cellular proteomics : MCP*. 2007;6(10):1680-1689.
191. Bruno S, Grange C, Deregibus MC, et al. Mesenchymal stem cell-derived microvesicles protect against acute tubular injury. *Journal of the American Society of Nephrology : JASN.* 2009;20(5):1053-1067.
192. Eirin A, Zhu XY, Jonnada S, Lerman A, van Wijnen AJ, Lerman LO. Mesenchymal Stem Cell-Derived Extracellular Vesicles Improve the Renal Microvasculature in Metabolic Renovascular Disease in Swine. *Cell transplantation.* 2018;27(7):1080-1095.
193. The Role of UC-MSC and Conditioned Medium in Inhibiting Impairment of Vision in Retinitis Pigmentosa. In: https://ClinicalTrials.gov/show/NCT04315025.
194. Comparative Effectiveness of Arthroscopy and Non-Arthroscopy Using Mesenchymal Stem Cell Therapy (MSCs) and Conditioned Medium for Osteoartrithis. In: https://ClinicalTrials.gov/show/NCT04314661.
195. Therapeutic Potential of Stem Cell Conditioned Medium on Chronic Ulcer Wounds. In:https://ClinicalTrials.gov/show/NCT04134676.

196. Gottmann U, Notheisen A, Brinkkoetter PT, et al. Influence of donor pretreatment with dopamine on allogeneic kidney transplantation after prolonged cold storage in rats. *Transplantation.* 2005;79(10):1344-1350.
197. White E, Hildemann WH, Mullen Y. Chronic kidney allograft reactions in rats. *Transplantation.* 1969;8(5):602-617.
198. Casiraghi F, Azzollini N, Todeschini M, et al. Localization of mesenchymal stromal cells dictates their immune or proinflammatory effects in kidney transplantation. *American journal of transplantation : official journal of the American Society of Transplantation and the American Society of Transplant Surgeons.* 2012;12(9):2373-2383.
199. Perico N, Casiraghi F, Todeschini M, et al. Long-Term Clinical and Immunological Profile of Kidney Transplant Patients Given Mesenchymal Stromal Cell Immunotherapy. *Frontiers in immunology.* 2018;9:1359.
200. Sensebe L, Fleury-Cappellesso S. Biodistribution of mesenchymal stem/stromal cells in a preclinical setting. *Stem cells international.* 2013;2013:678063.
201. Francisco LM, Sage PT, Sharpe AH. The PD-1 pathway in tolerance and autoimmunity. *Immunological reviews.* 2010;236:219-242.
202. Davies LC, Heldring N, Kadri N, Le Blanc K. Mesenchymal Stromal Cell Secretion of Programmed Death-1 Ligands Regulates T Cell Mediated Immunosuppression. *Stem cells (Dayton, Ohio).* 2017;35(3):766-776.
203. Salehi S, Reed EF. The divergent roles of macrophages in solid organ transplantation. *Current opinion in organ transplantation.* 2015;20(4):446-453.
204. Hancock WW, Thomson NM, Atkins RC. Composition of interstitial cellular infiltrate identified by monoclonal antibodies in renal biopsies of rejecting human renal allografts. *Transplantation.* 1983;35(5):458-463.
205. Toki D, Zhang W, Hor KL, et al. The role of macrophages in the development of human renal allograft fibrosis in the first year after transplantation. *American journal of transplantation : official journal of the American Society of Transplantation and the American Society of Transplant Surgeons.* 2014;14(9):2126-2136.
206. Ikezumi Y, Suzuki T, Yamada T, et al. Alternatively activated macrophages in the pathogenesis of chronic kidney allograft injury. *Pediatr Nephrol.* 2015;30(6):1007-1017.
207. Estrada R, Li N, Sarojini H, An J, Lee MJ, Wang E. Secretome from mesenchymal stem cells induces angiogenesis via Cyr61. *Journal of cellular physiology.* 2009;219(3):563-571.
208. Gong M, Yu B, Wang J, et al. Mesenchymal stem cells release exosomes that transfer miRNAs to endothelial cells and promote angiogenesis. *Oncotarget.* 2017;8(28):45200-45212.
209. Liu B, Ding FX, Liu Y, et al. Human umbilical cord-derived mesenchymal stem cells conditioned medium attenuate interstitial fibrosis and stimulate the repair of tubular epithelial cells in an irreversible model of unilateral ureteral obstruction. *Nephrology (Carlton, Vic).* 2018;23(8):728-736.
210. Liu B, Ding F, Hu D, et al. Human umbilical cord mesenchymal stem cell conditioned medium attenuates renal fibrosis by reducing inflammation and epithelial-to-mesenchymal transition via the TLR4/NF-kappaB signaling pathway in vivo and in vitro. *Stem cell research & therapy.* 2018;9(1):7.
211. Liu P, Li F, Qiu M, He L. Expression and cellular distribution of TLR4, MyD88, and NF-kappaB in diabetic renal tubulointerstitial fibrosis, in vitro and in vivo. *Diabetes research and clinical practice.* 2014;105(2):206-216.

212. Ferreira JR, Teixeira GQ, Santos SG, Barbosa MA, Almeida-Porada G, Goncalves RM. Mesenchymal Stromal Cell Secretome: Influencing Therapeutic Potential by Cellular Pre-conditioning. *Frontiers in immunology.* 2018;9:2837.
213. Kim YS, Noh MY, Cho KA, et al. Hypoxia/Reoxygenation-Preconditioned Human Bone Marrow-Derived Mesenchymal Stromal Cells Rescue Ischaemic Rat Cortical Neurons by Enhancing Trophic Factor Release. *Molecular neurobiology.* 2015;52(1):792-803.
214. Bian S, Zhang L, Duan L, Wang X, Min Y, Yu H. Extracellular vesicles derived from human bone marrow mesenchymal stem cells promote angiogenesis in a rat myocardial infarction model. *Journal of molecular medicine (Berlin, Germany).* 2014;92(4):387-397.

7. Curriculum Vitae and Publications

PERSONAL INFORMATION

Name:	Sara Medina Balbuena
Date of Birth:	15.04.1987
Place of birth:	Las Palmas de Gran Canaria, Spain
Nationality:	Spanish
Civil status:	Single
Father's name:	Medina Alonso, Juan
Mother's name:	Balbuena Castellano, María del Carmen Rosa

SCHOOLING

2003-2005:	Instituto Tomás Morales. High School Diploma in Health Sciences. Las Palmas de Gran Canaria, Spain

UNIVERSITY EDUCATION

May 2016-Present:	Ph.D Student, Fifth Medical Department (Nephrology, Endocrinology, Rheumatology) of Mannheim University Hospital, University of Heidelberg, Germany
September 2011- February 2012:	M.Sc Environmental Toxicology, Faculty of Pharmacy, University of Valencia (UV), Spain. **Thesis title**: *'Determination of pesticides in honey and honeybees. Environmental and Public Health implications'*
September 2005- July 2011:	B.Sc. Veterinary Medicine, Faculty of Veterinary Medicine, University of Las Palmas de Gran Canaria (ULPGC), Spain

PUBLICATIONS AND POSTER PRESENTATIONS

Publications:

Torres Crigna A, Daniele C, Gamez C, **Medina Balbuena S**, Pastene D.O, Nardozi D, Brenna C, Yard B, Gretz N, Bieback K. Stem/Stromal Cells for Treatment of Kidney Injuries With Focus on Preclinical Models. *Frontiers in medicine*. 2018;5:179.

Poster presentations:

Medina Balbuena S, Torres Crigna A, Bieback K, Porubsky S, Krämer BK, Yard B. Human adipose-derived mesenchymal stromal cells reduce chronic peritubular infiltration after ischaemia-induced acute kidney injury (AKI-IR). Poster presented at the 27. Jahrestagung der Deutschen Transplantationsgesellschaft, 2018 Nov 07-10, Berlin.

Medina Balbuena S, Henn J, Torres Crigna A, Bieback K, Porubsky S, Krämer BK, Yard B. A comparison of long-term renal outcomes in ischaemia-induced acute kidney injury models with or without unilateral nephrectomy at the time of ischaemia. Poster presented at the 28. Jahrestagung der Deutschen Transplantationsgesellschaft, 2019 Oct 17-19, Hanover

8. Acknowledgements

First of all, I would like to thank my supervisor Professor Benito Yard for giving me the opportunity to work in this, at times hard and frustrating, but most of the time amazing project, that has given me the chance to grow so much professionally and personally. Thank you for your kindness, support and scientific guidance. I would also like to show my gratitude to the head of the Cooperative Research Training group `Tissue Analytics for Stem Cell based Diagnostics and Therapies' (TASCDT), Professor Norbert Gretz and to Professor Karen Bieback, for cooperating with us in this project. I would also like to express my gratitude to a fellow TASCDT member, Daniela Nardozi for the help, friendliness and patience she always had towards me. I cannot forget about Sina Schwalm, the most efficient person I have ever known, always willing to help and to make your life easier. Thank you to Andreas Kluth from TICEBA for making our cooperation so straightforward and pleasant. I offer my deepest thanks to Jonas Jarczyk, for literally saving this project. Thank you for your hard work and commitment. Additionally, I would like to express my greatest gratitude to my partner in crime Rahef Ouerdani for always being there for me, through laughter and (a lot of) tears. You made this journey much more endurable, I cannot thank you enough. Of course I cannot forget about my dearest co-workers, the house 11 gang: Angélica Rodríguez and Katharina Kohl. Thank you so much for the coffee breaks, the scientific brainstorming, the occasional freezing to death and the conversations about life. Also, I would like to express my deepest thanks to Diego Pastene, whose generosity knows no limit. Thank you for always being there to help, your constant support and the high blood pressure due to so many coffee breaks. I sincerely thank Katharina Prem for teaching me so much, for her constant willingness to help, extreme care and patience.

On a more personal note, I would like to acknowledge my dear friend Adriana Torres, not only for her scientific help but also for making this journey so much more enjoyable. Getting to know you has been one of the highlights of this experience, I will cherish it forever. I also want to thank my fellow Veterinarian colleagues in the 'Consejo de sabios' for their support, for the occasional help concerning clinical issues when I have been really lost and for always making me feel that time has not passed, and we are still in the faculty making the photosynthesis. Also, I cannot forget about my oldest, dearest friend Pablo, who sucks at Science, but has always been there for me, through thick and thin, and who still makes me laugh like no other. Last, but definitely not least, I have to say a huge thank you to my beloved Javier, for supporting me every step of the way, for telling me I could do it when I wanted to give up and for encouraging me to follow my aspirations and be better. Of course, I cannot leave behind the person I love the most in the world, my father. For that I reason I have to write this bit in Spanish. Querido papá: Este trabajo te lo dedico a ti. Si no fuera por tu esfuerzo, el haberte sobrepuesto a la adversidad y la constante dedicación para con tus hijas yo nunca habría llegado hasta aquí. Eres el mejor padre que he podido desear. Tu cariño, honestidad e integridad siempre me han inspirado, y espero haber aprendido un poco de ti para ser cada vez mejor persona. Nunca podré expresarte con palabras lo agradecida que estoy por todo lo que has hecho por mí, pero al menos espero haberte hecho sentir orgulloso.